Yearbook

2016

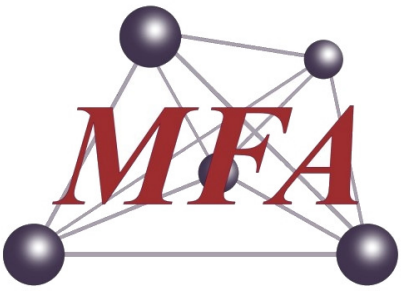

Institute of Technical Physics and Materials Science

http://www.mfa.kfki.hu/

Hungarian Academy of Sciences
Centre for Energy Research

Institute of Technical Physics and Materials Science

Director: Prof. Béla Pécz

Address: Konkoly-Thege Miklós út 29-33,
H-1121 Budapest, Hungary
Postal: P.O.Box 49, H-1525 Budapest, Hungary
Phone: +36-1-392 2225
Fax: +36-1-392 2226
E-mail: info@mfa.kfki.hu
URL: http://www.mfa.kfki.hu/

MTA EK MFA Yearbook 2016

Editor: Csaba S. Daróczi
Published by: MTA EK MFA, Budapest, Hungary, 2017

CONTENT

DIRECTOR'S FOREWORD

As the newly appointed director of MFA, it is my pleasure to welcome the reader. I recommend to browse the present yearbook which continues and contains results achieved in 2016. I am proud to be the follower of our former director, *Professor István Bársony*, who was heading the institute for twelve years and supported our researchers to achieve lot of successes. Remarkable point of last year was when István Bársony was appointed by the General Assembly of the Hungarian Academy of Sciences to "Ordinary" Membership in the Engineering Section. We, and personally myself, expect that his retreat from administrative load will contribute to an increased presence of him in laboratories and adds direct influence on research, increasing our efficiency and world wide acceptance.

In 2016, the most honorable event was the successful organization of an international conference, the "EUROSENSORS-2016" by co-workers of the institute, with Professor Bársony, as Chairperson. Furthermore, we are proud on increasing number of papers and conference talks, many of the latter were invited ones. Increasing number of citations reflect broad acceptance of those papers and our efforts. It is my mission to help and to lead the institution on this successful track.

We are extremely proud on numerous groups headed by young contemporaries, many of them honored by financing agencies. One of such financed "*Lendület*" (Momentum) research group was the Biosensorics group, which got to the end of the contract period and, accordingly, was subjected to an official audit. In that procedure, the group has received "Outstanding" qualification from the Academy of Sciences, which also meant that the previous extra support became part of the yearly budget. Another excellent group, the NanoFab2D research group was supported by an ERC starting grant. Immediately at the beginning of the project they announced a novel device concept on 2D materials exploiting magnetism at the zigzag edges of graphene nanoribbons. Thus, enabling control of both charge and spin signals within the simplest three-terminal field-effect transistor device configuration.

The Institute works under the Quality assurance system ISO 9000-2008. In this system, scientific publications are considered as products. Therefore we make a sum-up of them each year. Fortunately the scientific level of MFA's publications has increased again and the researchers receive more and more independent citations year by year. Cooperation with industrial partners has a growing importance in the life of MFA. Our researchers contributed substantially to the development of 3D fingerprint sensor devices. MFA researchers participate actively to the development of robotic

minimal invasive surgery by their tactile sensors. Our researchers participate actively in R&D processes and in the case of Hungarian industrial firms; it is our institute which initiates the projects. MFA clearly wants to show that the research conducted by the institute also benefits for the society. Therefore, each year we organize an Open Day, when everyone can take a personal visit to the institute and listen talks on the last activity and even visit some laboratories. MFA organizes scientific seminar talks weekly and those lectures are also open to the public. We are proud for the one-week summer school for high-school students, when they also get a chance to work inside our laboratories. These youngsters often return later in some form to the "nest".

Our applications for buying new equipment were awarded in 2016. A brand new fluid-AFM was bought for the Biosensorics research group from the support of our Academy. Beside that, our application in order to buy the first aberration corrected TEM/STEM was also awarded by NKFIH (National Research Development and Innovation Office) and by the Ministry of National Economy. Therefore the Thin Film Physics Department of MFA will purchase (by public procurement) a new microscope with a resolution below 0.1 nm (and EDS X-ray analysis device) from EU Structural Funds. There are further applications in the pipeline, which we hope will be awarded in 2017.

I congratulate to my colleagues: *György Szabó*, who was awarded by the Physics Grand prize of the Hungarian Academy of Sciences and also to *Levente Tapasztó*, who received the Physics prize of the Hungarian Academy of Sciences. We are also proud of those 9 Ph.D. students, who were supervised by colleagues at MFA defended their thesis successfully in 2016 and got the Ph.D. degree from different universities.

I hope that the Readers of this yearbook will find further interesting details on the following pages. Here I note that the former MFA Yearbooks are available electronically at http://www.mfa.kfki.hu/en/yearbook/ .

Budapest, March 21st, 2016

Dr. Béla Pécz

GENERAL INFORMATION

Organization of MFA

Director	- ***Béla PÉCZ***

Scientific Departments	
Nanostructures Department	- *Levente TAPASZTÓ*
"Lendület" group - 2D Materials	- *Levente TAPASZTÓ*
Thin film physics Department	- *Katalin BALÁZSI*
Complex Systems Department	- *György SZABÓ*
Photonics Department	- *Péter PETRIK*
Microtechnology Department	- *Gábor BATTISTIG*
"Lendület" group - NanoBioSensorics	- *Róbert HORVÁTH*

Directly supervised functions	
Head of Scientific Advisory Council	- *János LÁBÁR*
Scientific secretary, projects and PR	- *Krisztina SZAKOLCZAI*
Quality control, MTMT, REAL admin	- *Andrea BOLGÁR*
Technical support	- *Károly BODNÁR*
Financial administration	- *Zsuzsa KELEMEN*
Informatics	- *Gergely TAMÁS*
Technology transfer (IPR)	- *Antal GASPARICS*

Key Financial Figures of MFA

The turnover realized by the institute (and in general by the members of the Hungarian academic research network) always reflect the national and international political and financial system. The domestic subsidies did not change in the last 5 years; however the research overhead and expenditures are increasing worldwide. There is a certain periodicity in the income of the institute based on the changes by the domestic grant management system, and also by the European Commission's research schemes (FP6, FP7 and now H2020).

Until 2012 MFA was operating as an independent entity, but after the two reorganizations of MFA - first the merge with Research Centre for Natural Sciences, than the migration to Centre of Energy Research - made our financial status completely not plannable, totally unpredictable and non-transparent by our own grant administration group. We still do not have access to authentic budget; the data for 2015-2016 are based upon our own estimates.

Despite all these, all the project contract modifications due to reorganization were successful by mid-2016 (took more than one year to complete!), and also scientific achievements were granted with new financial sources both from national and international authorities. By the end of the year our income reached its record value in 14 years with 2,1 billion HUF.

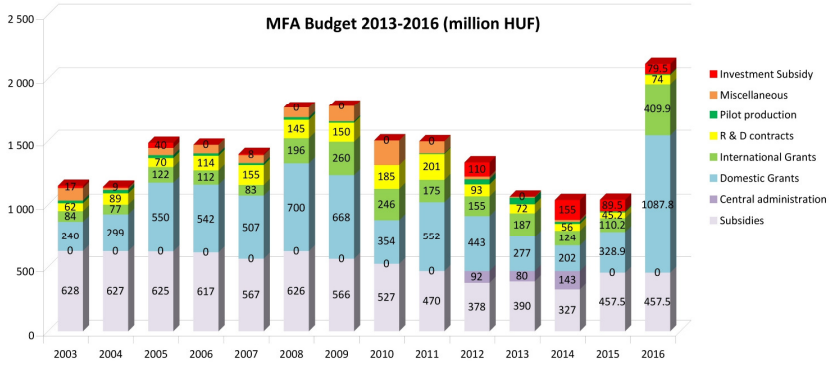

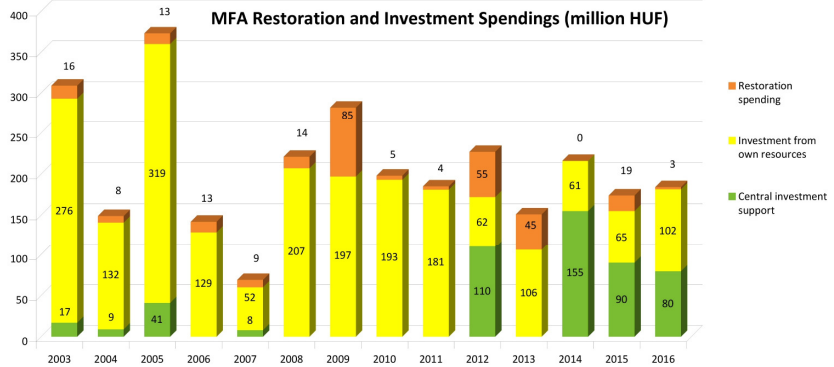

Publications & Citations

According to the Thomson-Reuters ISI "Web of Knowledge", and MTMT databases, the Institute has an average publication activity of ca. 100 scientific papers in IF journals a year.

MFA and its predecessor's publications

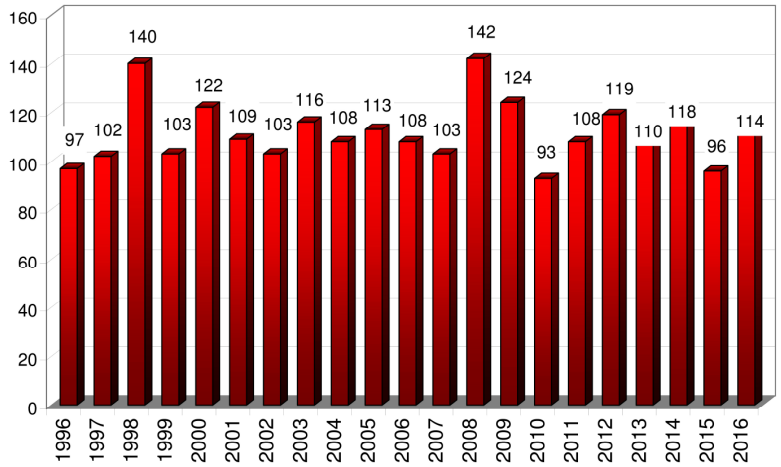

The complete 2016 publication list of MFA – with considerably more titles than listed by the ISI Web of Science and MTMT – is included at the end of this yearbook. A good measure of recognition of MFA's scientific activity is the h-index of 81.

MFA and its predecessor's citations

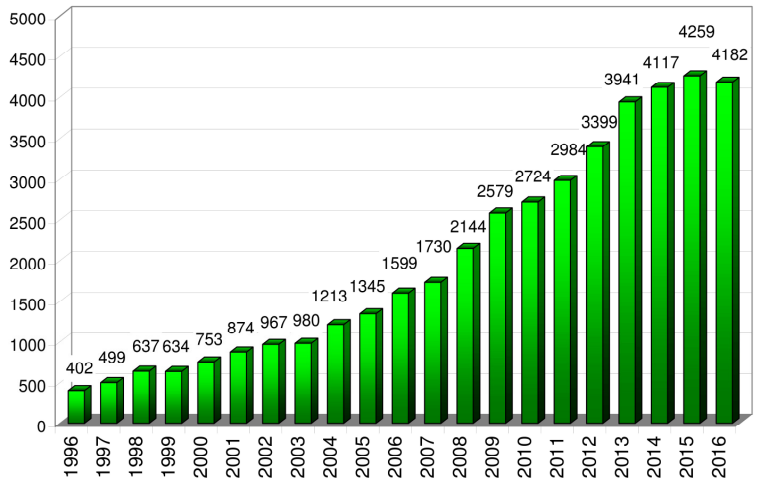

Prizes and Distinctions

BÁRSONY, István

Ordinary member of the Section of Engineering Sciences of the Hungarian Academy of Sciences

SZABÓ, György

Physics Grand prize of the Hungarian Academy of Sciences

TAPASZTÓ, Levente

Physics prize of the Hungarian Academy of Sciences

RADNÓCZI, György

Officer's Cross, Order of Merit of the Republic of Hungary

and

Professor Emeritus of the Hungarian Academy of Sciences

TÓTH, Attila Lajos

Golden Cross, Hungarian Cross of Merit of the Republic of Hungary

VONDERVISZT, Ferenc

Polinszky prize of Veszprém city

VANCSÓ, Péter

Young scientist prize of the Hungarian Academy of Sciences

KOLONITS, Tamás — Jenő Pócza prize of the Hungarian Society for Microscopy

CSIKÓSNÉ PAP, Andrea Edit — Óbuda University Kandó Kálmán Faculty of Electrical Engineering dean's laudation

SZOLNOKI, Attila — EPL award "Highlights 2015 -a compilation of the best papers published within the last year"

OLÁH, Nikolett — MTA EK Young scientist prize

BALÁZSI, Katalin — MFA Prize (Researcher)

OSVÁTH, Zoltán — MFA Prize (Postdoctoral)

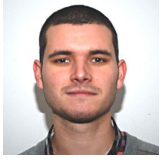

ZÁMBÓ, Dániel — MFA Prize (Ph.D. student)

HIGHLIGHTS

Taming defection – how we all might be better off with certain level of tolerance

(OTKA K-120785)

A. Szolnoki and M. Perc

Leaving the joint enterprise when defection is unveiled is always a viable option to avoid being exploited. While loner strategy helps the population not to be trapped into the tragedy of the commons state, the resulting three-strategy solution is rather disappointing. Namely, the average payoff is unable to exceed the income of a loner's strategy significantly, hence participating in a public goods game does not necessarily provide an attracting option for competing players. This failure suggests that perhaps it is not the best option for cooperators to leave the group when defectors emerge because by switching to loner state they loose all benefits of mutual cooperation immediately. In this way the original dilemma can be transformed into a new form where cooperator players should decide how many defectors they tolerate in their group before leaving the group for a modest, but guaranteed payoff.

To explore this new dilemma we introduce a spatial model of public goods game in which beside the unconditional defector (D), cooperator (C), and loner (L) strategies there are players with a certain degree of tolerance for the defectors among them. These players could choose to cooperate or abstain, depending on the actions of other players. By forming 5-member groups on a square lattice we allow the diversity of tolerance threshold. In particular, M_1, …, M_5 strategies behave as a cooperator as long as the number of defectors remains below a threshold value in the group but it switches to loner state otherwise. By following this approach we can check the viability of this mixed strategy and clarify if there is an optimal level of tolerance which provides the highest income for the whole population.

Such a complex system is generally characterized by the presence of strong fluctuations, unpredictable and non-linear dynamics, multiple scales of space and time, and frequently some form of emergent structure. To handle this complexity during the Monte Carlo simulation we should apply stability analysis of sub-system solutions and also finite-size analysis. An example of a stability analysis is illustrated in Fig. 1 where two subsystem solutions, namely the three-strategy DCL and the four-strategy DCM_1M_2 phase are compared. The series of snapshots in the upper row shows the separation of the population in two parts, each of which is initially randomly distributed with the strategies that will form one of the two competing subsystem solutions (Fig. 1(a)). In Fig. 1(b), the subsystem solutions are formed in both halves of the space and their proper competition starts after removing the border between them (thus allowing strategy transfer across the border). Fig. 1(c) shows an intermediate state during the competition in which the DCL phase will ultimately turn out to be the winner. Fig. 1(d), on the other hand, shows an intermediate state during

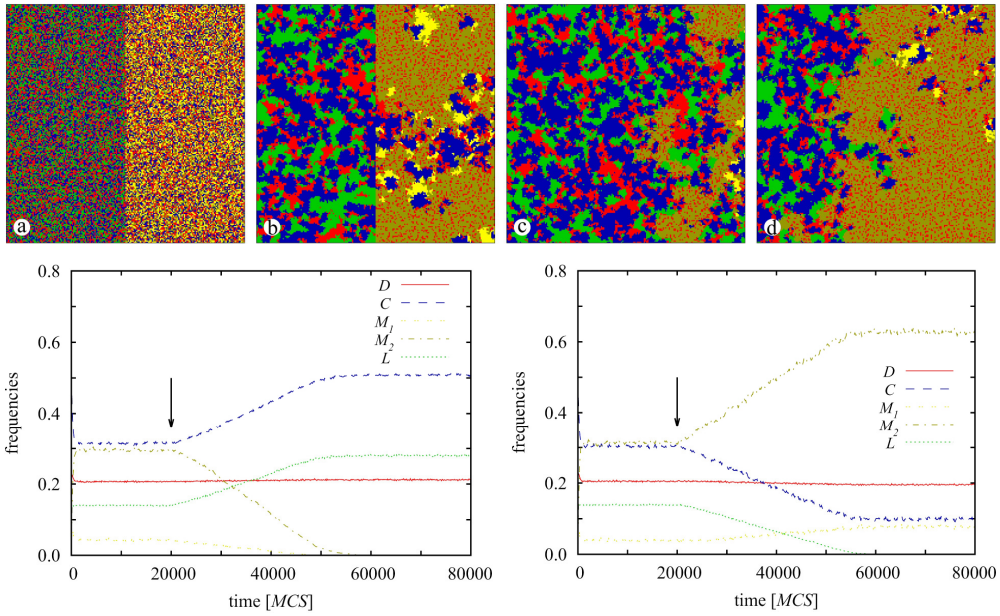

Figure 1. *Stability analysis of two subsystem solutions at both sides of the discontinuous phase transition point.*

the competition in which the DCM_1M_2 phase will ultimately turn out to be the winner. Here only the synergy factor r is changed slightly while all other parameters are unchanged. The two graphs in the bottom row depict the corresponding time evolution of the strategy densities. After a relaxation of 20 000 Monte Carlo steps (marked by an arrow), the two subsystem solutions start competing for space. On the left (r=2.80) the DCL solution wins, while on the right (r=2.81) the DCM_1M_2 solution wins. The linear system size used for this example was L = 2400, but the snapshots in the upper row contain just a 200×200 cutoff of the whole population for clarity. Here, in agreement with the colors of legends, defectors are marked by red, pure cooperators by blue, M_1 strategy by yellow, M_2 by ochre, and loners by green.

It is also worth stressing that simulations at small system can easily cause finite-size effects which may lead to misleading outcomes of the strategy competition. To illustrate it in Fig. 2 we start the evolution from a random initial state where all the eight strategies are present (Fig. 2 (a)). After relaxation only D (red) and M_2 (ochre) strategies survive, which also form a two-strategy solution (Fig. 2(b)). In Fig. 2(c), we then manually re-introduced small compact patches of three other strategies, namely strategy C (blue), strategy L (green), and strategy M_1 (yellow). Afterwards, loners die out (again) very soon within the DM_2 phase, as shown in Fig. 2(d). Later, C players also die out, but tolerant strategies M_1 and M_2 form a successful alliance, as shown in Fig. 2(e). Indeed, their formation turns out to be stronger than the previously declared victorious DM_2 phase, and the population terminates in a defector-free state, as shown in Fig. 2(f). Importantly, the defector-free state can evolve naturally from a random initial state if the system size is large enough.

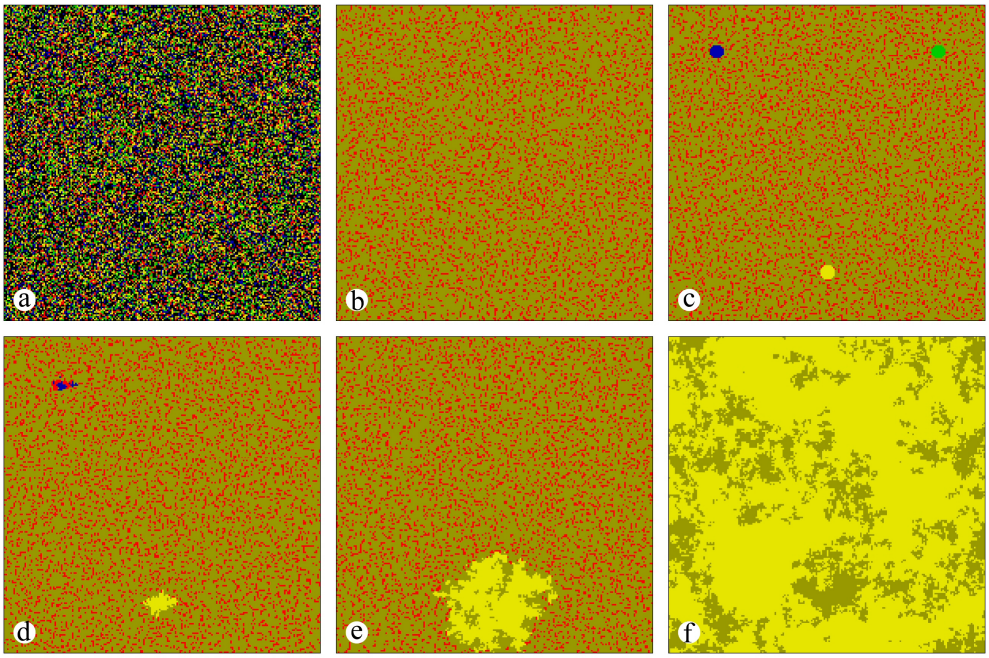

Figure 2 *Finite-size effect can easily cover the viable stable solution. The latter, plotted in (f), can only emerge spontaneously if the evolution is launched for sufficiently high system size.*

Our results are summarized in a phase diagram plotted in Fig. 3. It suggests that the diversity of tolerance proved optimal. When tolerant players had different thresholds for withstanding defection, they could turn the whole group towards cooperation in cases where defection would have otherwise dominated. As we noted, certain stable solutions only emerged when the number of players was large enough, lying largely undetected for smaller games. But once they emerged, they remained stable, even in small populations. These pattern formations may explain why tolerant behaviour remains stable during an evolutionary process especially when external conditions are demanding and they can only provide a modest benefit for cooperator strategy.

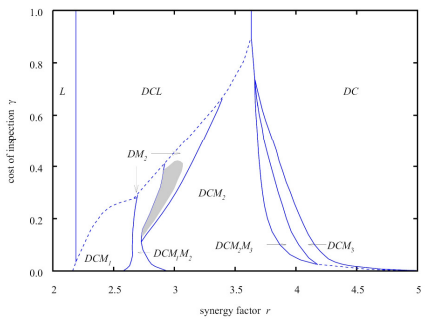

Figure 3 *Full phase diagram of our model on the* r − γ *(inspection cost – synergy factor) parameter plane. Dashed lines denote discontinuous, while solid lines mark continuous phase transitions. In structured population, in stark contrast to the well-mixed system, there also exist regions where the coexistence of different tolerance levels is the stable solution. The grey-shaded region in the two-strategy* DM_2 *phase denotes those parameter values where the population evolves into a full-cooperator, defector-free* M_1M_2 *phase, but only if the system size is large enough.*

Flagellin based biomimetic coatings: from cell-repellent surfaces to highly adhesive coatings

(Lendület LP2012-26/2012, ERC_HU NKFIH, OTKA NN117849)

B. Kovács, D. Patkó, I. Székács, N. Orgován, S. Kurunczi, A. Sulyok, N. Q. Khánh, B. Tóth, F. Vonderviszt, and R. Horváth

Biomimetic coatings with cell-adhesion-regulating functionalities are intensively researched today. For example, cell-based biosensing for drug development, biomedical implants, and tissue engineering require that the surface adhesion of living cells is well controlled. Recently, we have shown that the bacterial flagellar protein, flagellin, adsorbs through its terminal segments to hydrophobic surfaces, forming an oriented monolayer and exposing its variable D3 domain to the solution [*Analytical Chemistry* 85 (11), 5382-5389, 2013]. Here, we hypothesized that this nanostructured layer is highly cell-repellent since it mimics the surface of the flagellar filaments. Moreover, we proposed flagellin as a carrier molecule to display the cell-adhesive RGD (Arg-Gly-Asp) peptide sequence and induce cell adhesion on the coated surface. The proposed concept is visualized in Fig. 1.

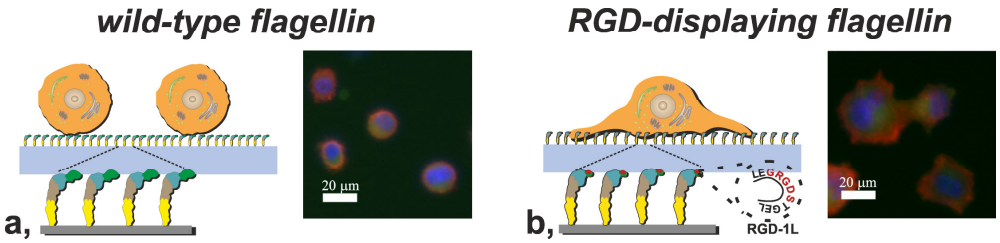

Figure 1 Schematic representation and fluorescent microscopic images of cells on anti-adhesive and adhesive surface coatings. a, Wild type flagellin hinder cell adhesion on the sensor surface. b, RGD displaying flagellin induce cell adhesion and spreading.

The details of this work have been recently published [53] and can be summarized as follows:

During the mammalian HeLa cell adhesion experiments, we recorded the cell adhesion data with OWLS (Optical Waveguide Lightmode Spectroscopy) and applied a PLL-*g*-PEG polymer monolayer as reference anti-adhesive surface coating. The ΔN_{TM} (effective refractive index change) signals recorded on surfaces coated with either wild-type flagellin or PLL-*g*-PEG both remained at the level of the baseline during the whole time span of the cell-based assay (Fig. 2a). Since ΔN_{TM} is proportional to the degree of the cell adhesion [*Journal of Receptors and Signal Transduction* 29 (3-4), 211-223, 2009], we concluded that both surfaces were highly cell-repellent. The changes in the full width of the TM_0 resonant peak at half maxima (changes of *W, i.e.* ΔW) were also monitored [*Applied Physics B: Lasers and Optics* 91 (2), 319-327, 2008].

Cellular activity provoked negligible shifts in *W,* further proving that there was no significant cell adhesion on either wild-type flagellin or PLL-*g*-PEG layers (Fig. 2b). Cell adhesion and spreading would make ΔW increase due to the micron-scale optical inhomogeneities caused by the adhering cells at the sensor surface. Our conclusions are well supported by the phase contrast images of cells captured on the coated sensor surfaces after the OWLS measurements (Fig. 3).

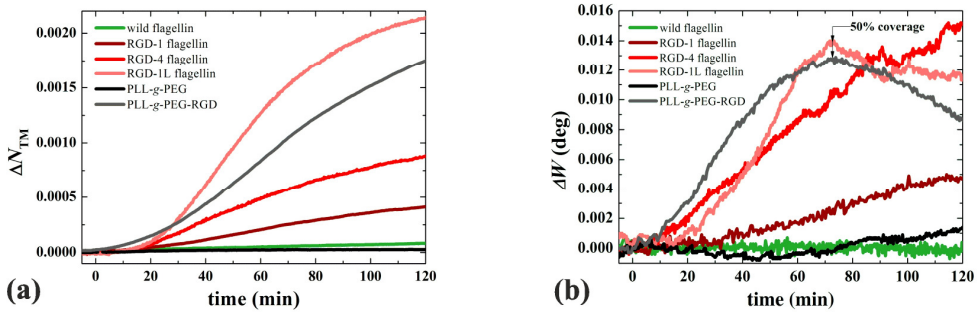

Figure 2 *OWLS signals recorded after living cells were seeded on the surfaces of the OWLS chips coated with the indicated layers. (a) The measured ΔN_{TM} values correlating with the strength of cellular adhesion. (b) Temporal evolution of the width of the OWLS resonance peak (W).*

We created flagellin-based fusion proteins in which the D3 domain of FliC is replaced by an oligopeptide segment containing one or more of the integrin binding RGD motif. Although the simple RGD motif is sufficient to mediate binding to integrin receptors, the flanking amino acid residues may further enhance binding affinity. Thus, we chose the more efficient GRGDS pentapeptide as the basic unit for insertion.

We tested the genetically modified flagellin variants as surface coatings, too. On the sensor surfaces coated with RGD-displaying flagellin variants, cells provoked a continuous increase (up to a maximum value) in N_{TM}. Cells seeded on the PLL-*g*-PEG-RGD-coated adhesive reference surface produced similar signals. The observed saturating sigmoid-shaped curves are clear characteristics of active cell spreading. The larger the signal the stronger is the cellular adhesion; cells induced the largest ΔN_{TM} signal thus showed the strongest adherence on the RGD-1L surface. The second, the third and the fourth highest cell adhesion were obtained with the PLL-*g*-PEG-RGD, RGD-4 and RGD-1 coatings, respectively (see Fig. 2a).

In conclusion, cells on the three different RGD-displaying flagellin layers adhered to different degrees, which could be explained by the fact that the RGD motif was integrated with different linker pairs, and most probably provided different accessibility and flexibility for the cells.

The temporal evolution of the width of the OWLS resonance peak (*W)* during cell adhesion was also recorded (Fig. 2b). In the case of the RGD-1 and RGD-4 flagellin-coated surfaces *W* increased monotonically and continuously until the end of the experiment. This suggests that the surface coverage did not reach 50% during the

time of the experiment. In contrast, in case of the PLL-*g*-PEG-RGD and RGD-1L surfaces ΔW first increased, then reached a very clear maximum, and then decreased again. Previous experiments and numerical simulations suggest that such kinetic behavior indicates that the cell coverage already increased above 50%. The half surface coverage is reached at the maximum value of the resonant peak width [*Applied Physics B: Lasers and Optics* 91 (2), 319-327, 2008]. This finding also suggests that the most intense cell adhesion and spreading took place on the PLL-*g*-PEG-RGD and RGD-1L coatings. The phase contrast images recorded well confirm the above findings (see Fig. 3).

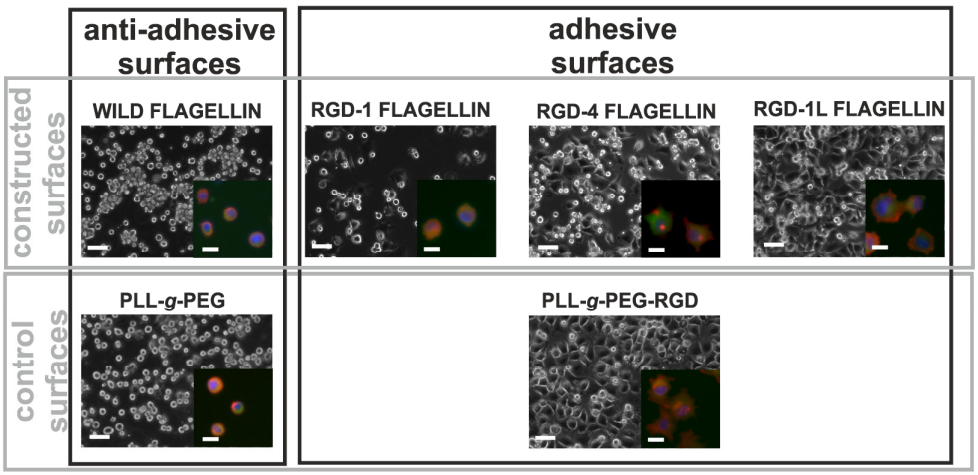

Figure 3 *Microscope images of the cells seeded on the investigated surfaces. The phase contrast images (scale bar 50 μm) show cells on the biosensor surfaces right after the OWLS experiments. The insets (scale bar 20 μm) show fluorescently labeled cells cultured on glass coverslips in parallel experiments (red: F-actin, blue: nuclei, green: vinculin).*

In conclusions, the application of flagellin-based fusion proteins for fabricating tunable surfaces opens up new avenues. Wild-type flagellin and its functionalized variants can be applied together in various mixing ratios. Thus, oriented affinity layers with negligible non-specific cell adhesion can be created with well controlled average distance between the binding sites.

Other peptide sequences can be easily introduced into flagellin in a similar manner. Therefore, surfaces with multiple functionalities can be fabricated in a straightforward manner. Flagellin variants exhibiting specific recognition functionalities offer the possibility to create a large variety of coatings on hydrophobic surfaces. Since flagellin does not adsorb at all on hydrophilic surfaces solution [*Analytical Chemistry* 85 (11), 5382-5389, 2013], patterned functional surfaces could be easily created in a straightforward and cost-effective manner by patterning the hydrophobicity of the surfaces and exposing them to the solutions of functionalized flagellin.

PUBLIC OUTREACH

The MFA summer school was organized 9th time in 2016, where 24 secondary school students from the Carpathian-basin have attended. For increasing the awareness our institute provided a one week opportunity to join scientific research.

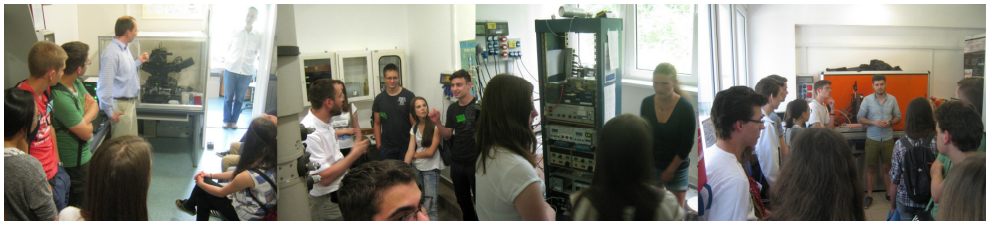

The students had the opportunity to get familiar with the MFA research facilities during the working hours, and to have many excursions sporting events and other social programs after it (http://alag3.mfa.kfki.hu/mfa/nyariiskola/).

From the left side: (1): rooting for the Hungarian national football team, (2): eating what we baked, (3): how we kill fire, (4): tunnelling-effect, (5): Min Kim receives her diploma.

Students supervised by MFA scientists achieved excellent results on Scientific Students' Contests and other national and international contests: *Domonkos Szegedi* won first prize at BME and also received special prize of the BME Pro Progressio Foundation; *László Ádám Gréczi* won the National Talent Program's scholarship with his Mag Car-4.0 project; *Orsolya Batiz* was awarded with gold medal on the 23rd International Conference of Young Scientists event (http://www.icys2016.com/); *Anna Borbála Tóth* won first prize at the Scientific Students' Contest of the Faculty of Information Technology and Bionics, Catholic University Péter Pázmány; *Péter Udvardi* won first prize at the 25th Youth Scientific and Innovation Student Contest and qualified to the European Union Contest for Young Scientists, Brussels (EUCYS), where he also won a honorable special prize.

The institute still participates in running the „All Colors of Physics" bus, mainly promoted by Wigner FK. The bus formerly known as Nanobus set up by MFA. The bus organizes entertaining science shows for raising the awareness for natural sciences (http://www.sokszinufizika.hu/) The bus show entertained several hundreds of people.

MFA joined the international Girl's Day event as well as the Researcher's Night series second time in 2016.

For educational and awareness purposes the institute maintains the http://www.nanotechnology.hu/ webpage, where the institute's nanotechnology related results are published plainly. Videos and articles can be downloaded from this site. The continuously developed software called Web-Schrödinger is also freely accessible; it can be used for numerical solution of stationary and time dependent Schrödinger-equation.

MFA upkeeps the http://www.nanobiosensorics.com/ webpage, where visitors can get information about the optical label-free detection of nanoscale (biological) objects.

MFA maintains the http://www.mems.hu/ webpage and publishes information here about the work of the Microtechnology Department and also about the latest MEMS, NEMS, BioMEMS and NeuroMEMS topics researched. The department runs an Open Access laboratory, therefore the detailed description of the instruments, clean rooms and technological background can also be reached, together with the access right conditions.

EVENTS

Professor István Bársony was appointed as a new ordinary member of the Section of Engineering Sciences of the Hungarian Academy of Sciences, by the 187th General Assembly. In January 2017 he held his inaugural lecture entitled “Silicon technology – and what we can thank for it” at the main hall of the Hungarian Academy of Sciences.

(MTA photos)

EUROSENSORS 2016, the 30th anniversary conference of the series was held from September 4 to 7, the second time in Budapest, Hungary. Twenty-three years ago the Technical University of Budapest (BME) was the host, this time the Engineering Section of the Hungarian Academy of Sciences.
For 30 years the EUROSENSORS Conference was the largest European forum for scientists and engineers from the academia, research institutes and companies, and especially for students to present and discuss the latest trends, and results in Sensors, Actuators, Micro- and Nanosystems.
EUROSENSORS 2016 was chaired by *Prof. Dr. István Bársony*, former director of MFA. The conference chair was *Dr. Gábor Battistig* head of Microtechnology Department. The Eurosensors School was organized by *Dr. Péter Fürjes*, the publication chair was *Dr. Zsolt Zolnai*.
The conference was attended by 550 participants, 78% of them came from academia and 22% from industry. 656 submissions were received from 46 countries for peer review, all were assigned to 5 reviewers. From the accepted ones 140 lectures (including 4 plenary talks and 7 keynote lectures) were selected and presented in 12 categories ranging from theory to special applications in the automotive and healthcare fields. 330 posters were presented and displayed for the entire duration of the conference to enhance discussions and networking possibilities.

The traditional EUROSENSORS trophy and the new flag inaugurated in Budapest was handed over to Prof. Jean-Paul Viricelle, the general chair of the next conference to be held in Paris, France EUROSENSORS 2017.

Group of EUROSENSORS volunteers related to MFA.

To maintain the strong connection with our Japanese partners and with the project members *Dr. Béla Pécz* held a talk at The Joint Visegrad 4 – Japan Seminar on Technology Transfer. For better understanding the Hungarian Embassy in Japan translated the slides to Japanese language.

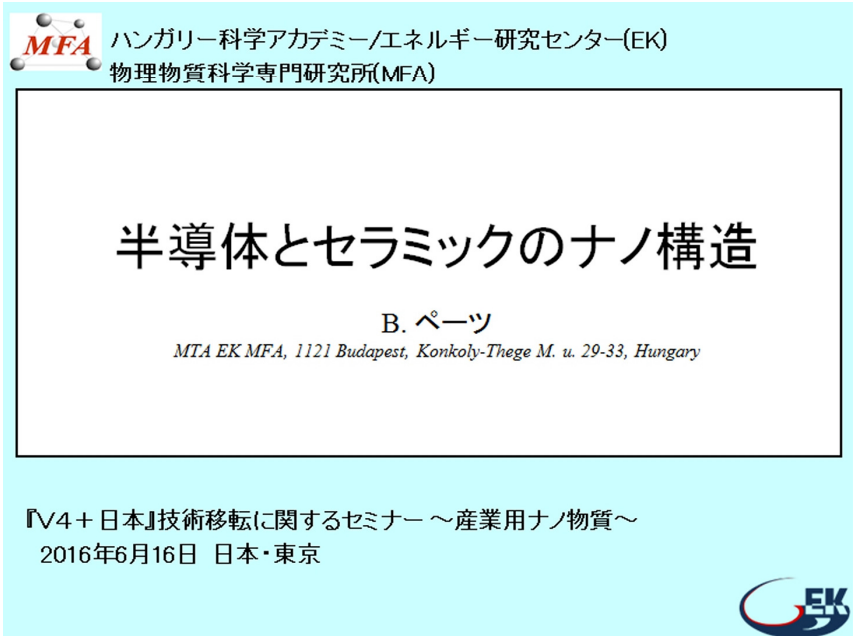

The Joint Visegrad 4 – Japan Seminar on Technology Transfer – Nanomaterials for Industrial Use, Tokyo, Japan, 16th June 2016.

SCIENTIFIC REPORTS

Nanostructures Laboratory & 2D 'Lendület' Research Group

Head: Dr. Levente Tapasztó

Research Staff

- Zsolt Endre HORVÁTH, Ph.D., Deputy Head of Laboratory
- Prof. László Péter Biró, Corr. Member of the HAS
- Gergely DOBRIK, Ph.D.
- Krisztián KERTÉSZ, Ph.D.
- Antal Adolf KOÓS, Ph.D.
- Géza István MÁRK, Ph.D.
- Péter NEMES-INCZE, Ph.D. (on leave)
- Zoltán OSVÁTH, Ph.D.
- Péter SÜLE, Ph.D. (from 2015-10-15)
- Péter VANCSÓ, Ph.D. (on leave)

Ph.D. students / Diploma workers

- Péter Lajos NEUMANN, Ph.D. student (on leave/left)
- Gábor PISZTER, Ph.D. student
- András PÁLINKÁS, Ph.D. student
- Zsófia JUHÁSZ, B.Sc. student

The Nanostructures Laboratory has nearly two decade long expertise in synthesis and characterization of various nanostructures. In recent years research efforts have been focused on 2D materials and on atomic precision lithography of nanostructures thereof. Besides graphene, our research interest was continuously shifting towards novel 2D materials, such as Transition Metal Dichalcogenide single layers, as well as their hetero-structures. In addition, bioinspired photonic nanoarchitectures were also investigated and applied for optical detection.

The most relevant results in 2016 have been:

- Novel device concept was developed based on magnetic phase transition in graphene nanoribbons that enabled electrical control of both charge and spin signals in a simple field effect transistor configuration.
- We were successful to image directly atomic-level oxidation processes of single layer transition metal dichalcogenides subjected to ambient conditions using Scanning Tunneling Microscopy.
- Anomalously large Moiré superlattices of graphene on Au (111) substrate were observed that can be interpreted as substantial distortions of the crystal lattices.

Moiré superlattices in strained graphene-gold hybrid nanostructures

(EU FP7 Marie Curie CIG No.334377, János Bolyai Research Scholarship, OTKA K101599, NKFIH TÉT_12_SK-1-2013-0018)

A. Pálinkás, P. Süle, M. Szendrő, Gy. Molnár, C.Hwang (KRISS,Korea), L.P. Biró, and Z. Osváth

Tailoring the atomic and electronic structure of graphene has been a subject of intense research, due to its possible applications in nanoelectronics. The local density of states (LDOS) can be modified, among other methods, by periodic potentials which create secondary Dirac points (SDP). Such periodic potentials can be induced in graphene by moiré patterns (Fig. 1) using crystalline substrates. The lattice mismatch and relative rotation between graphene and the crystalline substrate determine the period of the moiré pattern, and consequently the energy at which the SDPs appear.
Graphene grown by chemical vapor deposition was transferred on top of flat gold nanoislands and characterized by scanning tunneling microscopy (STM) and tunneling spectroscopy (STS). Here we show that the strength of graphene-gold interaction can be tuned by annealing the graphene-covered gold nanoislands at moderate temperatures and that graphene plays a key role in the formation of crystalline gold surfaces. Multiple annealing processes were applied: firstly, to increase the adhesion of graphene to the gold nanoislands, then to transform the supporting polycrystalline gold surfaces into (111) crystal planes. After annealing at 650 °C in Ar atmosphere, gold nanoislands covered by graphene have displayed Au(111) crystalline surfaces, while surface of non-covered nanoislands remained disordered.

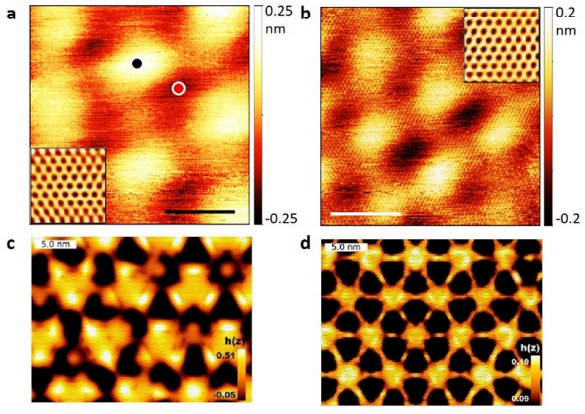

Figure 1 ***(a):*** *STM image of graphene on top of gold (111) showing a moiré of 7.7 nm. STS measurements taken on topographically high and low positions, marked with black and red dot, respectively, are shown in* ***(b)****. STM image of graphene on top of gold (111) showing a moiré of 5.1 nm.* ***(c)-(d):*** *DFT-adaptive CMD simulated images of the experimentaly observed moiré patterns.*

Considering the equilibrium interatomic distances of bulk Au (0.288 nm) and graphene (0.246 nm), a maximum moiré period of only 1.8 nm can be formed in graphene/Au(111), due to the significant misfit between the two lattice constants. This implies that large moiré periodicities (5.1 nm, 7.7 nm, see Fig. 1) can only be

explained by considerable lattice distortions both in the graphene and in the support layers.

Various moiré patterns found experimentally were successfully reproduced by classical molecular dynamics (CMD) simulations. A new DFT-adaptive interface interaction potential has been developed which proved able to describe adequately the weak van der Waals forces at the graphene/Au(111) interface. CMD simulations reveal that in the case of anomalously large moirés the standard lattice constants do not apply, the crystal lattices are considerably distorted. The misfit is reduced from 12.8 % to 4.2 % and the moiré periodicity increases from 1.8 nm up to 7.8 nm [91].

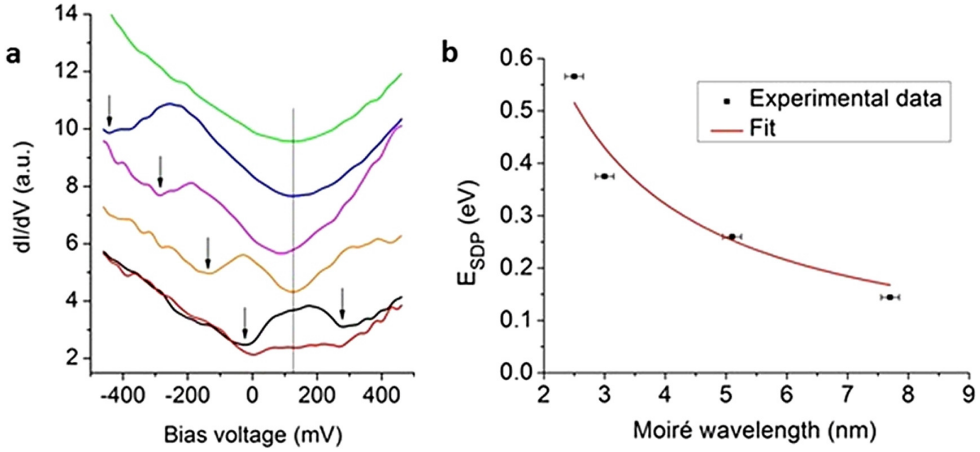

Figure 2 *Local density of states of graphene on Au (111) showing secondary Dirac points.* ***(a):*** *Experimental dI/dV curves for five different moiré wavelengths: 1.9 nm (green), 2.5 nm (blue), 3.0 nm (magenta), 5.1 nm (orange), and 7.7 nm. For this latter, spectra measured on both topographically high (black) and low (red) positions are shown. The secondary dips in the spectra are marked by arrows.* ***(b):*** *Energy of the secondary dips measured from the Dirac point, as a function of moiré wavelength. The black symbols are experimentally measured values, while the red line is the theoretical fit to the data.*

Tunnelling spectra were acquired on the moiré patterned graphene/Au(111) areas. The corresponding dI/dV curves display secondary dips in the LDOS. The energy of these secondary Dirac points depends on the moiré wavelength, as shown in Fig. 2(a,b). The experimentally measured values are in good agreement with the expected theoretical dependence $E_{SDP}=2\pi\hbar v_F/(\sqrt{3}\cdot\lambda_M)$, where λ_M is the moiré wavelength.

A magnetic phase-transition graphene transistor with tunable spin polarization

(ERC StG NanoFab2D, Lendület LP2014-14)

P. Vancsó, I. Hagymási (Wigner FK), and L.Tapasztó

Graphene has emerged as a material with strong potential for both electronic and spintronic applications, however the absence of a band gap in 2D graphene sheets turned the scientific attention towards graphene nanoribbons (GNRs). It has been shown that the semiconducting nature of zigzag nanoribbons (ZGNRs) is related to interaction effects and their oppositely spin polarized edge states. In this work, we propose a novel ZGNR device concept, enabling the control of both charge and spin signals, integrated within the simplest three-terminal device configuration (Fig 1). Our device is based on the strong interplay of the band structure and edge spin configuration in ZGNRs. While in the half-filled system antiferromagnetic (AF) state with oppositely spin-polarized edges is stable, in a doped ZGNR ferromagnetic (FM) state with parallel spin orientation on both edges can become energetically favorable. Therefore, by varying the carrier density of the ribbon a magnetic phase transition between AF and FM state can be achieved which is also an abrupt semiconductor (AF)-metal (FM) transition. This proposed switching mechanism is different as compared with the conventional FET devices, because the applied gate voltage can here dynamically open and close an interaction gap, with only a minor shift of the Fermi level.

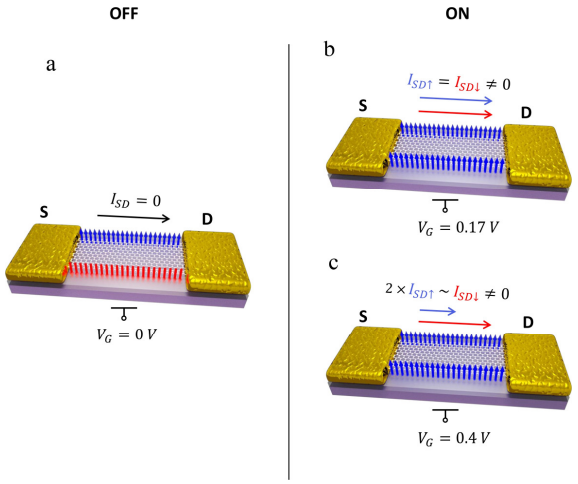

Figure 1 *Schematic representation of the three states of the proposed ZGNR FET.* ***(a):*** *an insulating OFF state with antiparallel spin orientation on opposite ribbon edges in the absence of a gate bias,* ***(b):*** *the conducting ON state characterized by parallel spin orientation on ribbon edges but no net spin polarization of the current induced by an applied gate voltage, and* ***(c):*** *spin polarized ON state achieved by further increasing the gate potential.*

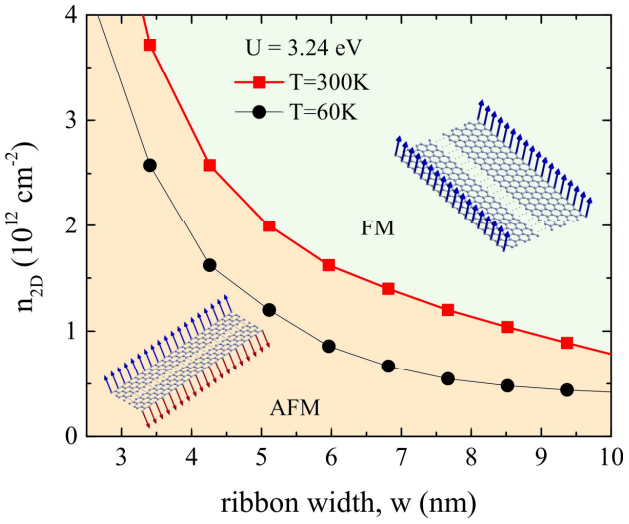

Figure 2 *Phase diagram of ZGNRs as a function of charge carrier concentration (n_{2D}) and ribbon width (w) at two different temperatures (T=60K and T=300K). The AF ground state is the only stable without external doping; however, the FM configuration can become favorable above a critical doping value and ribbon width.*

Our experimentally validated Hubbard model revealed that for realistic ribbon widths the magnetic phase transition occurs in the low doping regime ($n_{2D} \sim 10^{12}$ cm^{-2}) which can be easily accessed experimentally by simple electrostatic gating (Fig 2). We found that gate voltage where the ZGNR transistors can switch is in the range of 0.1-1, depending on the width of the ZGNR and the properties of the gate insulator layer (SiO_2, HfO). To explore the transport characteristics of the proposed novel device we have performed Landauer transport calculations by using the spin dependent Hamiltonian matrix from our Hubbard calculations (Fig 3). We have found that such devices can operate at high speed (S = 71 mv/dec.), while the spin polarization of the current can be tuned between 0 and 50% even at room temperature. The main advantage of our proposed device concept is that we are able to control both charge and spin currents by using a simple gate electrode, which could open new routes for novel data processing techniques.

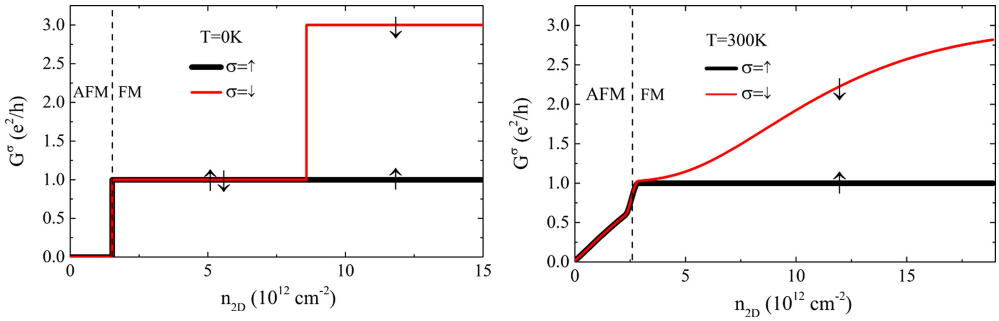

Figure 3 *Spin dependent conductance (G) as a function of charge carrier density (n_{2D}) for a 4.2 nm wide ZGNR at* ***(a):*** *T=0K and* ***(b):*** *T=300K. The AF-FM transition (dashed line) dynamically closes the bandgap of the ribbon switching the transistor into a conducting state. Further increasing the carrier concentration opens additional spin down channels leading to the spin polarization of the current.*

Oxidation of transition metal dichalcogenide monolayers

(Lendület LP2014-14, ERC StG NanoFab2D, Graphene Flagship)

J. Pető, P Vancsó, G. Z. Magda, and L. Tapasztó

The chemical modification of 2D crystals holds the potential of engineering their physical and chemical properties. While graphene oxide is a widely investigated material, much less is known about the oxidation of various transition metal dichalcogenide (TMDC) single layers. This process is of particular importance, as, in contrast to graphene, oxidation of 2D TMDC crystals can spontaneously occur under ambient conditions. Nevertheless, the underlying atomic mechanisms of oxidation process, as well as the atomic-scale structural modifications induced by the oxidation remained so far largely unexplored. Here, we were able to image directly the ambient oxidation process of 2D MoS_2 crystals by Scanning Tunneling Microcopy (STM).

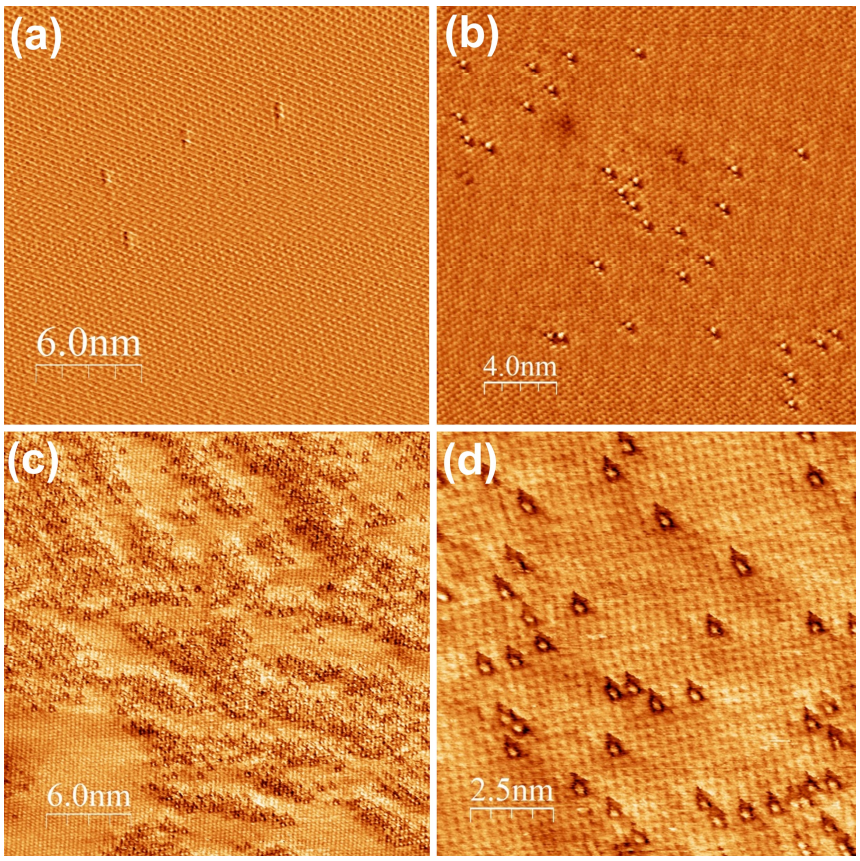

Figure 1 *Atomic resolution STM images of the oxidation process of MoS_2 single layers exposed to ambient conditions.* ***(a):*** *as-prepared,* ***(b):*** *for 1 month and* ***(c):*** *for 1 year.* ***(d):*** *Higher resolution image revealing the substituion of S atoms by oxygen atoms.*

In contrast to graphene, where the oxidation induces a massive amount of structural disorder, we found that the oxidation of 2D MoS_2 proceeds through individual atomic substitutions all over the 2D MoS_2 surface, while fully preserving the crystal lattice. Furthermore, such oxidized MoS_2 single layers can be easily reduced to a perfect MoS_2 lattice by a simple annealing step in H_2S. Such atomically ordered and reversible defect formation mechanism can be exploited in the defect engineering of various physical and chemical properties of 2D MoS_2.
By contrast, a strikingly different oxidation behavior has been identified in $MoSe_2$ single layers, where, under ambient conditions, the surface remains structurally intact even after a year exposure to ambient, while the oxidation proceeds only at the edges.

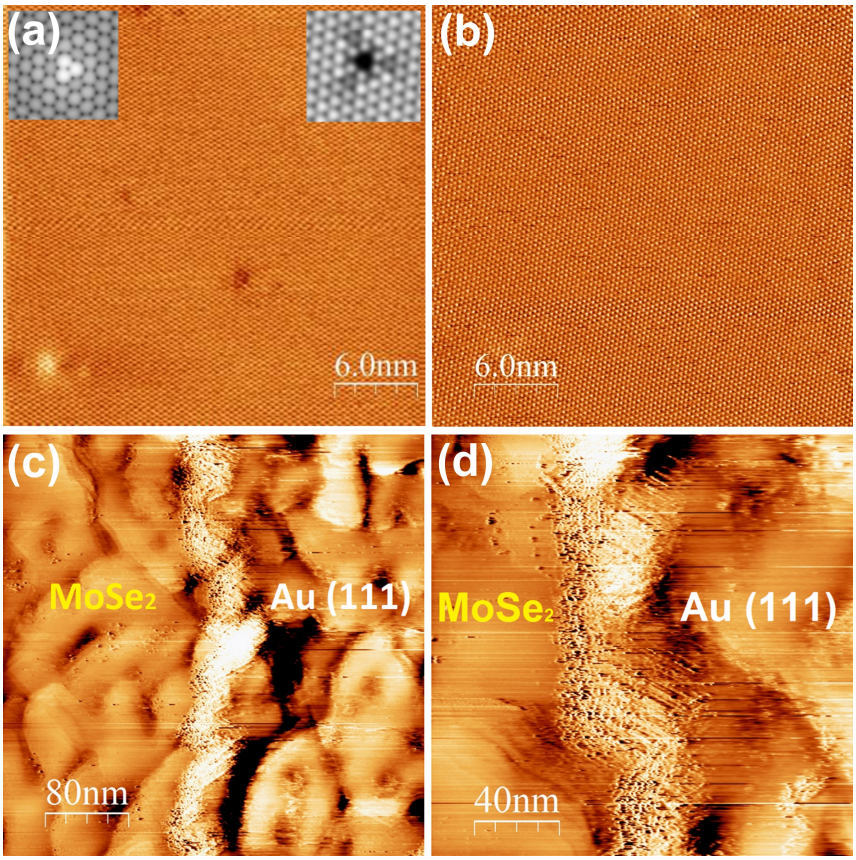

Figure 2 *Atomic resolution STM images of $MoSe_2$ single layers exposed to ambient conditions for 1 year show no sign of oxidation on the surface* ***(a-b)****. By contrast, STM images of $MoSe_2$ edges clearly reveal edge oxidation effects* ***(c-d)****.*

Monitoring the oxidation processes of TMDC single layers at the atomic scale, on one hand enables us to identify materials with increased chemical stability under ambient conditions, on the other hand, it opens the way towards understanding and exploiting the role of defects in various properties of 2D crystals, such as electrical transport, photoluminescence or catalysis.

Determination of the STM tip-graphene repulsive forces by comparative STM and AFM measurements on suspended graphene

(EU FP7 Marie Curie CIG No.334377, János Bolyai Research Scholarship, OTKA K101599, NKFIH TÉT_12_SK-1-2013-0018)

A. Pálinkás, Gy. Molnár, C. Hwang (KRISS, Korea), L. P. Biró, and Z. Osváth

Graphene grown by chemical vapor deposition was transferred on top of flat gold nanoislands and characterized by scanning tunneling microscopy (STM) and atomic force microscopy (AFM). Graphene bubbles were formed with lateral dimensions determined by the size and shape of nanoislands. These graphene bubbles could be squeezed during STM imaging using bias voltages of less than 250 mV and tunneling currents of 1 nA (see Fig. 1). Nanoindentation measurements performed by AFM show that the squeezing of graphene bubbles occurs at repulsive forces of 20 – 35 nN. Comparing the AFM and STM results, this study reveals that mechanical forces of the order of 10^{-8} N occur between the STM tip and graphene under ambient imaging conditions and typical tunneling parameters [88].

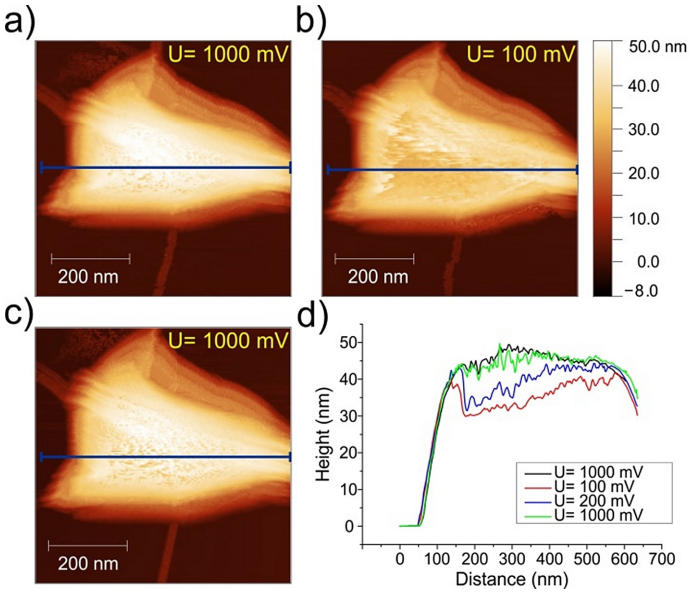

Figure 1 *Series of STM images of a graphene nanobubble measured at bias voltages of* ***(a):*** *U = 1000 mV,* ***(b):*** *U = 100 mV, and* ***(c):*** *U = 1000 mV. Tunneling current: I = 1 nA.* ***(d):*** *Height profiles taken at different bias voltages along the same line section shown with horizontal line in* ***(a-c)****.*

The graphene bubble shown in Fig. 1, formed on the top of a gold nanoisland, is imaged first at U = 1000 mV (Fig. 1(a)). The height profile measured along the line section in Fig. 1(a) is shown in Fig. 1(d) (black line). Decreasing the bias voltage to U = 100 mV we observed that the graphene was pushed against the top of the gold nanoisland (Fig. 1(b)), as shown also by the corresponding height profile in Fig. 1(d) (red line). Somewhat higher graphene z-values were obtained for the same height profile as the bias voltage was increased to U = 200 mV (Fig. 1(d), blue line).

Furthermore, when the bias voltage was increased again to U = 1000 mV, the graphene bubble recovers to the initial shape (Fig. 1(d), green line). The current was kept constant throughout the measurements (I = 1 nA). The results show that by decreasing the bias voltage the repulsive force regime starts to dominate the tip-graphene interaction, and the graphene bubble can be squeezed.
In order to evaluate the mechanical forces acting between STM tip and graphene, AFM measurements were performed in PeakForce® mode on similar graphene nanobubbles. The AFM image of a flat gold nanoisland with graphene bubble on top is shown in Fig. 2(a). This AFM image was obtained by scanning with a very low (F = 1.5 nN) force.

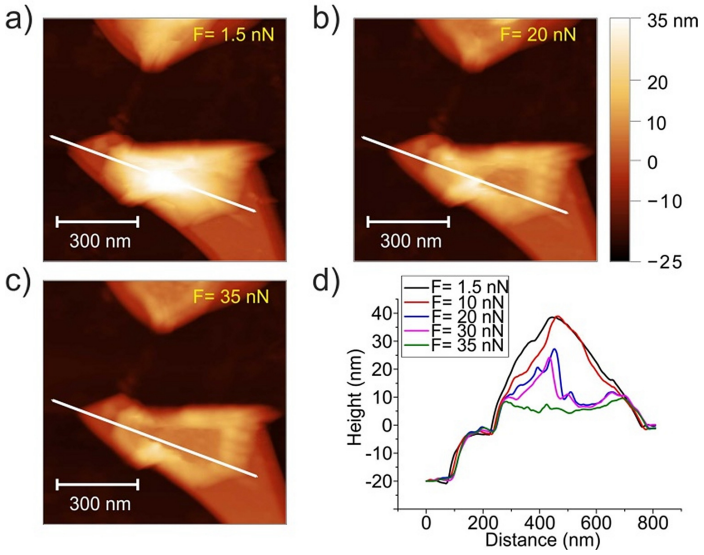

Figure 2 *PeakForce AFM images of a graphene nanobubble measured with compressive forces of* ***(a):*** *F = 1.5 nN,* ***(b):*** *F = 20 nN, and* ***(c):*** *F = 35 nN.* ***(d):*** *Height profiles taken at different forces along the same line section shown in* ***(a-c)*** *(white line).*

The height profile measured along the line section in Fig. 2(a) (white line) shows that the height of the graphene bubble is about two times the height of the gold nanoisland (Fig. 2(d), black solid line). AFM images were registered on the same area using forces up to 40 nN. A complete image was recorded for every force setpoint (F). It was observed that by increasing the scanning force the graphene bubble starts to collapse. This is shown in Fig. 2(b) and Fig. 2(c), which are topographic images measured with forces of 20 nN and 35 nN, respectively. Obviously, the shape of the graphene bubble is altered. Selected height profiles are shown in Fig. 2(d), which were taken along the same line section shown in Fig 2(a) (white line), extracted from the AFM images measured with the corresponding tip-sample force values. The bubble is considered 'squeezed' at F = 35 nN (Fig. 2(d), green line).

Electromagnetic and thermal properties of three-dimensional printed multilayered nano-carbon/poly(lactic) acid structures

(OTKA K101599, Graphene Flagship)

A. Paddubskaya (Minsk), N. Valynets (Minsk), P. Kuzhir (Minsk), K. Batrakov (Minsk), S. Maksimenko (Minsk), R. Kotsilkova (Sofia), H. Velichkova (Sofia), I. Petrova (Sofia), I. Biró (3D Wishes), K. Kertész, G. I. Márk, Z. E. Horváth, and L. P. Biró

Microwave is the ultimate range for open space communication. However, the drastic growth of the satellite data transmission in the past decade makes spectral bands allocated to different communication channels overcrowded. Along with the ever-increasing density of emitters in the environment, this jam makes the electromagnetic (EM) compatibility an important issue. In other words, any new equipment must have adequate immunity in order to function consistently and reliably, be resilient to major disturbances, and coexist with other equipment. The electromagnetic interference (EMI) shielding effectiveness (SE) is determined by material absorptivity, surface reflectivity, and multiple internal reflections. For a continuous metal sheet, the latter mechanism is negligible, not to mention the weight of metals, which may be prohibitive for space applications.

The EMI SE of a composite material mainly depends on the filler's intrinsic conductivity, dielectric constant, and aspect ratio. Nano-carbon fillers, such as graphene nanoplatelets and carbon nanotubes, are indeed interesting materials from the point of view of electromagnetic shielding. Though graphene/polymer heterostructures have several advantages in comparison with conventional metal shielding layers, such as its light weight, resistance to corrosion, and flexible absorption mechanism of shielding, their fabrication process is quite difficult because of the graphene transfer stage.

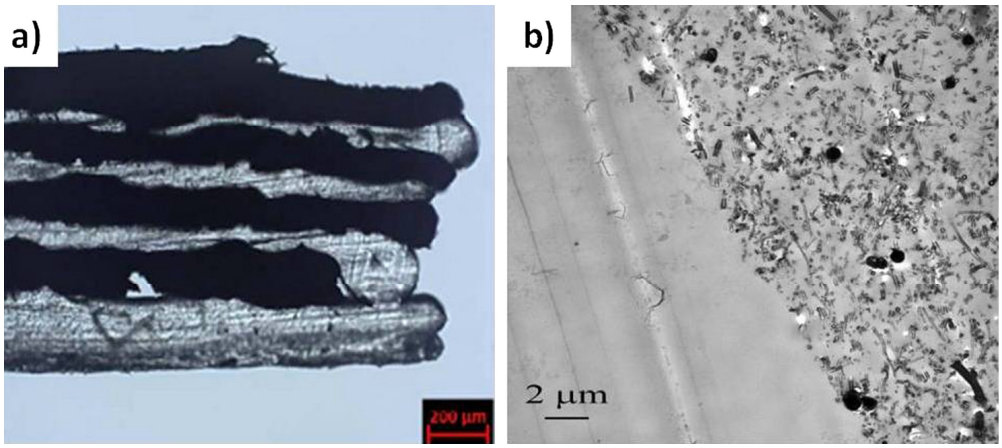

Figure 1 ***(a):*** *Optical image of the cross section of 3D printed multilayered sample with 4 nano-carbon layers (black stabs), and* ***(b):*** *X-TEM image of the PLA/nano-carbon doped interface.*

In this study, our goal was to design a new type of light material having tunable electromagnetic absorption properties, by 3D printing of photonic type band gap structures by layer by layer deposition of nano-carbon doped polymer layers and pure (dielectric) polymer layers, Fig. 1. The source material for the nano-carbon layer is a commercial nanocomposite filament, named 3D Black Magic (3DBM), consisting of a nano-carbon filler incorporated in a polylactic acid (PLA) polymer, while the pure polymer layer is printed from a pure PLA filament.
The results demonstrate, Fig. 2, the potential of the 3D printing technique for producing multilayered structures by layer by layer deposition. The sandwich structure composed of continuous nano-carbon doped polymer layers and pristine polymer layers, the mixed nano-carbon filler consisting of graphene, short carbon nanotubes, and graphene sheet-like structures obviously determines both the microwave and the thermal properties of the complex material.

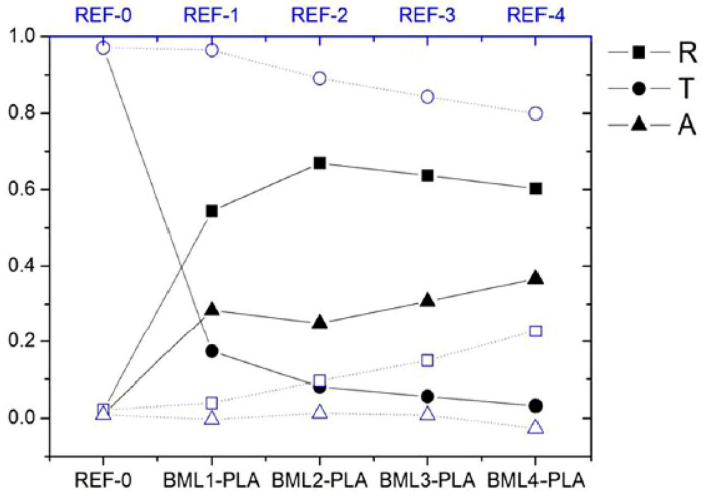

Figure 2 *Reflectance, absorbance, and transmittance reconstructed from the experimental data of reference samples (open symbols) and samples contacting 1–4 nano-carbon layers (solid symbols) at 30 GHz.*

The electromagnetic measurements promise a great potential of such a type of materials for electromagnetic compatibility applications in microwave frequency range. Sandwich structures containing only two nano-carbon layers already become nontransparent to microwaves, giving EMI SE at the level of 8–15 dB, and the contribution of absorption of the plane stratified sandwich structure is quite significant (30%–40%). In case of upgrading the structure with proper anti-reflection geometry – inspired from our work on biological photonic nanoarchitectures – we may obtain the same zero transmission originated from the full absorption of EM radiation.

Pretreated butterfly wings for tuning of selective vapor sensing

(OTKA K 111741, OTKA K 115724)

G. Piszter, K. Kertész, Zs. Bálint, and L. P. Biró

Photonic nanoarchitectures occurring in the scales of the blue butterflies are responsible for their vivid blue wing coloration. These nanoarchitectures contain quasi-ordered nanocomposites which are constituted from a chitin matrix with embedded air holes. Therefore, they can act as chemically selective sensors due to their color change when mixing volatile vapors in the surrounding atmosphere, which condensate into the nanostructure through capillary condensation. The condensed vapors can alter the refractive index contrast in the nanoarchitecture which results in the color change of the wings.
Using a home-built vapor mixing setup the spectral changes caused by the different air + vapor mixtures were efficiently characterized. It was found recently that the spectral shift is vapor specific and proportional with the vapor concentration.

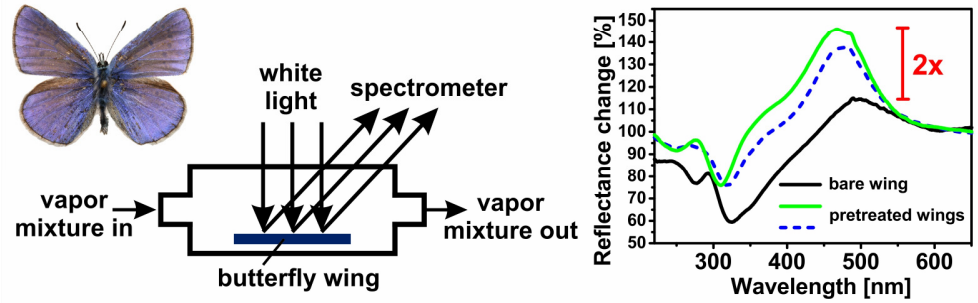

Figure 1 *The wings of Polyommatus icarus males are suitable for optical vapor sensing. The image shows a blue male specimen, the schematics of the vapor sensing cell, and the typical optical response of the bare and pretreated butterfly wings during vapor exposition. In the latter case the optical reference (100%) was the pristine butterfly wing in artificial air atmosphere. The two colored curves show the optical response of two ethanol pretreated wings.*

Both the chemical selectivity and the sensitivity could be improved if arrays of sensitized butterfly wings would be used. Therefore, P. icarus butterfly wings were pretreated in liquid ethanol for 14 days to modify the surface of the photonic nanoarchitecture. After the complete drying, the standard vapor sensing measurements, using seven volatiles, were carried out to investigate differences in chemical selectivity and sensitivity of the modified wings.
Optical response of ethanol pretreated samples can be seen in Fig. 1. During the vapor exposition the optical response (color change) of the wing can be measured using the initial color (wing in artificial air) as a reference. One can see in Fig. 1 that the maximal intensity of the optical response curves is more than doubled when butterfly wings were pretreated in liquid ethanol for two weeks as compared to bare wings. This enhanced vapor sensing is reproducible, too: two wings of the same specimen

were pretreated under the same conditions and after the measurements the significant spectral enhancement of both wings was observed.

The chemical selectivity of the bare and ethanol pretreated samples was analyzed using principal component analysis (PCA). In Fig. 2 the PCA results of the bare (A) and ethanol pretreated (B) samples can be seen. Both samples show similar chemical selective behavior as every vapor has individual trajectory in the graphs. The PCA score plot of the untreated and ethanol pretreated wings are compared in the low concentration range (C), too, where spread of the vapor sensing trajectories was significantly larger in case of the ethanol pretreated sample, showing the higher chemical selectivity in that concentration range.

These results show the way how to tune the chemically selective optical response of the photonic nanoarchitectures by modification of their surface.

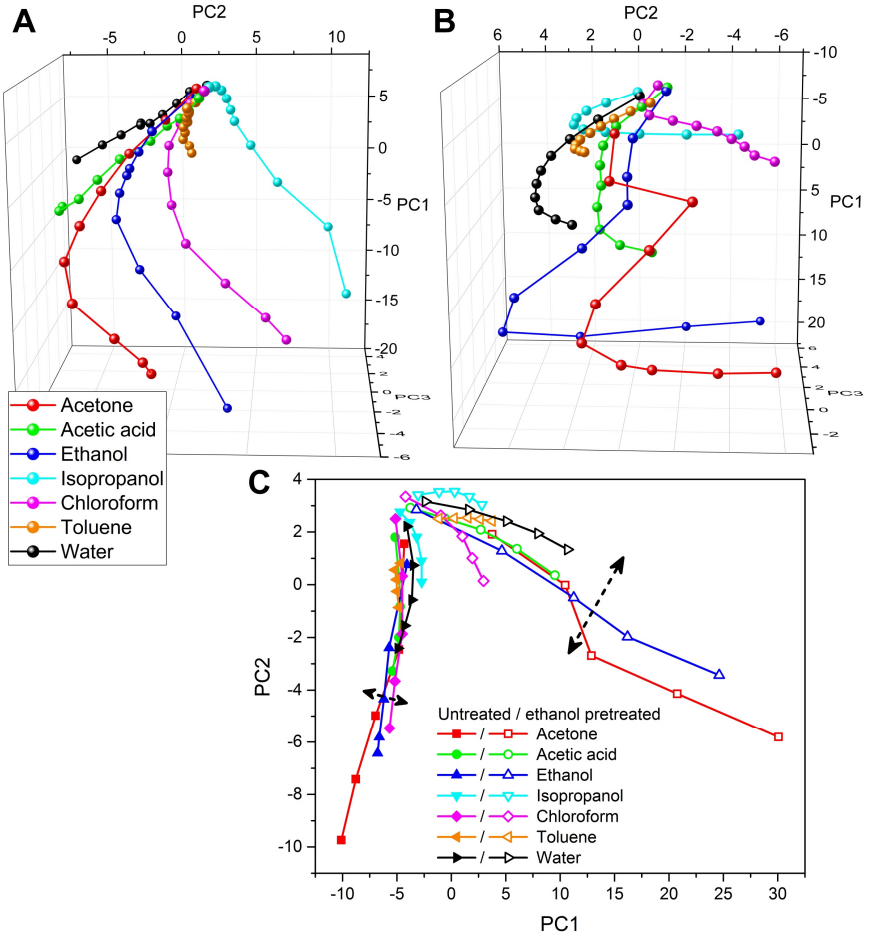

Figure 2 *PCA score plots of* ***(A)****: the untreated and* ***(B)****: the 14 day ethanol pretreated Polyommatus icarus wings when used as a sensor material. The vapor concentration increases from the top to the bottom (to saturated vapors) in both graphs.* ***(C):*** *The low-concentration (<50%) behavior was investigated in more detail using PCA, too.*

Photonics Department

Head: Miklós FRIED, D.Sc., scientific advisor

Research Staff

- Péter PETRIK, D.Sc., Head of Ellipsometry Laboratory
- András DEÁK, Ph.D., Head of Chemical Nanostructures Laboratory
- Emil AGÓCS, Ph.D., (on leave)
- Antal GASPARICS, Ph.D.
- András HÁMORI, dr. univ.
- Csaba S. DARÓCZI, dr. univ.
- György JUHÁSZ, dr. univ.
- György KÁDÁR, D.Sc.
- Tivadar LOHNER, D.Sc.
- Norbert NAGY, Ph.D.
- Judit NÁDOR, Ph.D.
- Ferenc RIESZ, C.Sc.
- Miklós SERÉNYI, D.Sc.
- Gábor VÉRTESY, D.Sc.
- Dániel ZÁMBÓ, Ph.D.

Ph.D. students

- Bálint FODOR, Ph.D. student (on leave)
- Szilárd POTHORSZKY, Ph.D. student
- Benjamin KALAS, Ph.D. student

Diploma workers

- Dániel SZEKRÉNYES, M.Sc. student
- László BICSÉRDY, M.Sc. student
- Enikő TRAPLY, M.Sc. student
- Bálint ÉLES, B.Sc. student
- Enikő MOLNÁR, B.Sc. student
- Alex SZENDREI, B.Sc. student
- Alekszej ROMANENKO, M.Sc. student
- Olívia KOZÁK, B.Sc. student

Technical Staff

- Tímea CSÁNYI

MFA Photonics Department was involved in several EU and domestic projects. A recently developed nondestructive material testing method called Magnetic Adaptive Testing (MAT), which is based on systematic measurement of minor magnetic hysteresis loops, was applied to detect local wall thinning in ferromagnetic plates. It was shown that even a relatively small, local variation in the sample thickness could be detected with an adequate signal/noise ratio from the far side of the specimen. The measurements also gave good results when the investigated plate was covered by other plate(s).

In a continuing cooperation with the GREMAN laboratory of the University of Tours, we characterized columnar meso-Porous Si (PSi) thin films and dense nanowire carpets (SiNW) by spectroscopic ellipsometry (SE) in the visible-near-infrared wavelength range. Isotropic, in-depth graded, anisotropic and hybrid effective medium approximation-based (EMA) models were investigated. At low current densities (< 100 mA/cm^2) in-depth inhomogeneity shows a feature in the SE spectra that is stronger than anisotropy. At high current densities (> 100 mA/cm^2), however,

this behavior turns around, and anisotropy becomes the dominant feature of the PSi-spectra. SiNW evaluations revealed that the layers are highly anisotropic as well, but derived prolate spheroid aspect ratios showed that the best ordered orientation is obtained for the sample formed of ≈1 μm nanowires. For the thicker layers, the long nanowires start to collapse into bundled states, decreasing the anisotropy.
In cooperation with the Fuel and Reactor Materials Laboratory and the Thin Films Physics Laboratory we characterized Zr tubes for nuclear fuel cladding, with special emphasis on the optical properties. We have shown that ellipsometry with focusing can routinely be used to measure thin layers and surface properties on Zr tubes with a diameter as small as 9.1 mm. Temporal behavior of the oxide thickness has been measured for oxidation temperatures of 600 °C and 800 °C.
We used low-molecular weight polyethylene glycol (PEG) to trigger the clustering of gold nanoparticles through the control of colloidal interactions. The clustering is attributed to the delicate interplay between the high ionic strength and elevated temperature and is explained in terms of chain collapse of the surface-grafted PEG molecules.
By partial masking of the particles (polymer layers deposited by spin-coating technique) gold/silica Janus particles were successfully fabricated and investigated by single-particle spectroscopy. On those gold/silica particles we have examined whether the change of the extent of coverage appears in the single-particle spectra and we have taken correlative SEM snapshots. In the range of 33% and 50% coverage 5-7 nm differences have been found in the position of the scattering maxima.
We are involved in 2 EU-projects („SEA4KET" and ENIAC-2012-2 "E450DL") to develop "Imaging Optical Inspection Device With A Pinhole Camera". We developed 30, 45-60 and 60-90 cm wide prototypes. As a demonstration, thin oxide film covered, NiSi covered and Plasma Immersion Ion Implanted Si-wafers were measured on the robotic arm in clean room environment.

Simulation of magnetic flux distribution during measurement of local thinning of ferromagnetic plates

(OTKA K 111662)

G. Vértesy, Cs. S. Daróczi, and A. Gasparics

For pipes used in industry, e.g. in chemical and power plants, wall thinning is one of the most serious defects. The detection and the evaluation of the thickness reduction of pipes are very important issues for the prediction of lifetime of the pipes in order to avoid severe accidents. There is a special concern on the local wall thinning at locations under an enforcement shield that covers outside of the pipe, where a branch pipe is connected to the main one. Because the enforcement shield and the pipe wall form two layers of metal, it is difficult to inspect inside of the pipe under the enforcement shield by currently used commercial methods. A recently developed

nondestructive method called Magnetic Adaptive Testing (MAT), which is based on systematic measurement of minor magnetic hysteresis loops, was applied for detection of local wall thinning in ferromagnetic plates. It was shown that even a relatively small, local modification of the sample thickness could be detected with adequate signal/noise ratio from the other side of the specimen. The measurements gave sufficient results also, if the investigated plate was covered by other plate(s) [NDT&E International, 47 (2012) pp.51-55.],[E-Journal of Advanced Maintenance, Vol. 4, No. 2. (2012) pp.96-104].

The efficiency of MAT measurement can be improved by the proper choice of the measurement conditions. In cooperation with the co-workers of Budapest University of Technology and Economics (Department of Broadband Infocommunications and Electromagnetic Theory), the magnetic flux distribution was simulated. A system of three ferromagnetic plates was used for simulation, the bottom plates having an artificial slot in the bottom (One quarter of the system is illustrated in Fig. 1, if the magnetizing yoke is over the centre of the slot). Magnetization of the plates was performed by an attached magnetized yoke on the top of plates. The change of the magnetic flux was calculated in the cross section (blue area) of the magnetizing yoke, as indicated in Fig. 1.

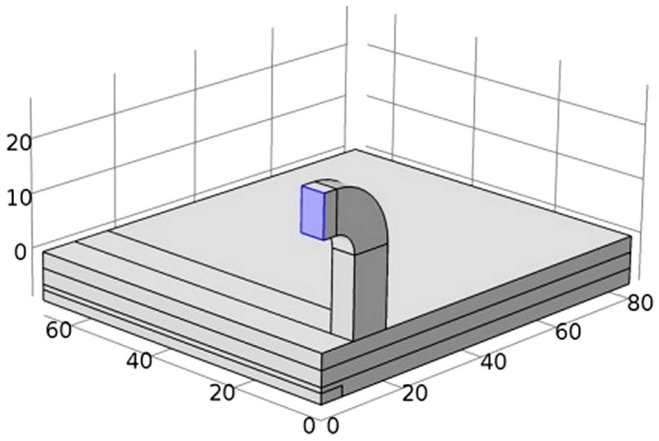

Figure 1 *The magnetizing yoke over the system of three iron plates (with 180x170x3 mm dimensions), the bottom has the artificial slot (with 170x10x2 mm dimensions).*

The magnetic flux was calculated according to the $\Psi = \int_A B * da$ expression, where "A" is the surface, indicated by blue color in Fig. 1. The influence of air gap was also taken into account, between the yoke and the surface, and also between the plates.

As an illustration, it is shown in Fig. 2, how the magnetic flux changes due to the presence of a 2 mm deep, 10 mm wide slot in the bottom layer if the distance between the yoke legs (size of the yoke) and air gap is modified.

Similar calculations were carried out also for 5 and 15 mm wide slots. Fig. 3 shows the result of a calculation, where the influence of the slots on the magnetic flux is

directly calculated. (In this case 50 μm airgap was supposed.) The influence of the size of the magnetizing yoke on the flux change is clearly seen. It is worth of mentioning as well, that the position of the maximal flux change depends on the size of magnetizing yoke, too. It turned out also (not shown here), that if air gap is increased, the position of the maximal flux change is significantly shifted towards larger size magnetizing yoke.

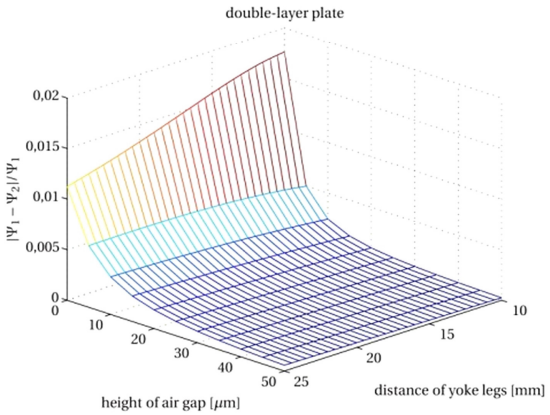

Figure 2 *The modification of the magnetic flux due to the slot in the case of double layer configuration at the cross section of the magnetizing coil, positioned over the slot as a function of air gaps and as a function of the distance between yoke legs..*

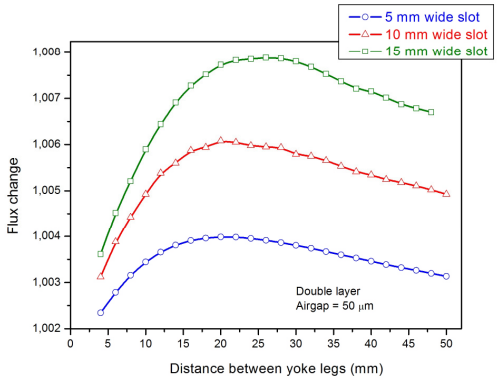

Figure 3 *The modification of the magnetic flux due to the slot in the case of double layer configuration at the cross section of the magnetizing coil, positioned over the slot as a function of air gaps and as a function of the distance between yoke legs..*

The above presented results help to optimize the parameters of the actual experimental arrangement for solving a given task.

Spectroellipsometric detection of silicon substrate damage caused by radiofrequency sputtering of niobium oxide

(OTKA K115852, M-ERA.NET "Watersafe")

T. Lohner, M. Serényi, E. Szilágyi, Zs. Zolnai, Zs. Czigány, N. Q. Khánh, P. Petrik, and M. Fried

Substrate surface damage induced by deposition of metal atoms by radiofrequency (rf) sputtering or ion beam sputtering onto single-crystalline silicon (c-Si) surface has been characterized earlier by electrical measurements. The question arises whether it is possible to characterize surface damage using spectroscopic ellipsometry (SE). In our experiments niobium oxide layers were deposited by rf sputtering on c-Si substrates in gas mixture of oxygen and argon. Multiple angle of incidence spectroscopic ellipsometry measurements were performed, multilayer optical models (niobium oxide layer, native silicon oxide layer and ion implantation-amorphized silicon (i-a-Si) layer) on a c-Si substrate were created in order to evaluate the spectra. The evaluations (fitting the layer thicknesses) yielded thicknesses of several nm for the i-a-Si layer. Better agreement could be achieved between the measured and the generated spectra by inserting a mixed layer with components of c-Si and i-a-Si applying the effective medium approximation (EMA, fitting the layer thicknesses and compositions) between the silicon oxide layer and the c-Si substrate.
In cooperation with Wigner Research Centre for Physics high depth resolution Rutherford backscattering (RBS) measurements were performed to investigate the interface disorder between the deposited niobium oxide layer and the c-Si substrate. High resolution cross-sectional transmission electron microscopy (HRTEM) investigation was applied to visualize the details of the damaged subsurface region of the substrate (see Fig. 1).

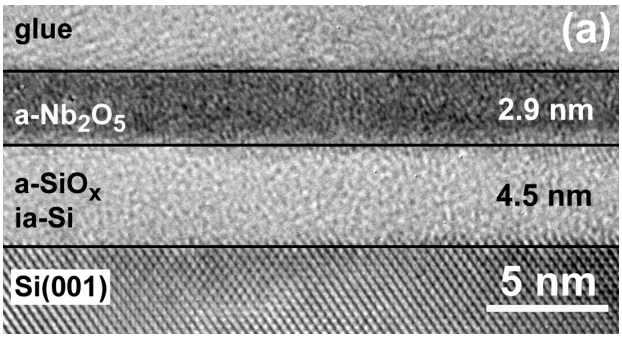

Nb-oxide layer, 2.88 nm

Silicon dioxide layer, 2.80 nm

EMA layer, 4.75 nm
(74% c-Si + 26% i-a-Si)

Single crystalline Si substrate

Figure 1 (a): *Cross sectional HRTEM image of a Nb-oxide sample rf deposited for 100 s (2.0 kV wall potential). The thicknesses of the amorphous layers are indicated in the image. On the right: The three-layer optical model constructed on basis of the results of the RBS and HRTEM measurement for the evaluation of the measured spectroellipsometric data. The values are from the SE evaluations.*

Sputtering at higher wall potential results in higher thickness of the mixed layer with i-a-Si and c-Si components in the damaged subsurface region. During the rf sputtering the energetic oxygen and argon ions and neutral atoms may penetrate into the c-Si substrate to a depth of several nm causing displacement of host silicon atoms and consequently producing damaged regions.

Makyoh topography

F. Riesz

Within the project KMR_12-1-2012-0226, in collaboration with Mirrotron Ltd and the Wigner Research Centre for Physics, the surface flatness of large-area (57 mm × 175 mm) polished Ni(P)-coated Al blocks were characterized for next-generation neutron guide applications. Using highly overlapping sub-aperture measurements with sample translation, it was concluded that the overall flatness of the samples is smaller than the measurement error, that is, it is below 0.5 µm (discounting some edge effects). The error margin was also confirmed by elementary calculations. In addition, a featureless and smooth surface morphology was confirmed. Fig. 1 shows the purpose-built sample positioning/translation stage.

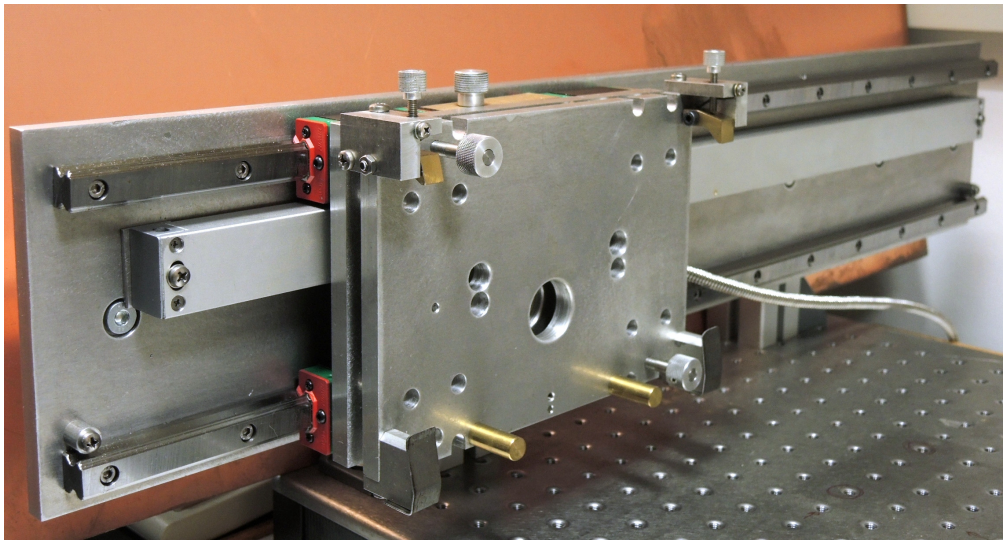

Figure 1 *Sample positioning stage for flatness characterisation of large-areas samples.*

The surface shape and morphology of hot-wall VPE SiC/Si heterostructures grown at IMEM–CNR, Parma, have been characterized with Makyoh topography in order to study the effects of the addition of methyl trichloro silane. Low amount of sample bow was obtained in an optimized growth process.

Grating coupled optical waveguide interferometry combined with in situ spectroscopic ellipsometry

(OTKA K115852, H2020-SMEINST-2-2014-683541, M-ERA.NET "Watersafe", FP7 ENIAC "E450EDL", "SEA4KET")

E. Agócs, P. Kozma, J. Nádor, A. Hámori, M. Janosov, B. Kalas, S. Kurunczi, B. Fodor, E. Ehrentreich-Förster, M. Fried, R. Horváth, and P. Petrik

Two surface-sensitive label-free optical methods, grating coupled interferometry (GCI) and spectroscopic ellipsometry (SE) were integrated into a single instrument. The new tool combines the high sensitivity of GCI with the spectroscopic capabilities of SE. This approach allows quantification with complex optical models supported by SE and accurate measurements with the evanescent field of GCI. A flow cell was developed to perform combined and simultaneous investigations on the same sensor area in liquid (or gas) environments. The capabilities of the instrument were demonstrated in simple refractometry and protein adsorption experiments.

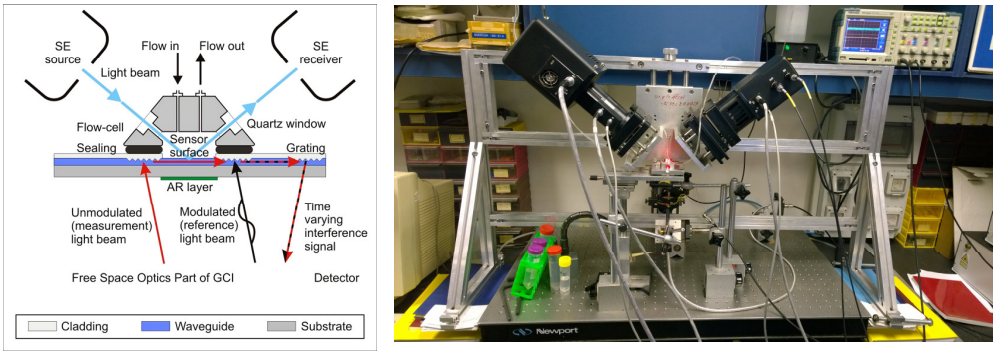

Figure 1 *Schematic representation of the configuration and the working principle of the combined GCI-SE setup.*

In the first experiment, Milli-Q water and glycerol solutions were applied in order to demonstrate the simultaneous measurement capabilities and to check the limit of refractive index detection of the two system components. The uncertainty of the refractive index determination was 9×10^{-7} and 4.8×10^{-5} for GCI and SE, respectively (Fig. 2 left).

In the second experiment, fibrinogen surface adsorption was monitored by means of the combined sensor tool in order to demonstrate its capabilities in biological experiments, as well. The phase shift measured by GCI informed us about the changing of the sensing area with high sensitivity. Exploiting the capabilities of SE for a more complex evaluation, the surface mass density of the fibrinogen layer was determined by analyzing the ellipsometric spectra, and it was found to be approximately 0.4 ng/mm^2 at the end of the adsorption process (Fig. 2 right).

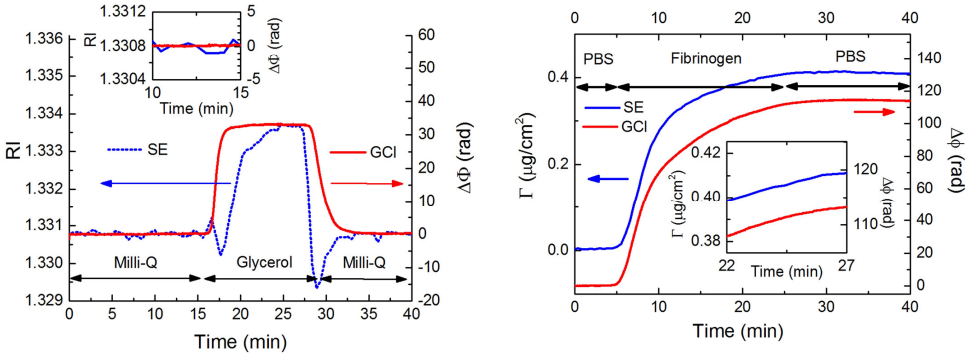

Figure 2 *Simultaneous GCI and SE refractometric measurements for the estimation of LOD values of the combined configuration (left) and for the investigation of the fibrinogen surface adsorption (right).*

Performance analysis of plasmon-enhanced ellipsometry for protein adsorption measurements

(OTKA K115852 and M-ERA.NET "WaterSafe", TÉT_12_DE-1-2013-0002)

B. Kalas, J. Nádor, E. Agócs, A. Saftics, S. Kurunczi, R. Horváth, M. Fried and P. Petrik

We studied gold nanolayers with six different thicknesses (5, 10, 20, 30, 40 and 50 nm), and the adsorption of protein nanolayers on these gold surfaces by *in situ* ellipsometry. The gold nanolayers were evaporated onto BK7 glass substrates with a 2-nm CrO_2 interface layer to enhance the adhesion of the gold to the glass.

We acquired the optical properties of the structures by a Woollam M-2000DI rotating compensator ellipsometer. During the *in situ* investigation we used a laboratory-built semi-cylindrical Kretschmann-Raether flow cell. By measuring the interface through the substrate we were able to exploit the surface plasmon resonance (SPR) phenomenon in order to increase the sensitivity (40 pg/mm^2) of the measurement.

This instrument has numerous advantages compared to our former constructions (using standard flow cell arrangement). For example, the signal to noise ratio is better and the probability of the appearance of a bubble in the flow cell is much lower. This makes the measurement faster and more stable. We used fibrinogen as a model protein to study the adsorption to the various gold surfaces.

In contrast to traditional SPR-devices the ellipsometer provides phase information of the reflected light, so we acquired more information that enabled us to increase the sensitivity by two orders of magnitude compared to the case of having only amplitude information. The other advantage was that we could choose the SPR-angle very

precisely (within 0.1 degree) and we used a broad wavelength range from 400 nm to 1690 nm. Using a spectroscopic ellipsometer gave us the opportunity to build a complex optical model and use it to determine optical properties and thicknesses of multi-layer structures simultaneously and quantitatively (Fig. 1). (The results are accepted for publication in the journal of Applied Surface Science.)

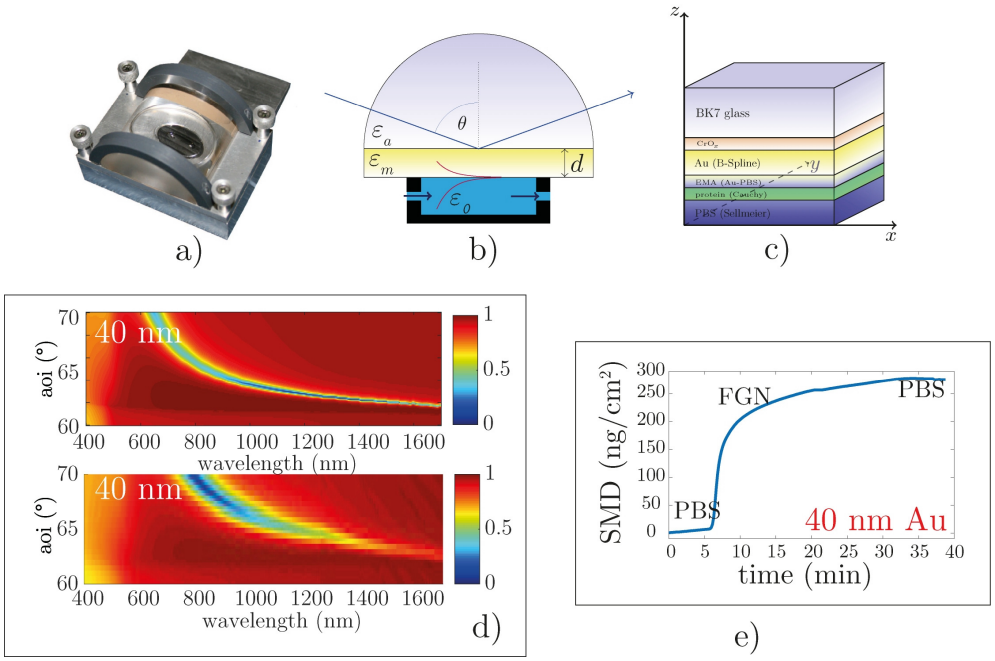

Figure 1 ***a)****: Photo of the SPR flow cell designed in the Photonics Laboratory,* ***b)****: schematic figure of the flow cell,* ***c)****: structure modelled to investigate the adsorption process,* ***d)****: the modelled (top) and the measured (bottom) tan(ψ) maps and* ***e)****: surface mass density of the adsorbed protein as a function of time.*

Optical characterization of columnar porous Si thin films and Si nanowires exhibiting large structural anisotropies

(OTKA K115852, H2020-SMEINST-2-2014-683541, FP7 E450EDL, SEA4KET, TÉT_14_FR-1-2015-0041, CampusFrance Balaton PHC)

B. Fodor; T. Defforge; E. Agócs; M. Fried; G. Gautier; and P. Petrik

In a continuing cooperation with the GREMAN laboratory of the University of Tours, we characterized columnar mesoporous Si thin films (PSi) and dense nanowire (SiNW) carpets by spectroscopic ellipsometry in the visible-near-infrared wavelength range. Porous Si layers were formed by electrochemical etching while structural

anisotropy was controlled by the applied current. Layers of highly oriented SiNWs, with length up to 4.1 µm were synthesized by metal-assisted chemical etching. Ellipsometric spectra were fitted with different multi-layered models, based on effective medium approximation (EMA). Isotropic, in-depth graded, anisotropic and hybrid EMA models were investigated with the help of the root mean square errors obtained from the fits. In the case of PSi, characterization revealed that, at low current densities (< 100 mA/cm^2), in-depth inhomogeneity shows a more important feature in the ellipsometric spectra than anisotropy. On the other hand, at high current densities (> 100 mA/cm^2) this behavior turns around, and anisotropy becomes the dominant feature of the spectra. SiNW evaluations revealed that the layers are also highly anisotropic, but derived prolate spheroid aspect ratios showed that the best ordered orientation is obtained in samples formed of ≈1 µm nanowires. For the thicker layers, the long nanowires start to collapse into bundled states, decreasing the anisotropy.

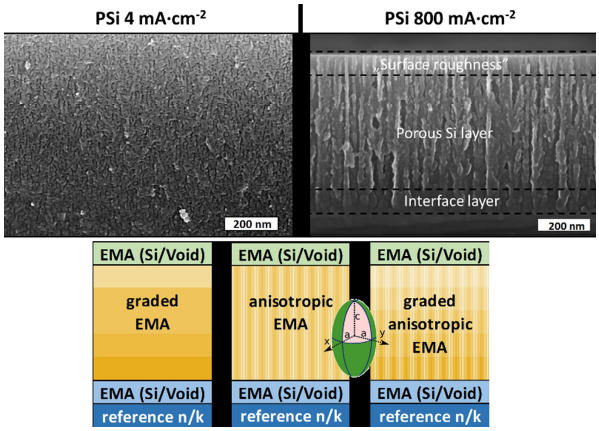

Figure 1 *Cross-sectional SEM images (top left) of a porous Si sample prepared by small current density showing a dendritic structure and of a sample prepared by large current density revealing a highly columnar structure (top right) and the three EMA-based model-structures (bottom) tested for all the PSi layers. The optical response of the dendritic structures shows an isotropic while the columnar structures show an anisotropic behaviour.*

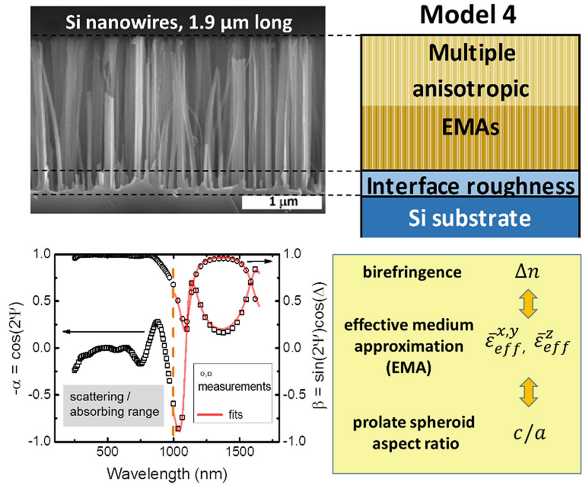

Figure 2 *Cross-sectional SEM image of one of the SiNWs (top left). EMA based model-structure (top right). Corresponding α and β measured and fitted ellipso-metric values at an AOI of 65° (bottom left). With the help of the anisotropic EMA models (Model 2, 3 and 4), we can fit the birefringence and the dichroism of the anisotropic structures and also derive an average ellipticity for either the pores of the PSi or for the NWs.*

Optical properties of Zr and ZrO_2

(OTKA K115852, MTA EK Grant, M-ERA.NET "Watersafe")

P. Petrik; A. Sulyok; T. Novotny, E. Perez-Feró, B. Kalas, E. Agócs, T. Lohner, M. Menyhárd, and Z. Hózer

In cooperation with the Fuel and Reactor Materials Laboratory and the Thin Films Physics Laboratory we characterized Zr tubes for nuclear fuel cladding, with special emphasis on the optical properties. We have shown that ellipsometry with focusing can routinely be used to measure thin layers and surface properties on Zr tubes with a diameter as small as 9.1 mm (see Fig. 1). Multi-sample and depth profiling models have been used to determine reference dielectric function spectra for both the Zr substrate and its oxide. Temporal behavior of the oxide thickness has been measured for oxidation temperatures of 600 °C and 800 °C. A vertical inhomogeneity of the oxide properties has been found by the optical measurements as well as by depth-profiling X-ray photoelectron spectroscopy investigations that revealed the formation of sub-oxides at the interface region of Zr and its surface oxide.

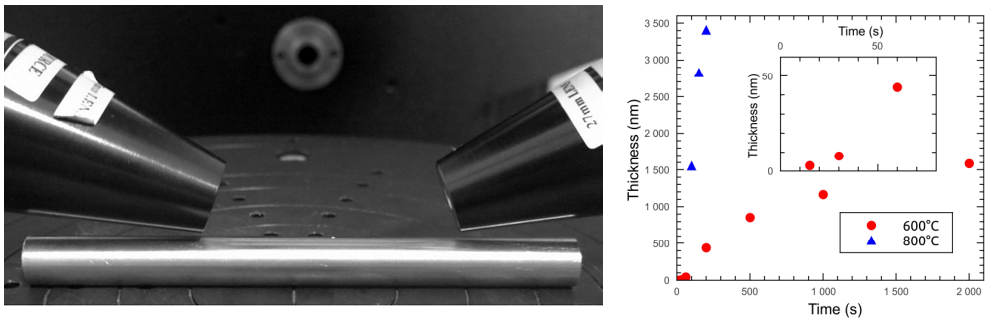

***Figure 1 (a)**: Ellipsometric measurement with focusing on a 9.1-mm diameter Zr tube for nuclear cladding. **(b)**: Thickness of oxides created at temperatures of 600 °C and 800 °C. The inset shows the behavior at small oxidation times.*

Development of optical metrology tool for in-line qualification of thin films on large area

(EU FP7 SEA4KET, ENIAC E450EDL)

Cs. Major, Gy. Juhász, P. Petrik, and M. Fried

We are involved in 2 EU-projects („SEA4KET" and the ENIAC-2012-2 "E450DL") to develop "Imaging Optical Inspection Device With A Pinhole Camera". We developed 30, 45-60 and 60-90 cm wide prototypes for mapping the optical properties of thin films of big area samples.

Figure 1 *We successfully installed our optical mapping device in the clean-room of IISB (Erlangen, Germany). A 300 mm diameter wafer can be seen on the robotic arm (left side).*

NiSi thin film covered and Plasma Immersion Ion Implanted 300 mm diameter Si-wafers were measured on the robotic arm in clean room environment. We determined the thickness maps on these big wafers.

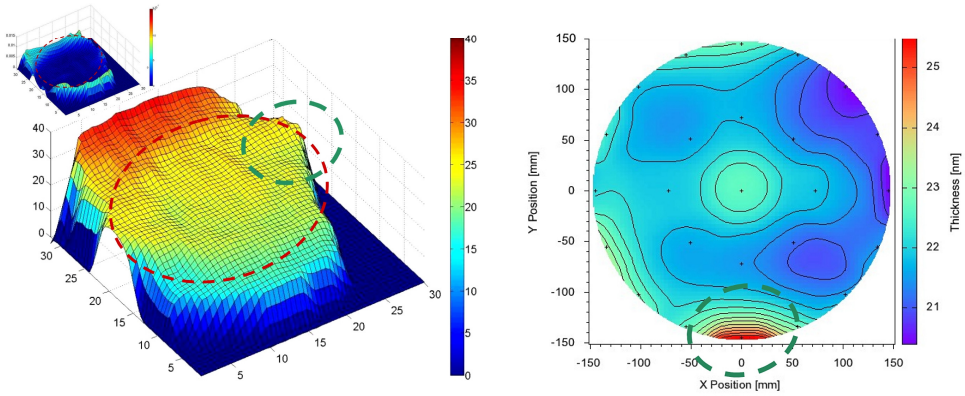

Figure 2 *Thickness-map of a NiSi covered 300 mm diam. Si-wafer (complete annealing at 350 °C) and control measurement by a SEMILAB-SOPRA SE (right). The big dashed curve shows the edge of the sample (from the inserted MSE-map, upper-left), the small dashed curves show the maximum place.*

Aggregation kinetics and cluster structure of amino-PEG covered gold nanoparticles

(OTKA K112114, PD105173 and FP7 No.310250)

D. Zámbó, Sz. Pothorszky, D. F. Brougham, and A. Deák

In this study, controlled clustering kinetics is demonstrated for PEG (polyethylene glycol) grafted gold nanoparticles, in response to applied environmental stimuli; the temperature and ionic strength of the medium (Fig. 1). It is also found that the rate of assembly determines the structure of the prepared nanoparticle clusters (NPCs). After the system is brought out of equilibrium, time-dependent extinction and dynamic light scattering data are used to follow the evolution of nanoparticle cluster formation in real time. The results show that the rate of assembly increases with increasing ionic strength or temperature of the medium. As a result, the nanoparticle cluster size scales with ionic strength and temperature, over a cluster size range from a few particle sizes up to the micron-scale. It is found that, even at the lowest ionic strength, the electric double layer repulsion is eliminated; hence the observed differences in kinetics and in cluster structure arise from modulation of the repulsive steric interactions between nanoparticles.

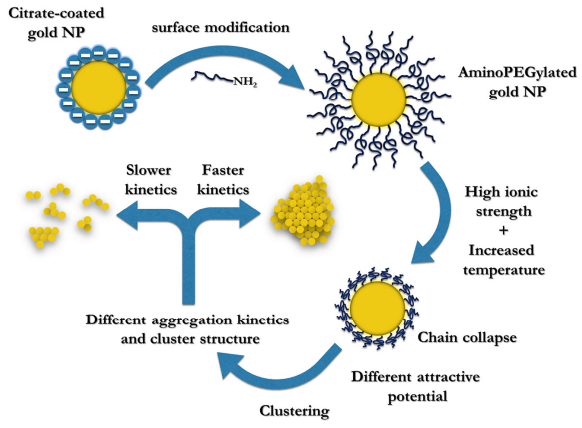

Figure 1 *Schematic representation of self-assembly of aminoPEGylated gold nanoparticles into different nanoparticle structures.*

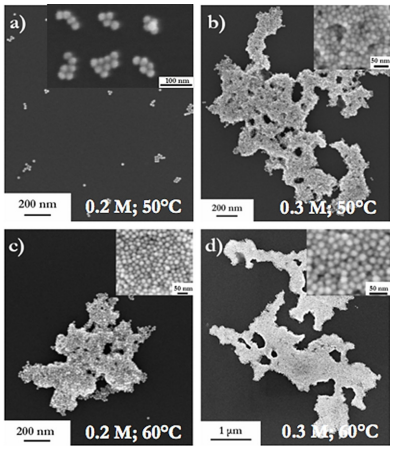

Figure 2 *Stucture of the gold NPCs evolved under different experimental conditions.*

For different sets of parameters, entirely different NPC structures evolved over time (Fig. 2), which can be attributed to the modulation of the steric repulsion arising from the PEG grafts. When the driving force for the clustering is smaller, only NPCs composed of a few particles are formed which can be effectively disassembled by providing external energy e.g. by ultrasonication. As the driving force increases, faster assembly occurs resulting in compact 3D assemblies. The approach should be extendable to suspensions of other nanoparticle types, where the nanoparticle stability is determined by surface-grafted responsive macromolecules [143].

Self-assembly of like-charged nanoparticles into Voronoi diagrams

(OTKA K104666, PD105173 and TÉT_12_JP-1-2014-0005)

D. Zámbó, K. Suzuno, Sz. Pothorszky, D. Bárdfalvy, G. Holló, H. Nakanishi, D. Wang, A. Deák, and I. Lagzi

The self-assembly of nanoscopic building blocks into higher order macroscopic patterns is one possible approach for the bottom-up fabrication of complex functional systems. Macroscopic pattern formation, in general, is determined by the reaction and diffusion of ions and molecules. In some cases, macroscopic patterns emerge from diffusion, and interactions exist between nanoscopic/microscopic building blocks. In systems where the distribution of the interaction-determining species is influenced by the presence of a diffusion barrier, the evolving macroscopic patterns are determined by the spatiotemporal evolution of the building blocks. A macroscopic pattern can be generated by the spatiotemporally controlled aggregation of like-charged carboxyl-terminated gold nanoparticles in a hydrogel (Fig. 1), where clustering is induced by the screening effect of the Na^+ ions that diffuse in a hydrogel. Diffusion fronts of the Na^+ ions and the induced nanoparticle aggregation generate Voronoi diagrams, where the Voronoi cells consist of aggregated nanoparticles and their edges are aggregation-free and nanoparticle-free zones (Fig. 2). We also developed a simple aggregation–diffusion model to describe the evolution of the observed Voronoi patterns.

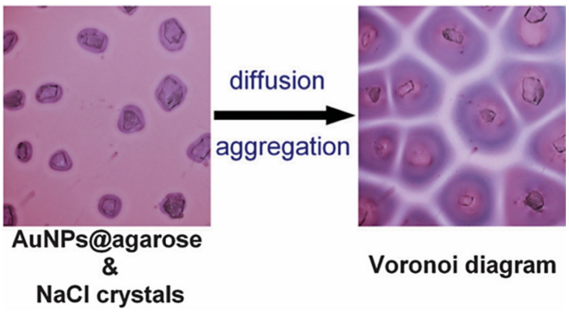

Figure 1 Representation of aggregation process triggered by the diffusion of sodium ions in a hydrogel.

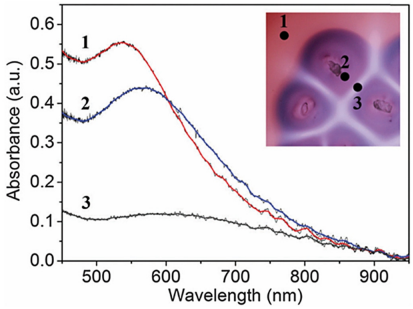

Figure 2 *UV-vis spectra of different regions in the hydrogel.* ***(1)****: Dispersed NPs;* ***(2)****: aggregated NPs;* ***(3)****: aggregation-free zones.*

The aggregation process of NPs was triggered by the electrostatic screening of negatively charged carboxyl protecting groups by Na^+ ions. The coupling diffusion of NPs and sodium ions and the aggregation of NPs generate Voronoi diagrams, where the Voronoi cells consist of aggregated NPs and their edges are aggregation-free and NP-free zones due to diffusion and fast aggregation processes. Our research provides an idea how to control spatiotemporally the self-assembly of nanoscopic building blocks by a diffusion front. Control of nanoscale systems by propagating reaction fronts could open up new avenues for research on nanostructured materials [144].

Assembling patchy nanorods with spheres: Limitations imposed by colloidal interactions

(OTKA K112114, PD105173, and FP7 No.310250)

Sz. Pothorszky, D. Zámbó, and A. Deák.

In the absence of external fields, the directed assembly of nanoparticles can be realized based on colloidal or other bio-specific interactions. Rod shaped nanoparticles can benefit simultaneously from shape and surface chemistry anisotropy (patchiness), making them excellent candidates for directed assembly.
Cetyltrimethylammonium bromide (CTAB) stabilized gold nanorods offer the possibility for regio-selective surface modification since they feature a less compact ligand shell at the tip region. By careful controlling the concentration of thiol-containing molecules during a ligand exchange, selective tip-functionalisation of the rods can be achieved. The aim of the present work was to perform directed assembly of patchy nanorods and nanospheres with precision control over the resulting structure. The driving force for spatially defined assembly is provided by carefully engineered surface chemistry of the assembling species. Two binding sites are created at the tips of gold nanorods where spherical particles can bind based on electric double layer interaction. The selectivity of the process is enhanced by covering the sides of the nanorods with large molecule polymer, providing an effective steric blocking in these regions of the nanorods (Fig. 1).

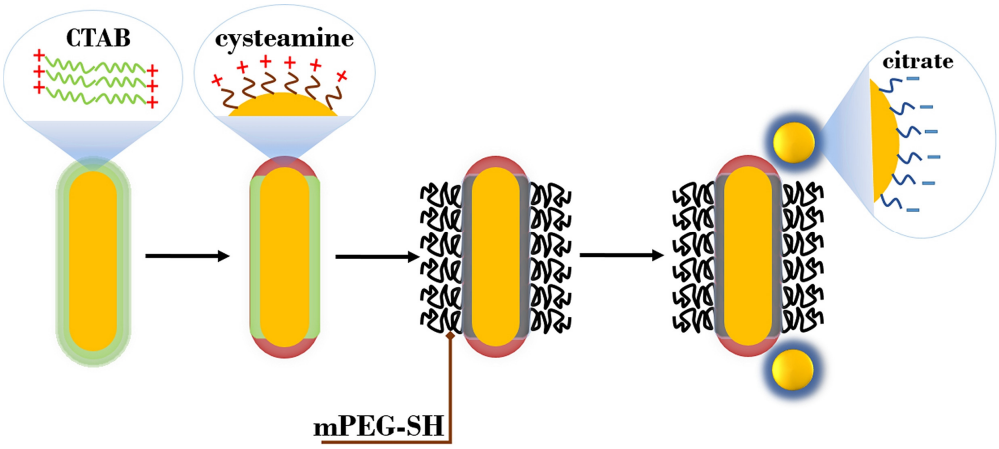

Figure 1 *Schematic display of the surface modification steps and the assembled structure.*

First, Au NRs with tip-selective surface modification were prepared using cysteamine-hydrochloride, starting from CTAB capped NRs. The second step of the procedure was the replacement of CTAB at the side region with mPEG-SH. For the self-assembly experiments the central building block was this patchy nanorod and citrate stabilized spherical gold particles. As observed in the SEM images, the rods preferentially accumulate two spheres in their tip regions at the opposite ends of the

rod (Fig. 2a). The ensemble extinction spectra measured in solution upon assembly (Fig. 2b) for the same system show a clear redshift and broadening of the longitudinal band position indicating plasmon coupling between the spherical particles and the nanorods' tip region, in agreement with structure observed in SEM.

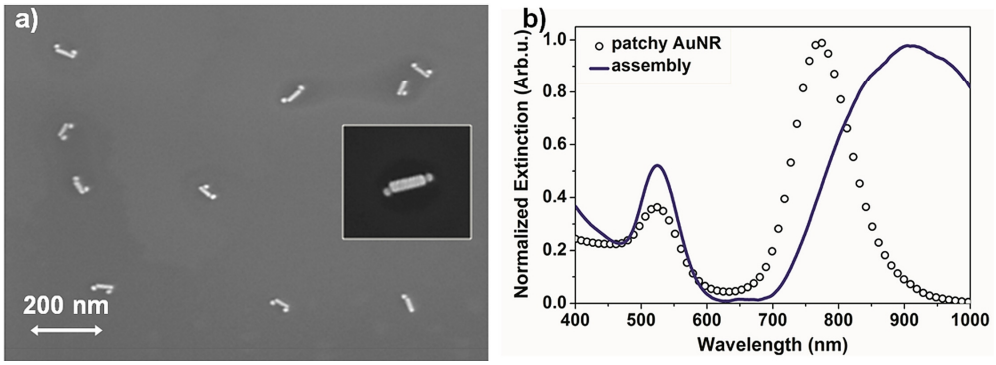

Figure 2 *The SEM image of the patchy nanorods (54x15 nm) assembled with 19 nm nanospheres* ***(a)****, and the corresponding extinction spectrum* ***(b)****.*

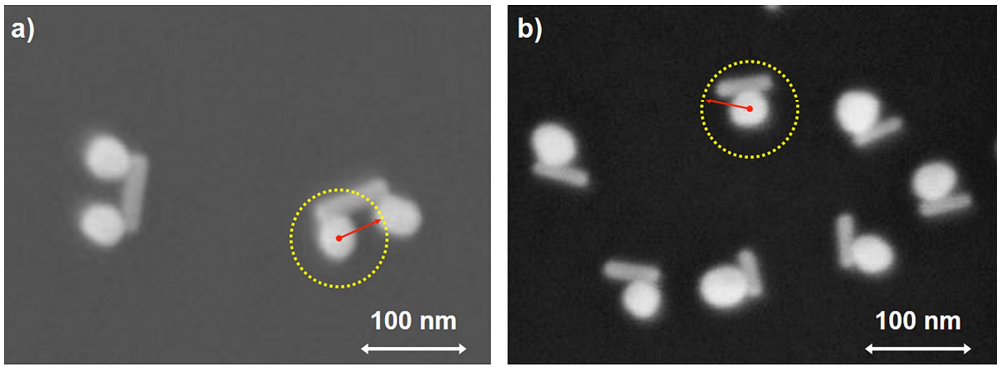

Figure 3 *Assembled structures using 40 nm gold nanospheres with gold nanorods having the same aspect ratio (3.8) but different dimensions: 80x21 nm* ***(a)****, and 60x16 nm* ***(b)****. The red arrows and the dotted circle indicate the separation distance where the value of the net particle-particle repulsion is 5 kT.*

As the relative size of the spherical particles increases, however, the two particles are shifted around the perimeter of the nanorod, finally only a single sphere gets assembled at the side of the rods (Fig. 3). The apparent cross-over of the regio-selectivity can be interpreted in terms of colloidal interactions, i.e. the second spherical particle is excluded due to nanosphere-nanosphere electric double layer repulsion, while the large van der Waals attraction results in a side positioning of the single adsorbed spherical particle. The results underline the importance of absolute values of the different interaction strengths and length scales in the programmed assembly of patchy nanoscale building blocks [98].

A different patchy particle type can be obtained by using interfacial templating. Instead of relying on the patchy surface coverage, structural and composition

inhomogeneity can be achieved by this approach. Our recent work connected to this field reports the preparation and optical properties of gold/silica "mushroom" nanoparticles, where a gold particle is only partially covered by the silica cap. The interfacial preparation method relies on partially embedding the gold particles in a polystyrene layer that masks the immersed part of the gold particle during silica shell growth from an aqueous solution. By adjusting sacrificial polystyrene film thickness and silica growth time, precise control over the coverage and cap thickness can be achieved (Figs. 4a,b).

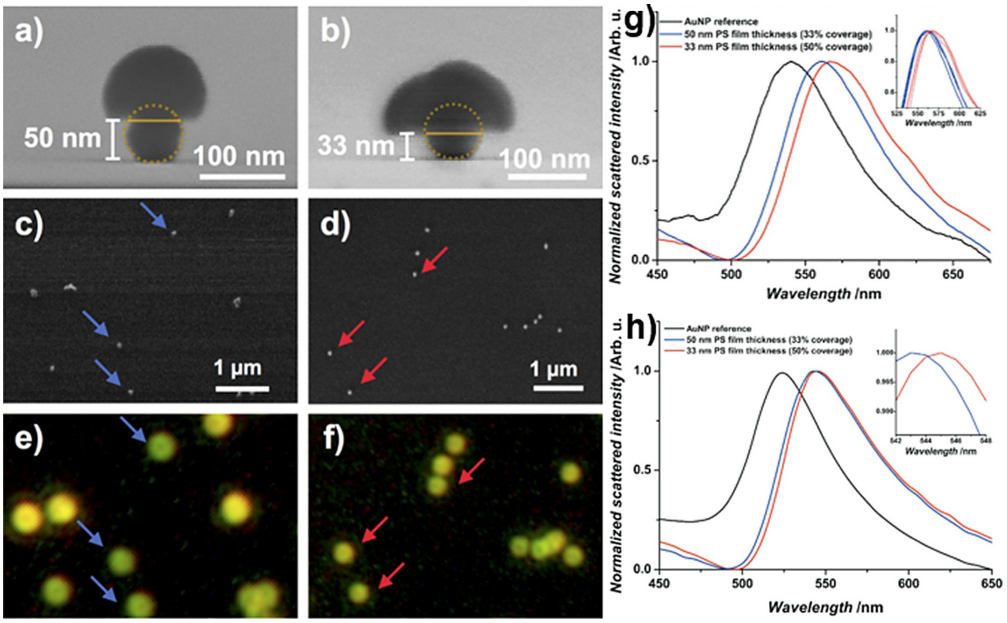

Figure 4 ***(a,b)****: Side-view, and* ***(c,d)****: top-view SEM images of the measured particles.* ***(e,f)****: Dark field scattering optical images of the same areas. Arrows mark the individual particles used to obtain single particle scattering spectra.* ***g)****: Averaged and normalized single particle scattering spectra. The inset shows the magnified region around the resonance peak for each individual spectra.* ***h)****: Simulated single particle spectra obtained for the reference particles (no coating), and the particles having 50% and 33% core-particle coverage by the silica cap after normalization.*

Correlative electron microscopy and single particle scattering spectroscopy measurements under-line the high precision and reproducibility of the method (Figs. 4c,d,e,f). The good agreement between the measured and simulated single particle spectra supported by near-field calculations indicates that the observed changes in the dipolar plasmon resonance are influenced by the extent of coverage of the gold core by the silica cap (Figs. 4g,h). The straightforward methods readily available for gold and silica surface modification using range of different (bio)molecules make these well-defined nanoscale objects excellent candidates to study fundamental processes of programmed self-assembly or application as theranostic agents [97].

Identification of dewetting stages and preparation of single chain nanoparticle rings by colloidal lithography

(OTKA K112114, PD105173, and FP7 No.310250)

N. Nagy, D. Zámbó, Sz. Pothorszky, E. Gergely-Fülöp, and A. Deák

Stages of drying after the wetting of template monolayer with aqueous gold nanoparticle solution were identified based on SEM images. Dewetting stages and characteristic particle deposits are summarized in Figure 1. During initial stage of drying, menisci are formed between neighboring template particles generating liquid bridges parallel to the substrate. This results remaining particles trapped at the lateral contact point of the particles (green square). Liquid level exceeds the equatorial plane of the particles which induces a faster evaporation in the triangular openings due to the 'chimney' effect.

This manifests in gold NP deposits at the triple points on the substrate (red square). During further evaporation, liquid film starts to evolve between neighboring PS particles and the silicon substrate, but these particles cannot be investigated from top-view. After the suspended film breaks up, liquid bridges evolve between neighboring particles whose thinnest point can be found at the midpoint between two PS particle. This causes random deposition of nanoparticles along the triple line, but trapped ones at the midpoints (purple square).

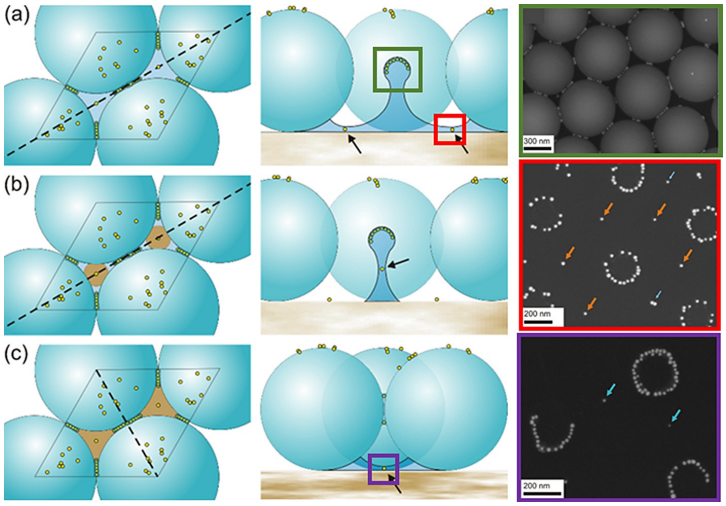

Figure 1 *Stages of the dewetting process below the equatorial plane of the template particles. Left panel shows the top view of the unit cell, where dashed lines indicate the plane of cross sections showed in the middle panel.* ***(a)****: Nanoparticle trapped at the triple point, where the liquid film is the thinnest;* ***(b)****: assumed particle trapping at the thinnest point of the liquid bridge between two neighboring template particles;* ***(c)****: nanoparticles trapped at the midpoint of the liquid bridge. SEM images of colored regions are represented in the right panel.*

In the final stage of the drying, the volume of these circular films decreases and the nanoparticles will be pressed into the wedge between PS and the substrate. Finally, the nanoparticles accumulate in a circular shape underneath the template particle forming single chain nanorings. Nanorings formed from 45 nm and 65 nm Au NP and different PS template particle sizes are demonstrated in Figs. 2(a-d). Diameter of produced nanorings shows dependency on the template particle diameter: using smaller PS beads smaller nanorings can be created. The internal diameter of gold nanorings can be estimated theoretically as well. Calculations and real internal diameters have excellent agreement demonstrated in Fig. 2(e).

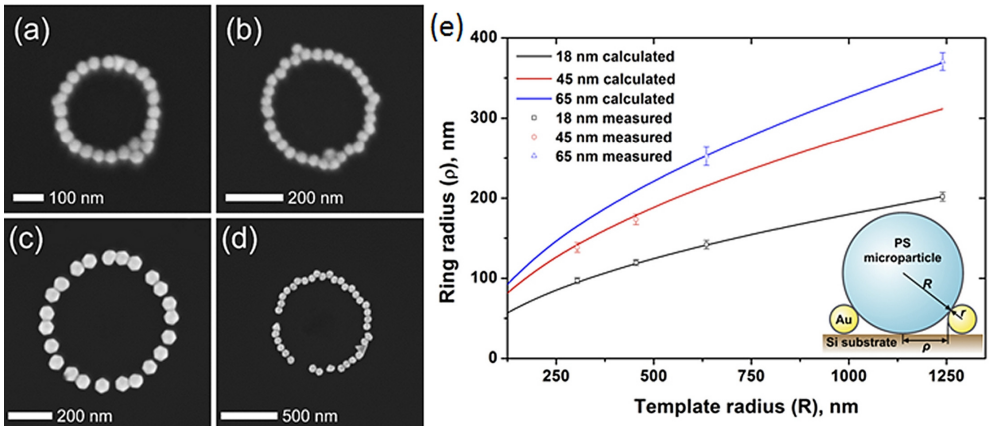

Figure 2 *Single chain gold nanoparticle rings of* ***(a,b)****: 45 nm, and* ***(c,d)****: 65 nm nanoparticles under* ***(a)****: 608 nm,* ***(b)****: 909 nm, (c): 1.27 μm and* ***(d)****: 2.48 μm PS particles.* ***(e)****: Calculated (solid line) and measured (scatter plots) internal ring radii in a function of template radius. Inset shows the calculation parameters according to hard sphere contact model.*

Effect of local defects and defect sides in template monolayer on the resulting structure was also investigated. Vacancies in the monolayer induce NP accumulation in the middle of the vacancy according to the "chimney" effect (Fig. 3(a)). Line defects indicate particle deposition between four PS particles (Fig. 3(b)). Domain boundaries cause broad disordered regions, where the surface coverage of the microparticles is smaller and the hexagonal order is missing [74]. Here random depositions, thick rings and connected wires can be observed (Fig. 3(c)).

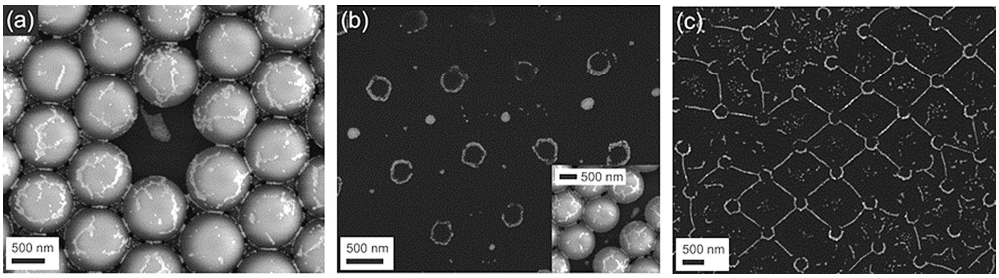

Figure 3 *Effect of vacancies* ***(a)****, defect sites* ***(b)****, and domain boundaries* ***(c)*** *on the structure after the drying process.*

Microtechnology Department

Head: Gábor BATTISTIG, Ph.D., senior research fellow

Research Staff

- Zsófia BAJI, Ph.D. (on maternity leave)
- István BÁRSONY, Member of HAS
- Orsolya BÁLINT-HAKKEL, Ph.D.
- László DÓZSA, Ph.D.
- Csaba DÜCSŐ, Ph.D.
- Zoltán FEKETE, Ph.D. (on leave)
- Péter FÖLDESY, Ph.D.
- Péter FÜRJES, Ph.D.
- Zoltán HAJNAL, Ph.D.
- Nguyen Quoc KHÁNH, Ph.D.
- Zoltán LÁBADI, Ph.D. (moved to Photonics Department)
- István LUKÁCS, Ph.D.
- György MOLNÁR, Ph.D.
- Andrea Edit PAP, Ph.D. (part time)
- Anita PONGRÁCZ, Ph.D. (on maternity leave)
- Vilmos RAKOVICS, Ph.D.
- István RÉTI, Ph.D.
- János VOLK, Ph.D.
- Zsolt ZOLNAI, Ph.D.

Ph.D. students / Diploma workers

- Zsófia BÉRCES, Ph.D. student
- Zoltán SZABÓ, Ph.D. student
- Ferenc BÍRÓ, Ph.D. student
- Máté TAKÁCS, Ph.D. student
- Tamás KÁRPÁTI, Ph.D. student
- Eszter HOLCZER, Ph.D. student
- Eszter TÓTH, Ph.D. student
- Éva JELINEK, Ph.D. student
- János RADÓ, Ph.D. student
- Anita ZÁTONYI, Ph.D. student
- Ágoston HORVÁTH, Ph.D. student

Technical Staff

- János FERENCZ, (engineer)
- Levente ILLÉS, (engineer)
- Csaba LÁZÁR, (engineer)
- Róbert HODOVÁN, (engineer)
- András LŐRINCZ, (engineer)
- András STRASZNER, (engineer)
- Erika TUNYOGI, (engineer, on maternity leave)
- Katalin VERESNÉ VÖRÖS, (engineer)
- György ALTMANN, (technician)
- Gabriella BÍRÓ, (technician)
- Tibor CSARNAI, (technician)
- Magda ERŐS, (retired)
- Károlyné PAJER, (technician)
- Csilla ARIAS-SOTONÉ FARAGÓ, (technician)
- Attila NAGY, (technician)
- Magda VARGA, (technician)

The task of the Microtechnology Department is

***Fundamental research on*:**

- sensing principles;
- novel materials and nanostructures;
- novel 3D fabrication techniques.

Research and development of physical, chemical/biochemical sensors and integrated systems:

- **MEMS** – R&D on gas sensors, 3D force sensors, thermal sensors, CMOS compatible and related techniques.
- **BioMEMS** – Development of novel microfluidic systems, their application in new fields of biochemistry.
- **NeuroMEMS** – Development of Si- and polymer based sensors for biomedical applications with special focus on brain science.
- **NEMS** – Synthesis and characterization of quasi-one-dimensional semiconducting nanostructures, semiconductor nanodevices, their integration into functional sensors, optoelectronic and photovoltaic devices.

Modeling, structural and device characterization methods available:

- Electrical characterization;
- Thermo-mechanical characterization;
- Scanning Microprobes;
- Ion beam analysis methods;
- SEM, TEM, EDX;
- Spectroscopic Ellipsometry.

The Department runs two clean labs (300 m^2 + 160 m^2 - Class 100-10000) comprising *a complete Si-CMOS processing line and a mask shop*, unique facility in Hungary. The technology allows to manufacture layers, patterned structures and devices with line resolution of 1 µm by optical and down to ≈10 nm by e-beam lithography on 3" and 4" Si and glass wafers.

Competencies (available also for our industrial and academic partners and customers):

- High temperature annealing, diffusion and oxidation; Rapid Thermal Treatment;
- Low Pressure Chemical Vapour Deposition of poly-Si, SiO_2 and Si_3N_4 layers;
- Low Temperature Chemical Vapour Deposition;
- Plasma Enhanced Atomic Layer Deposition;

- Physical Thin Film Depositions – Electron beam evaporation, DC and RF Sputtering;
- Ion implantation;
- Reactive Ion Etching, Deep Reactive Ion Etching;
- Photolithography with back-side alignment and Nanoimprinting;
- E-beam lithography;
- Nanopatterning, deposition and etching by Focused Ion-Beam;
- Wafer-bonding;
- Wet chemical treatments;
- Electro-chemical porous Si formation;
- Liquid Phase Epitaxy of III-V compound semiconductors;
- Mask design, laser pattern generator;
- Polymer (PDMS, SU8, Polyimide) structuring by photolithography and micro-molding techniques,
- Chip dicing, packaging especially for sensor applications;
- Materials and structural analysis & characterization:, SEM, FIB, EDX, Atomic Force Microscopy, Electrochemical Impedance Spectroscopy, Stylus Profiler;
- Electrical and functional modeling and characterization.

For detailed information please visit our web-sites:
www.mems.hu,
www.biomems.hu,
www.nanomems.hu,
www.neuromems.hu,
www.nems.hu
or contact us by e-mail: **dragon@mfa.kfki.hu**

MEMS

Activity leader: Cs. Dücső

Group members: Z. Baji, I. Bársony, G. Battistig, L. Dózsa, P. Földesy, P. Fürjes, Z. Hajnal, Gy. Molnár, A.E. Pap, V. Rakovics, J. Radó, I. Réti, Zs. Zolnai, F. Biró, and M. Takács

Projects:

- OTKA K109674 - Graphene based Terahertz modulators (2013-2017)
- OTKA PD116579 – ZnO and Ga_2O_3 nanostructures by Atomic Layer Deposition (2015-2018)
- OTKA K112114 – Combined micro- and nanotechnology methods and analytics – from patterning to applications (2014-2017)
- PAMIAQ, EURIPIDES / EUREKA 13-1610 - Particle Matter sensors for indoor air quality (2013-2016)
- NKFIH-NVKP16 – Up-to-date functional materials for autonomous sensor nodes and sensor networks (2016-2019)
- Italian-Hungarian joint program (CNR-IMEM – MTA EK MFA) - Synthesis, characterization and study of semiconducting materials for energy conversion, sensors, electronics and medical applications (2016-2019)
- ENIAC CALL 2013-1 - Intelligent Catheters in Advanced Systems for Interventions (2014-2017)

Force Feedback Control System for Robin Heart Surgical Robot

Minimally invasive surgery (MIS) offers several advantages for the patient and also for the society. The smaller trauma and faster recovery are obviously essential for the patient, whereas the reduced hospitalization and recovery time helps the society to spend the medical costs more effectively. INCITE project is intended to reveal and describe the advantages of the integration and application of various sensing capabilities in Minimal Invasive Surgery (catheter or surgery robot) systems. The future aim is to improve the functional characteristics, safety and standards of medical devices (catheters, robotic tools) applicable to minimal invasive cardiac intervention and surgery.

The lack of force feedback is one of the main barriers in the progress and widespread application of robotic surgery. The main tasks of the surgical robot control (Fig. 1) are the mapping and analysis the movements of the surgeon operator (position/velocity and possibly other physical parameters), as well as facilitating arm movement by providing control signals to the actuators. Additionally, it is desirable to feed-back the force/touch information to the person handling the tools. These signals

can help the operator to make immediate correcting actions during the operation: cutting, separation, handling and moving tissues, to execute vascular clamping, to tie a knot, to recognize the type of tissue (pathology, calcification), to manipulate between different elements of internal organs without the risk of harming neighboring tissue, and also to sense collision of arms/or tools by automatic recognition.

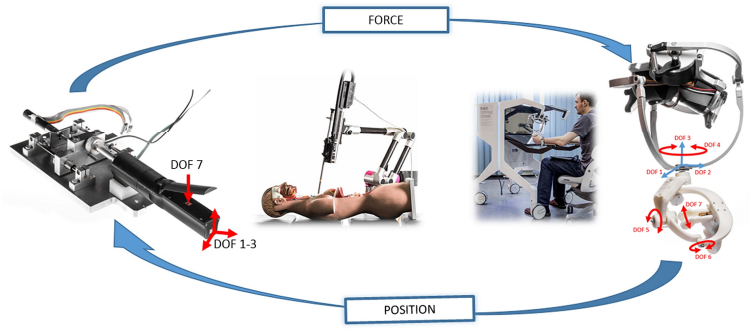

Figure 1 *Schematic representation of the master-slave systems with force-feedback and manipulation.*

Fabrication and integration of the 3D MEMS force sensors

3D force sensors were developed to further integration in laparoscopic heads of surgery robots. The Si sensors operate with piezoresistive transduction principle by measuring the stress induced signals of the symmetrically arranged four piezoresistors in a deforming membrane (Fig. 2). As the chip size has to be reduced to a few mm2, the conventional anisotropic alkaline etching technique was replaced by deep reactive ion etching (DRIE) for membrane formation. Moreover, DRIE enables to form any geometry of the membrane and offers the formation of monolith force transfer rod protruding over the chip surface (Fig. 2). This rod increases shear sensitivity of the structure, thereby plays a crucial role in tactile sensing. The technology applies SOI (silicon on insulator) wafers of appropriate device layer thickness. This results in highly uniform membranes and good reproducibility of the process.

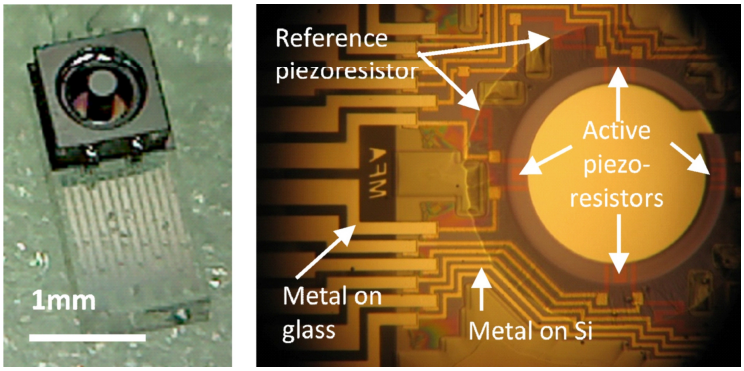

Figure 2 *Optical views of glass bonded chip from the top (left) and the same chip from the glass side (right).*

According to the medical and functional requirements the sensors must be covered by biocompatible and sterilisable elastic polymers. As the elastomer drastically affect the performance of the device, the proposed sensor structures were modeled by coupled finite element simulation to determine the appropriate geometric parameters to meet the functional requirements. Sensors were covered with spherically shaped PDMS (polydimethylsiloxane) polymer and the effect of the elastic coating was studied in terms of sensitivity and response time. The standard test included the measurements of the four out-of-balance voltages over the applied force range. As experienced the geometry and elasticity of the elastic coverage may result in sensitivity loss up to 50-90%.

Preliminary functional tests of the force sensors

Model tools were equipped with two 3D force sensors of MFA: one mounted on a tip of grasper for generation of a tactile signal, whereas the other directly placed inside the tool for measuring the gripping forces (Fig. 3). Appropriate control systems and test beds have been developed at FRK.

Figure 3 *Model of INCITE tools with tactile sensor on the tip and the 3D force sensor for gripping inside the grasper.*

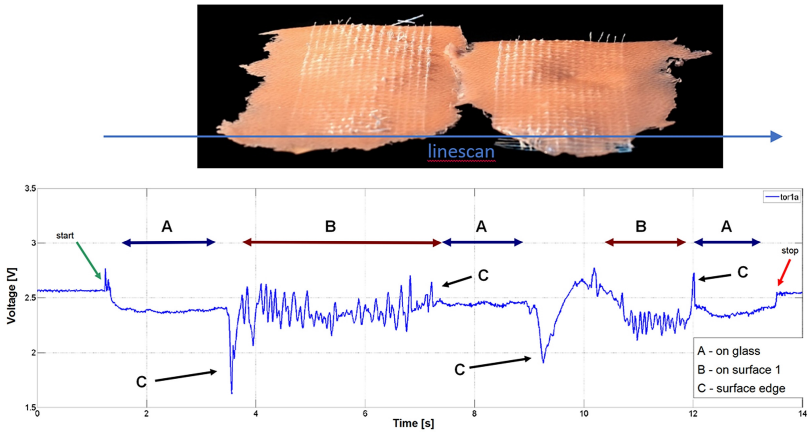

Figure 4 *Preliminary measurements for surface characterization by tip integrated tactile sensor.*

Preliminary tests were accomplished to reveal the possible information the force/tactile sensors integrated in the laparoscope head can provide. Our work is also focused on the preliminary definition of the biomechanical effects present during surgical operations. Tactile measurements were also accomplished on artificial and real animal tissues to evaluate the applicability of the sensors for biomechanical screening during MIS surgery (Fig. 4).

Development of gas sensing microstructures

The existing micro-hotplate structure was further developed to investigate the limits of possible applications. A double-spiral Pt filament was integrated in a cantilever type hotplate built up from a reduced stress $SiO_2/Si_3N_4/SiO_2$ multilayer elaborated earlier. The hotplate exhibits 15% less power dissipation of the full membrane type reference as revealed from resistance and micro-melting point measurements (Fig. 1). Nevertheless, the average temperature provides limited information about the temperatures distribution across the hot-plate, thereby may lead to false consequences when the sensing principle is governed by chemical reactions. To clarify this a detailed investigation was started to identify degradation mechanism and optimize the layout according to the requirements of the targeted applications.

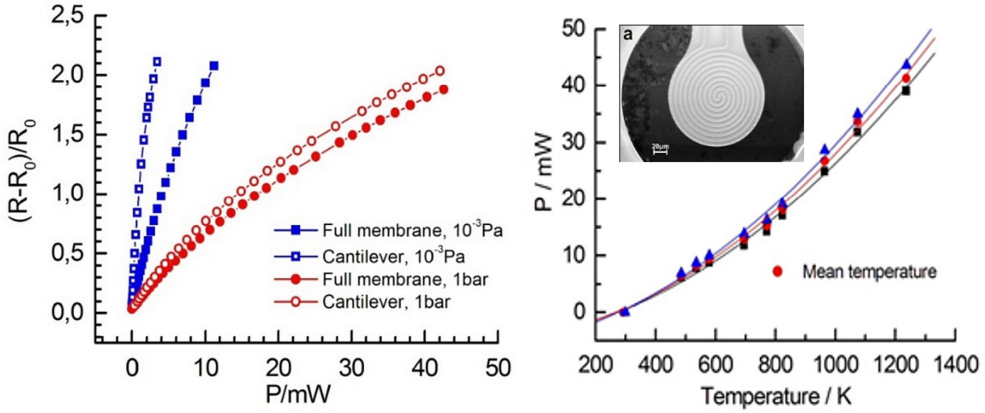

Figure 1 *Power dissipation of the double spiral Pt heater hotplate (insert on the right) as measured by resistance (left) and micro melting point technique (right).*

Deposition of catalyst in nano-porous sensing layers

Pt and Au nano-particles were deposited in the porous sensing layer formed on the top of the micro-hotplates. The WO_3 nano-rod based conductivity sensors were sensitized by Pt and Au nanoparticles (28nm, 20nm) and the effect of catalyst was investigated in detail. Drop deposited Au nanoparticles enhanced the sensitivity by a factor of 20 and showed the best performance by selective detection of H_2S over NH_3 in the ppb range (Fig. 2).

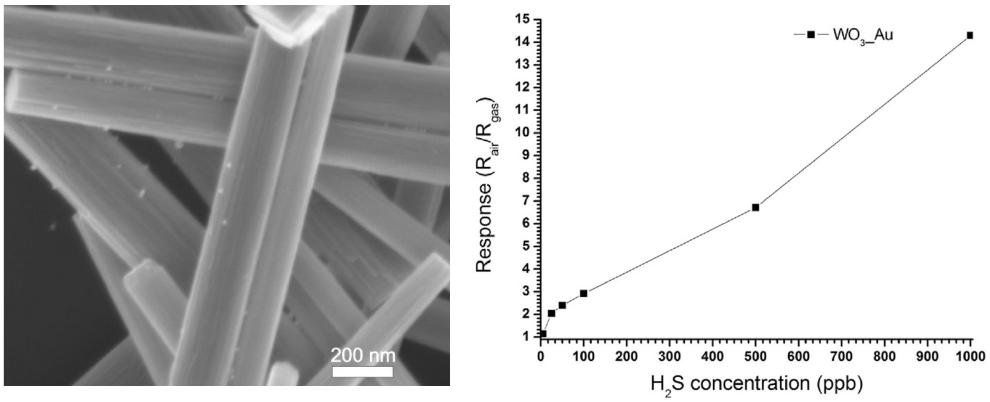

Figure 2 *WO_3 nano-rods sensitized with 20 nm Au nano-particles (left). Sensor responses for H_2S exposure in the ppb range (right).*

For the catalytic-calorimetric devices high operation temperature and large surface catalyst is needed to generate sufficiently large heat to be measured by the change of filament resistance. In order to meet this requirements ALD deposition technology of Pt was elaborated to cover uniformly the electrochemically formed porous Al_2O_3 layer on the top of the micro-hotplate (Fig. 3). The ongoing characterization of the device aims at the detection of hydrocarbons (LPG and methane) below the lower explosion limit (LEL) for commercial safety application.

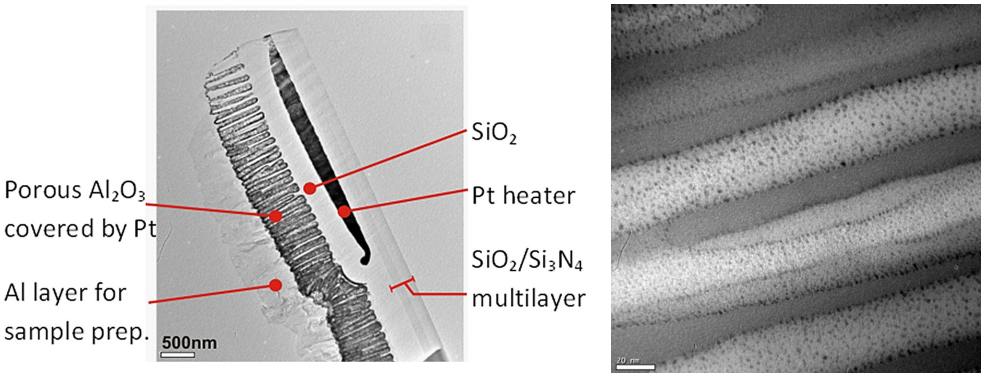

Figure 3 Cross sections of the micro-hotplate with ALD coated porous Al_2O_3 on top (left). Magnified view (right) shows the uniformly distributed Pt nano-particles in the full depth of pores. TEM images.

BioMEMS

Activity leader: P. Fürjes

Group members: Zs. Baji, O. Bálint-Hakkel, P. Földesy, Z. Hajnal, E. Holczer, E.L. Tóth, and J. Radó (A.B. Tóth, B.V. Farkas, A. Füredy are M.Sc. students)

Projects:

- ENIAC CALL 2013-1 - Intelligent Catheters in Advanced Systems for Interventions (2014-2017)
- OTKA CK 83821 – Preparation of microchannels by proton-beam micropatterning and their application in Lab-on-a-chip devices
- KTIA VKSZ_14 – Development of Multiparameter Point of Care in vitro diagnostic systems
- EURIPIDES / EUREKA 13-1610 - Particle Matter sensors for indoor air quality – PAMIAQ (2013-2016)
- GINOP-2.3.2-15 – Application of chip-technology for the improvement of the success rate in human in vitro fertilisation

Significant efforts were made in the recent period to construct and organize a competitive infrastructure and concentrate a solid knowledge background in the MEMS Laboratory of MFA works to support development of biosensors, biointerfaces and microfluidic systems. The developing scientific field concentrated around the micro- and nanofluidical, bioanalytical and medical diagnostic (BIOMEMS) research. These are highly challenging topics as proven by the numerous research projects , emerging industrial interest and increasing number of attracted students. The group – covering postdoc researchers, Ph.D. and gradual students – is able to efficiently support scientific research of national and international institutes, development at industrial partners or the education at partner universities also beyond its own scientific topics.
As a result of novel and innovative biosensing and sample preparation principles new possibilities are being proposed in medical applications. These bioanalytical systems are expected to integrate the micro and nanoscale transducers with sample preparation microfluidic systems also composing Lab-on-a-Chip devices. Our main goal is to develop integrated devices and systems for industrial and medical applications.

Effective flow control in autonomous polymer microfluidic systems based on surface modification and bioinspired micropatterning

Precise and fast PoC monitoring of disease related blood protein marker levels could be crucial in effective therapies. Due to the development of microtechnology and

especially Lab-on-a-Chip (LoC) and microfluidic devices these cost-effective complex but miniaturized analytical systems became available and applicable for implementing the overall sample analysis from preparation to molecular diagnostics. The microfluidic system has to transport the sample and the washing buffer to the active area of the chip while mixing and incubate the sample with reagents. As the incubation and read-out needs a specified time, precise sample handling and flow control are crucial. The use of biological sample also requires bioinert surface properties with minimized non-specific adsorption and coagulation in the channels. The medium term target of our work is to develop a polymer based microfluidic cartridge for autonomously controlled sample transport and preparation to be incorporable into bioanalytical device.

Surface modification of self-driven microfluidic systems

Polymer based microfluidic sample transport system with multiple functions was developed for further application in bioanalytical devices detecting blood protein biomarkers or cells. Significant flow controlling subparts of the overall microfluidic system were designed, fabricated and characterized considering different surface modifications and microscale geometries. In order to fulfil the requirements the polydimethylsiloxane (PDMS) based material was modified by embedding PDMS-b-PEO molecules into the PDMS matrix. PDMS-b-PEO molecules change the inherent hydrophobicity of the polymer ensuring adequate capillary pressure for self-driven transport simultaneously affecting the level of the non-specific protein adsorption. The non-specific adsorption of the major blood proteins on the surfaces were recorded by fluorescent microscopy (Fig. 1). It was proven that precise sample handling and flow rate control with minimized non-specific adsorption on the surface can be achieved by combination of these surface modification techniques and bio-inspired microstructures.

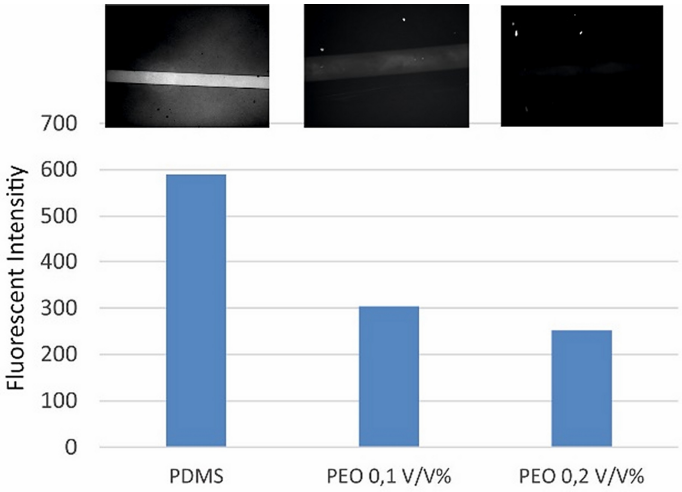

Figure 1 *Non-specific fluorescent labelled HSA molecule adsorption on the microfluidic channel-surface in case of different PDMS-b-PEO concentrations.*

Bioinspired microcapillary systems

We tested different geometries including biomimetic structures to form both special capillary and flow stopping or rectifying structures to set (to enhance or decrease) local flow rates in the autonomous microfluidic system. The influence of the micropatterning of the transport channels was also analyzed. Enhanced capillary pump systems were designed, fabricated and evaluated to prove the advantage of secondary microstructures inspired by natural water transport systems (Fig. 2).

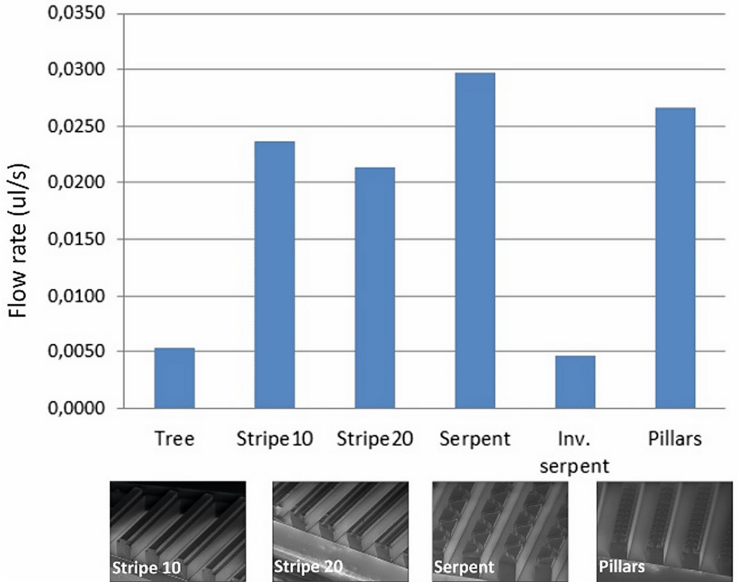

Figure 2 *Micro-patterned capillary channels in surface modified PDMS: secondary structures significantly modify the flow rates.*

Asymmetric capillary structures were implemented to enable unidirectional or at least direction dependent sample transport by mimicking the micro ornamentation of the natural surfaces (Fig. 3).

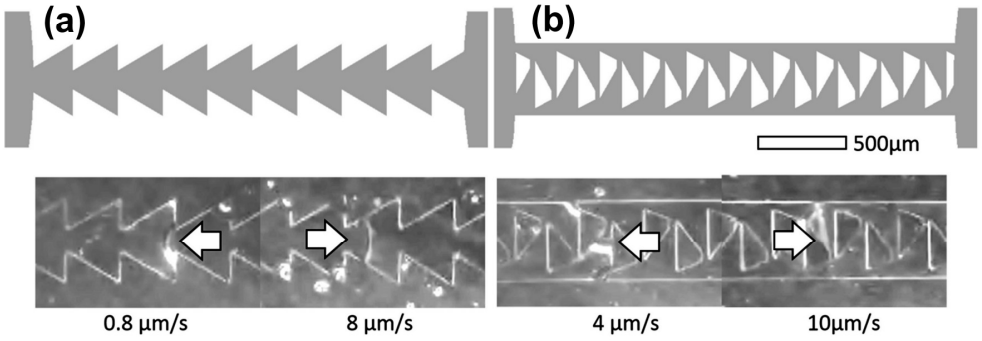

Figure 3 *Direction dependent flow rates in asymmetrically patterned microfluidic structures.* ***(a)****: flow stop,* ***(b)****: Texas horned lizard's skin.*

Biosensing applications

In cooperation with the MTA-ELTE Immunology Research Group we have identified and optimized the physical conditions suitable to promote strong interactions. Permanent binding, between RBCs and functionalized microfluidic channel surface results in altered flow properties of the test blood sample. This deviation is characterized by an overall retardation of blood flow and a concomitant, as well, as a more pronounced retardation of the RBC components of blood (Fig. 3). Using the model system of blood type group AB0 we also demonstrated that this phenomenon can be applied to reliably identify the blood group without the need of any preanalytical steps.

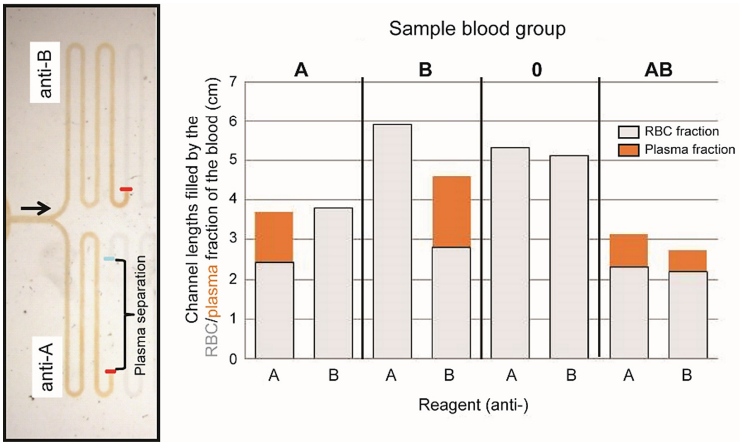

Figure 3 *Development of plasma front in samples of (a): 0,* ***(b)****: A,* ***(c)****: B, and* ***(d)****: AB blood types.*

Autonomous sample transport microfluidic systems were designed and fabricated to be integrated in Point-of-Care Lab-on-a-Chip based diagnostic cartridges in cooperation with 77 Elektronika Ltd.

Particle manipulation in microfluidic systems

The rapid development of microscale diagnostic (Lab-on-a-Chip) devices has underlined the importance of microfluidics enabling fast and effective preparation and analysis of liquid samples. This leads to the development of novel microfluidic structures based on the physical laws of this size domain.

Hydrodynamic particle separation in microfluidic systems

The aim of our work was to develop a passive microfluidic separation system applicable for pre-sorting pollutant particles (pollens, bacteria, grains) in environmental samples having different geometric or physical parameters. To achieve effective size dependent sorting of the particles dispersed in the liquid sample a

combination of different inertial separation methods were applied, utilizing the pinched flow fractionation, the Dean and the lateral migration based separation subsequently.
Microfluidic systems were designed and fabricated for particle separation and sorting by their hydrodynamic parameters such as cell size or density to be applied for sample preparation in optical scattering based pollution monitoring device. The hydrodynamic behavior of the microfluidic structure was modeled and predicted by Finite Element Method (FEM) using COMSOL Multiphysics code to calculate the flow field and the geometry dependent particle trajectories. The separation of black (10 µm particle diameter) and white (16 µm diameter) lines were visible and also demonstrated by their spatial distribution in Fig. 1.

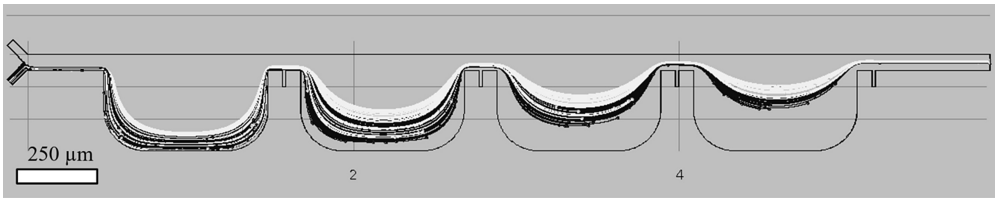

Figure 1 *Modelled particle trajectories developing in the lateral migration based passive separation system (particle diameters: 16µm – white lines and 10µm – black lines).*

The microfluidic system was manufactured by soft lithography and verified by fluorescent microscopy applying two differently labeled particles with 10 and 16µm diameters. The results of the experiment were in good agreement with the prior FEM estimations and proved successful size dependent sorting of particles (Fig. 2).

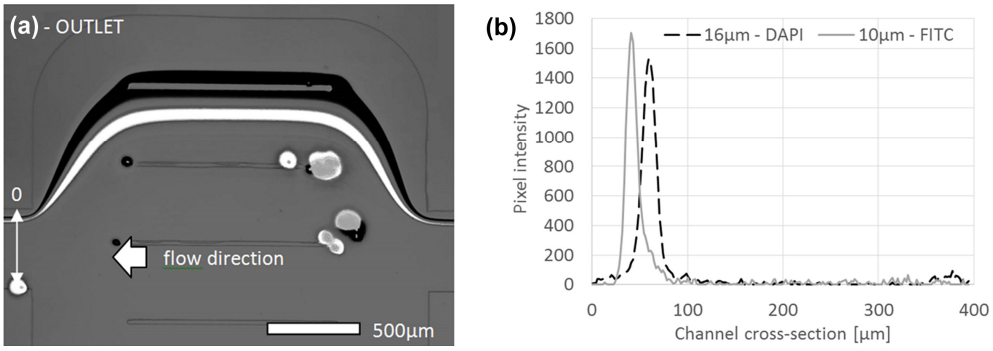

Figure 2 *Recorded trajectories **(a)**, and intensity analysis **(b)**, of different fluorescent labelled beads at the outlet (diameters: 16µm – white lines – DAPI and 10µm – black lines – FITC). The two bead sizes are separated by their respective peak positions.*

Particle trapping in microfluidic magnetic separation (MMS) system

Particle separation is challenging since the particles often have physical parameters (density, dielectric constant, etc.) similar to that of the solvent. Active separation techniques could offer several effective solutions, although they require an external field and power. Microfluidic Magnetic Separation (MMS) devices utilize the effective magnetophoresis based magnetic bead manipulation applying

microfabricated paramagnetic patterns to locally amplify the magnetic field. Microfluidic magnetic particle trapping system was modeled, designed and manufactured to characterize and improve the separation efficiency during sample preparation and analysis.
Coupled multiphysics model of the evolving magnetic field, fluid dynamics and particle trajectories was implemented in COMSOL Multiphysics. The movement and entrapment of magnetic beads in the MMS system were analyzed and the spatial distribution of the trapped magnetic particles was compared to experimental results (Fig. 3).

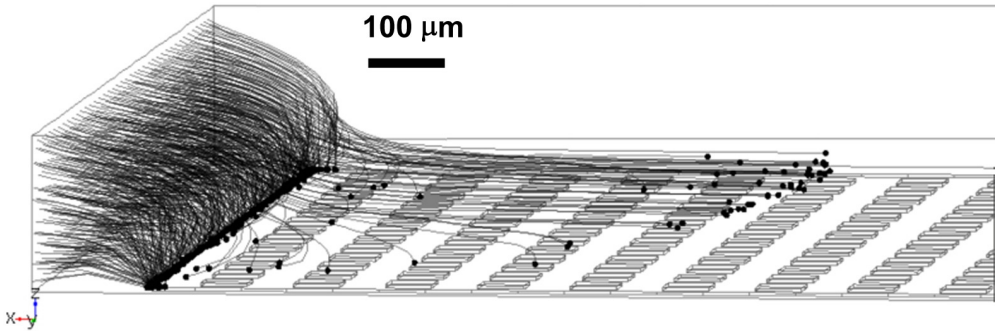

Figure 3 *Particle trajectories over the grid type paramagnetic pattern in the MMS structure.*

For functional validation the microfluidic system was manufactured in polydimethyl-siloxane (PDMS) by soft lithography technique, and special Fe-Ni pattern was deposited onto a glass wafer to amplify the magnetic field locally inside the chip. Experimental results showed the capturing effect of the paramagnetic grid (Fig. 4(a)). Untrapped particles followed the gridlines parallel to the flow direction (Fig. 4(b)) and maintained these trajectories after leaving the pattern as well.

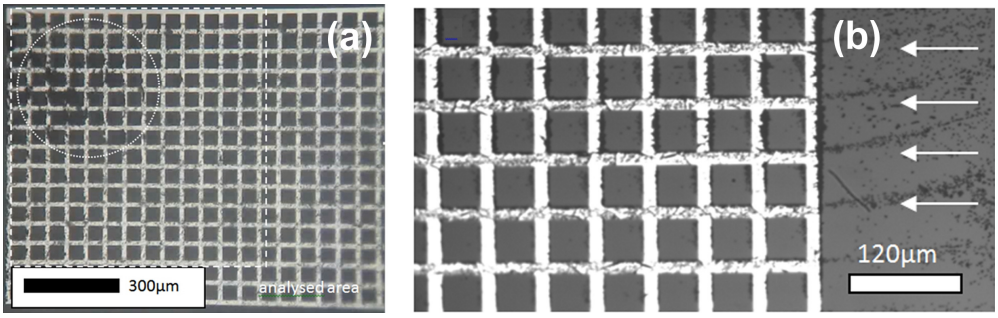

Figure 4 *Movement of the magnetic beads over the paramagnetic pattern: trapped magnetic beads on the paramagnetic (Fe-Ni) pattern of the MMS chip (a), untrapped particles follow the grid lines parallel to the flow direction (b).*

Precisely tailored solid state nanopores for molecule recognition

Nanoporous membranes are the fundamental components of the transport modulation based label free electrochemical biosensors envisioned to be applicable for high sensitive molecule detection. The sensitivity and the specificity of these sensors are significantly affected by the evolved pore geometry which has to be fitted to the target molecule size and conformation. Commercialization of the nanopore based biosensors or Lab-on-a-Chip devices seems to depend on the development precise and high throughput nanofabrication techniques enabling reliable and reproducible shaping nanopore geometries in solid state membranes.

Controlled nanopore fabrication by focused ion beam (FIB) milling

This work is intended to demonstrate a significant improvement regarding reliability and reproducibility of the Focused Ion Beam (FIB) milling for nanofabrication solid state nanopore arrays to achieve precise and predictable nanopore geometries fit to the targeted molecule conformation to be recognized. Solid state nanopores were fabricated by the combination of MEMS and NEMS technology. First a dielectric membrane was released by alkaline or DRIE etching from the backside, and then the nanopores were drilled by program controlled Focused Ion Beam (FIB) milling using accelerated Ga^+ ions applying different milling currents and doses to obtain various pore geometries. The geometries of the nanopores were analyzed in detail by high resolution SEM and TEM imaging (Fig. 1(a-b)).

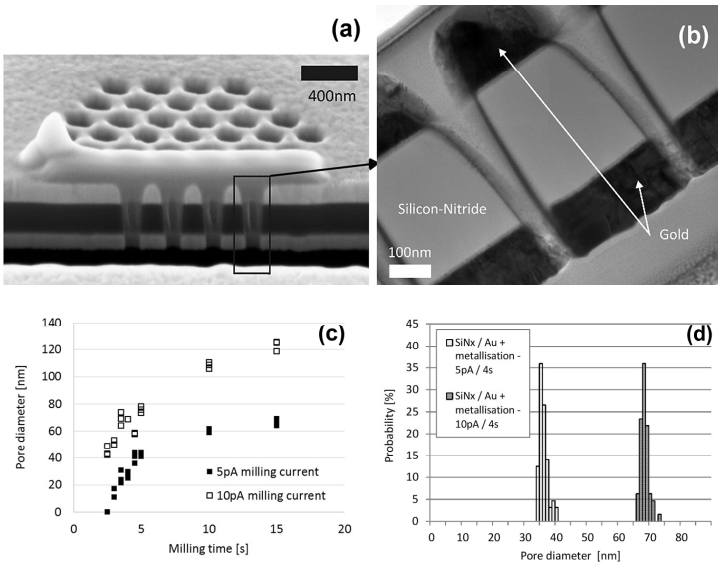

Figure 1 *Cross-sectional SEM* ***(a)****, and TEM view* ***(b)*** *of the nanopore array revealed by FIB milling of Au/SiN_x/Au membrane and the measured time dependent pore diameters in case of Au/SiNx layer structure and different ion currents (5pA and 10pA)* ***(c)****. Statistical pore diameter distribution was significantly improved by additional front side metallisation* ***(d)****.*

The statistical geometric parameters of the fabricated nanopores as a function of the fabrication parameters were recorded and studied (Fig. 1(c)). To improve the reproducibility of geometrical parameters of the nanopores an additional metallization

step was applied. During the fabrication process it had to passivate the sensor structure while applying the Focused Ion Beam milling for the complex material composition of the sensor structure. The work proved that the conformity of the pore geometry and the reliability of the fabrication process could be significantly improved by the advanced nanofabrication process (Fig. 1(d)).

NeuroMEMS

Activity leader: Z. Fekete

Group members: A. Pongrácz, Á.Cs. Horváth, A. Zátonyi, Zs. Bérces, D. Szegedi, B. Csernyus, Sz. Barna, D. Pinke

Projects:

- NKFIH K 120143 Investigation of novel implant materials for high-resolution, multi-parametric imaging of cortical activity (2016-2020)
- OTKA 116550 Understanding the impact of nanostructuring to control neural cell - solid surface interactions at brain-machine interfaces (2015-2018)
- Nemzeti Agykutatási Program – NAP B - Design, fabrication and validation of novel microelectrodes for optogenetic and infrared neural stimulation in the hippocampus and deep-brain areas (2015-2017)

Silicon microelectrodes for infrared neural stimulation

Infrared neural stimulation (INS) was discovered in 2005, when action potentials were successfully elicited using infrared light. Histology performed after revealed that there is a radiant exposure range, where action potentials are elicited without damage.

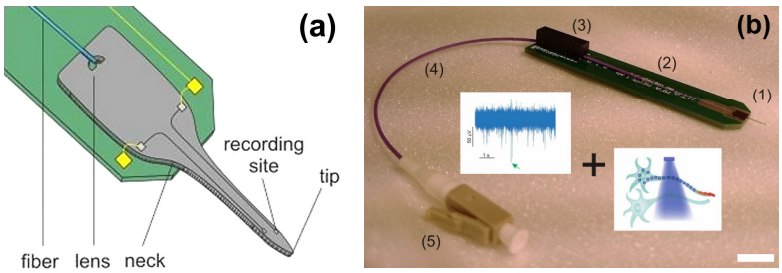

Figure 1 ***(a)****: Concept of a silicon microelectrode that provides infrared stimulation and records the electrical activity of neurons simultaneously.* ***(b)****: Implantable MEMS device for simultaneous optical stimulation and electrical recording of neural activity. Scale bar: 10 mm Components of the system:* ***(1)****: Silicon microelectrode chip,* ***(2)****: PCB,* ***(3)****: Electrical connector,* ***(4)****: Optical fiber,* ***(5)****: Optical connector.*

In our work, a Michigan-type silicon microprobe for infrared neural stimulation was designed and investigated in terms of technology induced surface roughness and optical transmission. The fabrication of such optrode was realized by deep reactive ion etching and subsequent wet chemical polishing (Fig. 1).

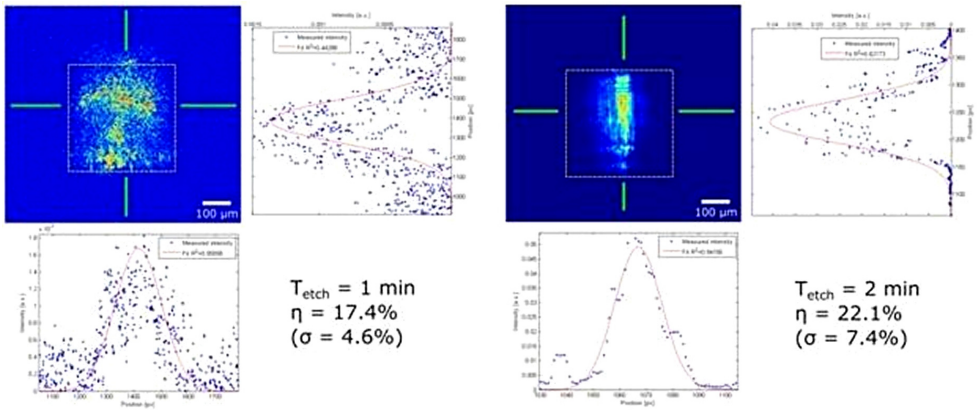

Figure 2 *Beam profile of P1 (left) and P2 (right). Dashed yellow lines represent the contour of the probe shaft, while green lines indicate the X and Y cross-section of represented data on optical power (reprinted from Kiss et al., 2016, Sens. & Act. B).*

The overall efficiency was further boosted by integrated couplers and focusing microlenses etched into the silicon substrate. By the proposed fabrication approach, 22.1% in system efficiency was achieved at a wavelength of 1310 nm. We observed that system efficiency does not increase significantly by increasing the time of sidewall polishing, however, the beam shaping effect of the coupling lens is more significant, when the tip roughness is reduced to 8.7 nm RMS value. The spatial distribution of the delivered light can also be controlled through integrated micromirrors at the probe tip, which facilitates lateral out-coupling with a Gaussian beam profile (Fig. 2).

Simultaneous in vivo recording of local brain temperature and electrophysiological signals with a novel neural probe

Temperature is an important factor for neural function both in normal and pathological states, nevertheless, simultaneous monitoring of local brain temperature and neuronal activity has not yet been undertaken. In our work, we propose an implantable, calibrated multimodal biosensor that facilitates the complex investigation of thermal changes in both cortical and deep brain regions, while recording multiunit activity of neuronal populations in mice. The fabricated neural probe contains four electrical recording sites and a platinum temperature sensor filament integrated on the same probe shaft within a distance of 30 µm from the closest recording site. The feasibility of the simultaneous functionality is presented in

in vivo studies. The probe was tested in the thalamus of anesthetized mice while manipulating the core temperature of the animals. We obtained multiunit and local field recordings along with measurement of local brain temperature with accuracy of 0.14 °C. Brain temperature generally followed core body temperature, but also showed superimposed fluctuations corresponding to epochs of increased local neural activity. With the application of higher currents, we increased the local temperature by several degrees without observable tissue damage between 34-39 °C.

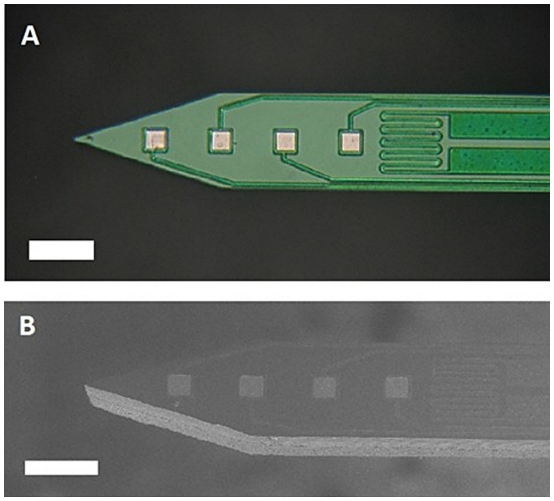

Figure 1 ***A)****: Optical microscopy views of a 4-channel microelectrode with integrated platinum temperature sensor filament.* ***B)****: Perspective scan-ning electron micrograph of an as-fabricated probe shaft. Scale bar represents 100 µm on each figure. (Reprinted from Fekete et al. 2017, J Neural Eng.)*

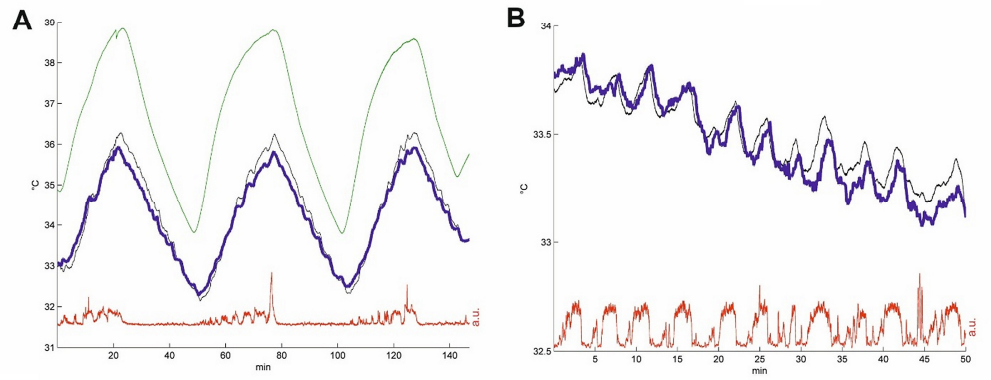

Figure 2 *Validation of the thermoelectrode by temperature measurement in vivo* ***(A)****: Parallel changes of core body temperature, brain temperature, and neural activity. Effect of a series of heating cycles between 34-39 °C performed by a heating plate directly placed under urethane anaesthetized mouse.* ***(B)****: Brain temperature and multiunit activity in an anaesthetized mouse without active heating. Microfluctuations in brain temperature are associated with elevated multiunit activity. Green line: rectal temperature sensor, black line: contralateral reference NTC thermistor, blue line: temperature sensor of our thermoelectrode. Red curves show the smoothed multiunit activity (arbitrary units) recorded simultaneously by the thermoelectrode (reprinted from Fekete et al. 2017, J Neural Eng).*

A Multimodal, SU-8 - Platinum - Polyimide Microelectrode Array for Chronic In Vivo Neurophysiology

Utilization of polymers as insulator and bulk materials of microelectrode arrays (MEAs) makes the realization of flexible, biocompatible sensors possible, which are suitable for various neurophysiological experiments such as in vivo detection of local field potential changes on the surface of the neocortex or unit activities within the brain tissue. In this paper the microfabrication of a novel, all-flexible, polymer-based MEA is presented. The device consists of a three dimensional sensor configuration with an implantable depth electrode array and brain surface electrodes, allowing the recording of electrocorticographic (ECoG) signals with laminar ones, simultaneously. In vivo recordings were performed in anesthetized rat brain to test the functionality of the device under both acute and chronic conditions. The ECoG electrodes recorded slow-wave thalamocortical oscillations, while the implanted component provided high quality depth recordings. The implants remained viable for detecting action potentials of individual neurons for at least 15 weeks.

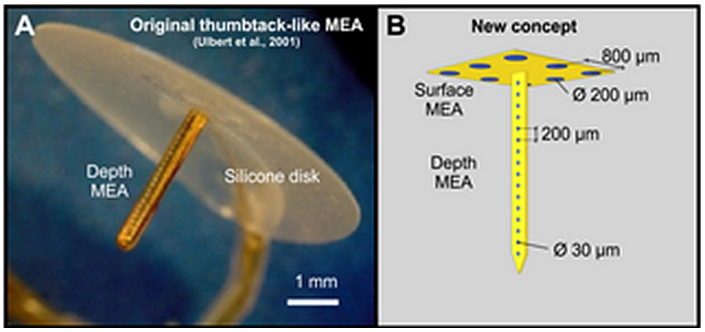

Figure 1 *Design concept.* ***(A)****: The thumbtack electrode, containing a 3 mm long shaft with an array of insulated fine wires and a silicone disk (www.plexon.com).* ***(B)****: Design concept of the multimodal polymer-based MEMS electrode array (reprinted from Márton et al., 2016, PLOS One).*

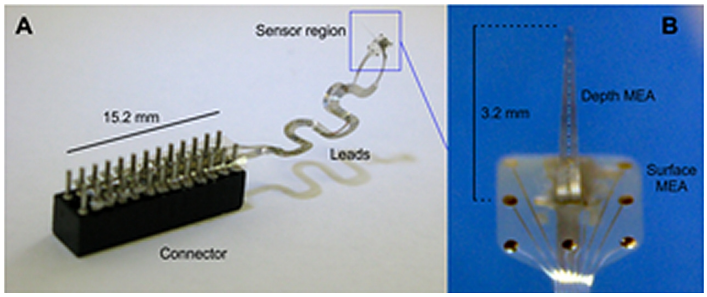

Figure 2 *Photographs of the assembled device.* ***(A)****: Macroscopic view.* ***(B)****: A microscopic image of the sensor region, containing the microelectrodes (reprinted from Márton et al., 2016, PLOS One).*

Neurobiochemical changes in the vicinity of a nanostructured neural implant

Neural interface technologies including recording and stimulation electrodes are currently in the early phase of clinical trials aiming to help patients with spinal cord injuries, degenerative disorders, strokes interrupting descending motor pathways, or limb amputations. Their lifetime is of key importance, however, it is limited by the

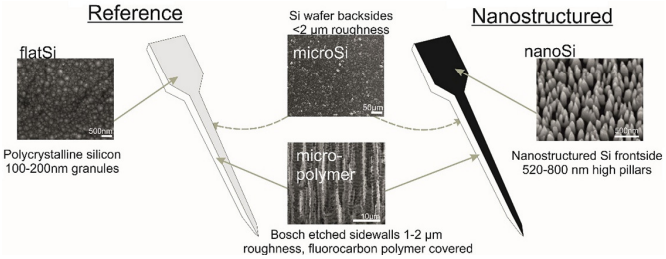

Figure 1 *The two types of fabricated devices are: the one with nanostructured shank (right side) and a reference with polycrystalline Si front-side (left side). The two sidewalls of both devices are microstructured with a fluorocarbon polymer layer on the Si wafer as a result of the Bosch etching step (micro-polymer). The backside of the devices are the non-polished Si wafer (microSi). Front-side of the reference device is a polycrystalline Si layer with 100-150 nm grain size (flatSi), and the front-side of the nanostructured device has 520-800 nm high pillars in a 18-70 pillars/µm^2 density (nanoSi) (reprinted from [8]).*

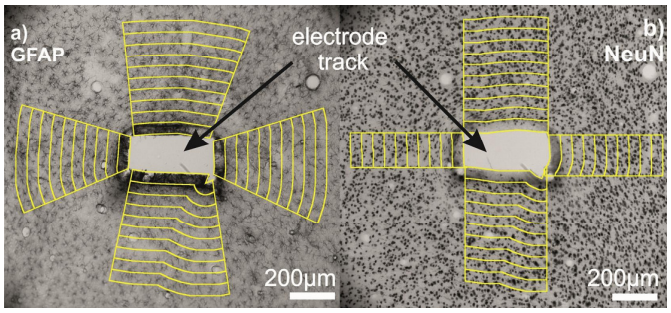

Figure 2 *Light micrographs of the electrode tracks were segmented by a custom made ImageJ macro. From the manually defined track outlines 50 µm wide regions were segmented up to 500 µm along the selected shape of the track. Yellow-edge stripes represent the 50 µm wide manually selected ROIs. Different sides of the electrode track were also selected manually. In the case of GFAP staining (a), average pixel intensities were calculated in each ROI. On the NeuN stained images (b), cell numbers were determined manually in each ROI (reprinted from [8]).*

foreign body response of the tissue causing the loss of neurons and a reactive astrogliosis around the implant surface. Improving the biocompatibility of implant surfaces, especially promoting neuronal attachment and regeneration is therefore essential. In our work, bioactive properties of implanted black polySi nanostructured surfaces (520-800 nm long nanopillars with a diameter of 150-200 nm) were investigated and compared to microstructured Si surfaces in eight-week long *in vivo*

experiments (Fig. 1). Glial encapsulation and local neuronal cell loss were characterized using GFAP and NeuN immunostaining respectively, followed by systematic image analysis (Fig. 2). Regarding the severity of gliosis, no significant difference was observed in the vicinity of the different implant surfaces, however, the number of survived neurons close to the nanostructured surface was higher than that of the microstructured ones. Our results imply that the functionality of implanted microelectrodes covered by Si nanopillars may lead to improved long-term life.

NEMS

Activity leader: J. Volk

Group members: Zs. Baji, A. Békési, G. Battistig, Cs. Dücső, P. Földesy, N. Q. Khánh, I. Lukács, Gy. Molnár, A. L. Tóth, Zs. Zolnai, Z. Szabó, and I. Bársony

Projects:

- OTKA K109674 - Graphene based terahertz modulators (2013-2017)
- OTKA PD116579 - Preparation of ZnO and Ga_2O_3 nanostructures by atomic layer deposition (2015-2018)
- OTKA K112114 - Combined micro-nanotechnology supported by local probe analytical techniques: from pattern formation toward applications (2014-2017)
- FP7-ICT-2013-10 - 611019 - High-resolution fingerprint sensing with vertical piezoelectric nanowire matrices (PiezoMAT) (2013-2016)
- NKFIH-NVKP16 - Korszerű funkcionális anyagok hálózatba szervezhető autonóm érzékelőkhöz (KoFAH)

Piezoelectric based nanowire sensors

The aim of the project is to demonstrate a novel tactile sensor for ultrahigh resolution fingerprint detection using vertical piezoelectric nanowires (NW). Three different configurations have been selected by the project partners: NWs contacted at the side (Option 1), at the bottom with multiple electrodes (Option 2), whereas in Option 3 NWs are sandwiched between top and bottom contacts. ZnO nanowires were grown for all types of chips by MFA (Fig. 1). Research partners at Tyndall, Ireland, succeeded in the fabrication of side-contacts using electron beam induced deposition (EBID) and recorded a significant signal upon nanowire bending. We optimized the fabrication of Option 2 type chip having 8×8 active NWs (Fig. 2(a)). Acrylate based polymer encapsulation was used for strengthening (Fig. 2(b)).
In 2016 we focused on the characterization of these sensors. The static bending tests were carried out by the simultaneous detection of lateral force signal of an AFM and

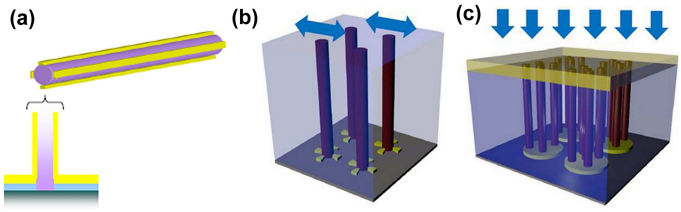

Figure 1 *Targeted contacting schemes: sideways (a), multiple bottom (b), top-bottom (c).*

the source-drain current (Fig. 3). Lateral force signal was calibrated by a vertically mounted compliant AFM cantilever. At first the selected NW was localized in dynamic AFM mode, which was followed by a carefully driven vertical approaching. After reaching a direct contact the AFM tip was pressed against the NW.

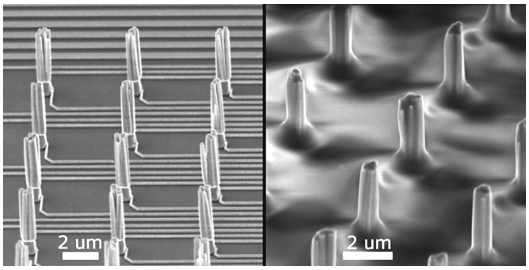

Figure 2 *SEM images of ZnO NWs before and after polymer encapsulation.*

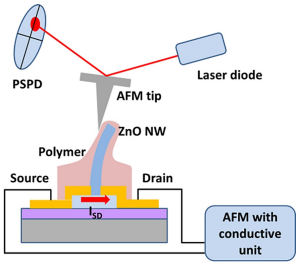

Figure 3 *Schematics of the AFM based NW bending setup.*

Current-voltage curve of the circuit changed significantly upon the influence of the NW bending, as shown in Fig. 4. Time domain cyclic tests carried out at a fix bias voltage have also revealed a strong correlation between the source-drain current and the lateral bending load, which offers itself for novel high resolution tactile imaging sensors having large gauge factor.

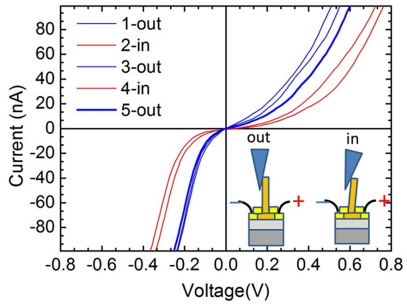

Figure 4 *Current-voltage curves taken at subsequent loading cycles.*

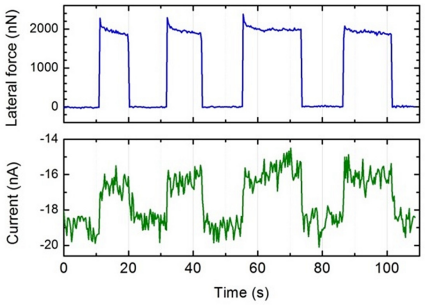

Figure 5 *Time domain measurement of the lateral bending force and source-drain current at a bias voltage of 0.2V.*

In 2017 we plan to extend the AFM tests to reveal the influence of the contact material, the geometry, and the free carrier concentration, besides macroscopic "pressing tests" to study the tactile imaging capabilities of the sensors.

Thin Film Physics Department

Head: Dr. Katalin Balázsi, Ph.D., senior scientist
(from 2016. August 15th)

Research Staff

- Ildikó CORA, Ph.D.
- Zsolt CZIGÁNY, D.Sc.
- László DOBOS, Ph.D. (retired in November, 2016)
- Zsolt FOGARASSY, Ph.D.
- Viktória KOVÁCSNÉ-KIS, Ph.D.
- János LÁBÁR, D.Sc,
- Fanni MISJÁK, Ph.D.
- Béla PÉCZ, D.Sc., MFA director, deputy general director (from July)
- György RADNÓCZI, D.Sc. (Prof. emeritus from November)
- György Zoltán RADNÓCZI, Ph.D.
- György SÁFRÁN, C.Sc.
- Attila SULYOK, Ph.D.
- Péter SÜLE, Ph.D. (left from September)
- Orsolya TAPASZTÓ, Ph.D.
- Lajos TÓTH, C.Sc.

- Árpád BARNA, D.Sc., emeritus inst.
- Péter B. BARNA, D.Sc., emeritus inst.
- György GERGELY, D.Sc., emeritus inst.
- Miklós MENYHÁRD, D.Sc., emeritus inst.

Ph.D. students / Diploma workers

- Erzsébet DÓDONY, Ph.D. student (maternity leave from June)
- Mónika FURKÓ, Ph.D. student
- Klára HAJAGOS-NAGY, Ph.D. student (maternity leave to November)
- Tamás KOLONITS, Ph.D. student
- Nikolett OLÁH, Ph.D. student
- Adél RÁCZ, Ph.D. student
- János SZÍVÓS, Ph.D. student
- Márton SZENDRŐ, Ph.D. student
- Haroune Rashid BEN ZINE, Ph.D. student (Hungaricum stipendium)
- Awais QUADIR, Ph.D. student (from October, Hungaricum stipendium)

Technical Staff

- Noémi SZÁSZ
- Sándor GURBÁN
- Andor KOVÁCS
- István KOVÁCS
- Katalin PUSKÁS (50%)
- Viktor VARGA
- Fenyvesiné Andrea JAKAB
- Valéria OSVÁTH
- Tamás ZAGYVA

The Thin Film Physics Department has been working on several main research subjects in 2016; ceramic coatings and composites, semiconductor layers, polycrystalline layers, high-entropy alloys.
Development of biocompatible coatings on surgical implants was an important research subject. The next topic based on ceramic was the development of ceramic/graphene nanocomposites prepared by powder technology for tribological applications in different aqueous environment. The third main subject was the research of semiconductor layers, heterostructures. A large amount of new

information was collected on how nickel can induce the crystallization of amorphous silicon.
Structure evolution in polycrystalline layers, development of thin coatings, and layers for hard coatings, for magnetic layers and for composites were also studied. As new research topics, development of high-entropy alloys and 316L steel based composites reinforced with ceramic nanoparticles were introduced. The last main field of study was the development of methodology in electron diffraction and on ion-solid interactions.
In 2016, 35 papers were published in refereed journals with a cumulative impact factor of 91, in addition, 6 papers in conference proceedings were published with no impact factor. Members of the group presented 6 invited lectures, 29 oral talks and 18 posters at international conferences. The group received 1587 independent citations in the examined interval of the last two years.
Summarizing other activities, members of the group lectured three courses at universities and four members held laboratory practices, all courses were for full semesters (Eötvös Loránd University (ELTE), Budapest, Budapest University of Technology and Economics (BME), Pannon University (PE), Veszprém). In addition to participants of courses, 10 graduate students were supervised in doctoral courses.
Social activity of the group is landmarked by 15 membership in different committees of the Hungarian Academy of Sciences and in boards of societies, giving two elected representatives to the General Assembly of the Hungarian Academy of Sciences.

New approaches in the development of Hypoallergenic implant material in Orthopaedics: steps to personalized medicine

(EU FP7 "HypOrth", OTKA 105355)

K. Balázsi, N. Oláh, Zs. Fogarassy, V. Varga, T. Sopcák, T. Zagyva, L. Illés,
D. Delfonse (Mathys, Switzerland), C. Lohman (Magdeburg Un., Germany),
J. Lorenzen (Teknologisk Institute, Denmark), M. Ignatiev (INOP, Poland), Cs. Balázsi

Joint replacement is one of the most successful areas in current orthopaedics. Although many improvements have been made, tissue reactions to biomaterials, infection and lacking osseointegration are still the main reasons for the failure of implants and for revision surgery. Various materials - considered as "ideal" to wear resistance (e.g. CoCr-alloys) or "bioinert" (Ti-alloys) – are found to induce adverse tissue reactions or to support biofilms. Patients with a known metal allergy are at a higher risk of developing sensitivity against biomaterials. HypOrth Program helps understanding local adverse reactions around artificial joint replacements and to improve integration of potential hypoallergenic implants with improved biocompatibility.
HypOrth has already developed bioactive implant surfaces including bioceramics. Those surfaces and implant materials are being tested in material tests as well as cell

culture experiments. From these results, prototypes are being designed. A very unique surface coating will be realized by using eggshells and seashells as a source for calcium/ hydroxyapatite coating to enhance osseointegration and mimic biocompatibility. This technology has been proven to be efficient and effective in simulator tests.
It can be assumed that the initiative HypOrth has direct impact on the health of European citizens but also on the technology transfer by stimulating metal forming industries. Already today, the prototype surfaces are expected to show superior properties as compared with existing technologies.

Mechanical characterization and corrosion of protective TiC/amorphous C nanocomposite coating as surface thin film

(Young Research Fellowship of HAS (FIKU), EU FP7 "HypOrth")

N. Oláh, Zs. Fogarassy, A. Sulyok, J. Szívós, T. Csanádi (IMR SAS, Slovakia),
M. Furkó, Z. May (MTA TTK), and K. Balázsi

Ceramic titanium carbide / amorphous carbon (TiC/a:C) protective nanocomposite thin film may be a potential candidate for such a surface protection coating to the different implant materials which serve as barrier layer. Our developments are focused on the biological application of these thin films [www.hyporth.eu].
The main goal of our current research work is to investigate the relationship between mechanical and corrosion properties of the different films. For this purpose, coatings with different structures were developed by co-depositing Ti and C on SiO_2/Si, TiAl6V4 and Titanium wafers (blasted and unblasted) using DC magnetron sputtering system in argon (0.25 Pa) at room temperature. Roughening the surface by sandblasting was applied for better adhesion between the TiC/a:C protective coating and the substrate. The DC magnetron sputtering of TiC/a:C surface thin films on sandblasted (s.b.)/polished Ti and TiAl6V4 substrates showed improved corrosion properties as compared with known implant materials. The comparison of structural changes before and after corrosion tests as well as any release of metal ions was investigated. The mechanical and tribological properties of TiC/a:C nanocomposite coatings on s.b./polished Ti and TiAl6V4 substrates were also examined and compared with those of bare substrates. Hardness (H) of ~ 26 GPa and elasticity (E) of ~220 GPa with μ of ~0.268 was observed in case of the film prepared at ~ 38 at% Ti content which consisted of 4-10 nm width TiC columns separated by 2-3 nm thin a:C layers. The H^3/E^2 ratio was ~0.4 GPa that predicts high resistance to plastic deformation of the C-Ti nanocomposites besides great wear-resistant properties (H/E of ~0.12) [81]. It was also shown, that the hardness and the tribological property of the bare implant materials was improved by four orders of magnitude with application of TiC/a:C nanocomposite coating with a moderate elastic modulus value (Fig. 1.). In the case of this (~38 at% Ti content) TiC/a:C coated s.b. TiAl6V4 alloy, after 10 days

of immersion time its j_{corr} value started to decrease with increasing its Rp value, while the SEM micrograph does not show any special changes of the surface morphologies of the samples after the corrosion tests. It is proved that roughening the surface by sandblasting can enhance the corrosion resistance. However, the presence of V was detectable in each case, the Al and Ti ions have been detained by the TiC/a:C thin film coated s.b. TiAl6V4. The main conclusion of our research is that a ceramic TiC/a:C thin film with ~20 at% a:C and ~38 at% Ti contents would be a suitable choice for a protective nanocomposite coating.

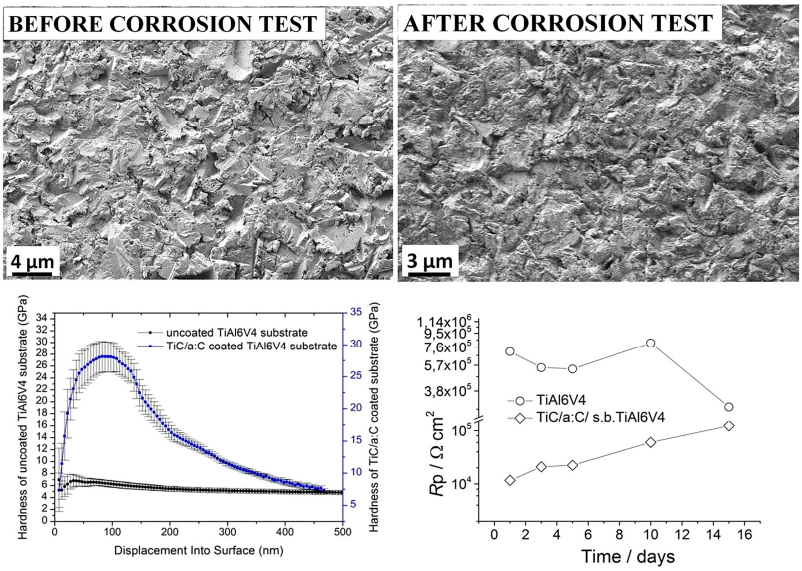

Figure 1 *SEM images about the TiC/a:C/s.b. TiAl6V4 before and after corrosion tests, comparison of the H values of the uncoated with μ of ~0.60 ±0.04 and TiC/a:C coated with μ of ~0.20 ±0.07 TiAl6V4 substrate and Rp values of TiC/a:C coated and uncoated s.b. implant materials derived from potentiodynamic curves depending on the immersion time.*

Development and characterization of multi-element doped hydroxyapatite coatings on metallic implant materials

(Young Research Fellowship of HAS (FIKU))

M. Furkó, and Cs. Balázsi

The research scope is to develop coatings onto implant materials which possess simultaneous antimicrobial and biocompatible properties. The coatings were prepared by pulse current deposition method. The coatings were also doped with silver (Ag) zinc (Zn) magnesium (Mg) and strontium (Sr) elements either with co-deposition or with surface post-treatment with solutions containing the corresponding element. The

basic electrolyte solution contained $Ca(NO_3)_2$, NH4H2PO4 and H_2O_2 at pH 4.3 at 70 °C. Since the as-deposited calcium phosphate coating is mainly in Monetite phase, after deposition, the samples were immersed into 1 M NaOH solution at 70 °C to achieve phase transformation into Hydroxyapatite phase. The biodegradable properties of the layers were evaluated by electrochemical tests in simulated body fluid (SBF) at temperature of 37 °C. Electrochemical Impedance Spectroscopy (EIS) measurements were performed also to test the samples' corrosion stability. All the electrochemical tests were carried out using a classical three-electrode cell with platinum as counter electrode, using saturated calomel electrode SCE as reference electrode and the samples themselves as working electrode. The surface morphologies and grain size of samples were also observed by SEM measurements (Figs. 1 and 2). These materials, which are reached already at low graphene contents, offer the possibility to reduce efforts in manufacture and to create new functionalities that may be utilized for technical applications.

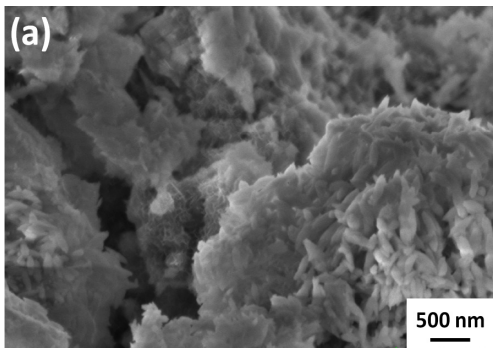

Figure 1 *SEM images of multi-element doped HAp.*

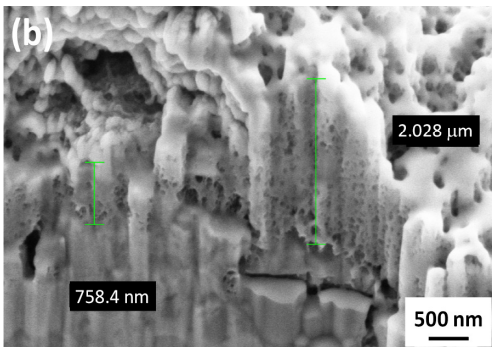

Figure 2 *Cross sectional analysis of coating by SEM/FIB measurement.*

Graphene-ceramic composites for tribological application in aqueous environments

(OTKA M-ERANET "Grace")

Cs. Balázsi, Zs. Fogarassy, V. Varga, M. Knoch (FCT), J. Dusza (IMR SAS, Slovakia), A. Kailer (IMW Franhoufer, Germany), and K. Balázsi

There is a strongly growing demand for high wear resistant and reliable ceramic materials that may be widely used in industrial applications and in energy production. Special attention is paid to components to be used under severe conditions and lubricated by the surrounding media which is mainly aqueous. Reliability and efficiency of these components need to be improved by using high performance ceramics with superior tribological (low friction, high wear, and corrosion resistance) and mechanical (fracture toughness, strength) properties.

The main aim of this work was development of novel, highly efficient tribological systems on the basis of ceramic/graphene nanocomposites, to prove their superior quality, and to demonstrate their suitability for technical applications, e.g., for slide bearings and face seals in aqueous media. The ceramic nanocomposites show that it is possible to prepare ceramic materials with improved mechanical and tribological properties by incorporating graphene into the Si_3N_4 structure using different sintering methods. Multilayered graphene (MLG) was prepared by attritor milling at 10 hours intensive milling of graphite powder with few micrometer size. The rather large quantity, cheap and rather quick preparation process are main strengths of our MLG technique. The Si_3N_4 / MLG nanocomposites were prepared by attritor milling and sintered by hot pressing (HP, Fig. 1), or hot isostatic pressing (HIP, Fig. 2) and with spark plasma sintering (SPS, Fig. 3). The Si_3N_4 ceramics were produced with 1wt%, 3wt%, 5wt% and 10wt% content of MLG. The tribological behavior of composites in different environment was investigated and showed the decreasing character of wear with increased MLG content. This new approach is very promising, since ceramic microstructure can be designed with high toughness and provide improved wear resistance at low friction.

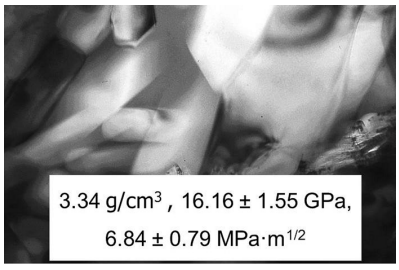

Figure 1 *Si_3N_4/MLG prepared by hot press (HP).*

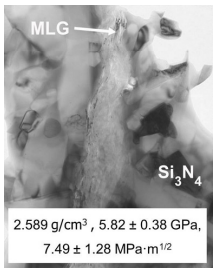

Figure 2 *Si_3N_4/MLG prepared by hot isostatic press (HIP).*

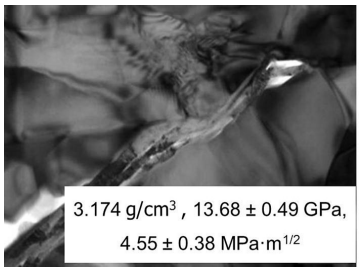

Figure 3 *Si_3N_4/MLG prepared by spark plasma sintering (SPS).*

In all composites, densities between 97 and 100 % were obtained (as compared to fully densified reference Si_3N_4). The alpha-Si_3N_4 to beta-Si_3N_4 phase transformation was completed during hot pressing. The structural investigations and phase analysis measurements confirmed the presence of MLGs in all composites after the sintering process. The presence of very fine nanostructred zirconia on the silicon nitride grains is the effect of high efficient milling process. Vicker hardness (HV) values decreased with increasing of MLG content from 18.86 GPa to 9.69 GPa. The small increase to 18.86 GPa of HV at 1wt% MLG content in comparison to 17.01 GPa reference Si_3N_4 might be attributed to smaller grain sizes. The results show that improved tribological properties, more stable frictional behaviour and a significant increase of the wear resistance at MLG contents beyond 5 wt% can be achieved in case of composites sintered by HP.

Improving the tribological performance of ceramic composites by a continuous few-layer graphene tribo-film

(Bolyai János Research Grant; OTKA PD 121368)

O. Tapasztó, J. Balko (Slovak Academy of Sciences-SAS), V. Puchy (SAS), J. Dusza (SAS), P. Kun, and L. Tapasztó

Graphene nanoplatelets (GNPs) are regarded as a particularly promising nanoscale filler material for various composites. Improvement in the tribological properties of ceramic composites could be achieved. Here, we propose to employ a novel mechano-chemical method, based on the ball milling of graphite with melamine addition to increase the exfoliation efficiency, but without chemically modifying the resulting few-layer graphene sheets. We have prepared Si_3N_4 composites reinforced by these ultra-thin few-layer graphene nanoplatelets (FL-GNPs) using the Spark Plasma Sintering method. We found that the composites prepared with only 5wt% of FL-GNPs are characterized by more than 20 times increased wear resistance, while their friction coefficient is reduced to nearly its half, as compared to monolithic Si_3N_4 (Fig. 1).

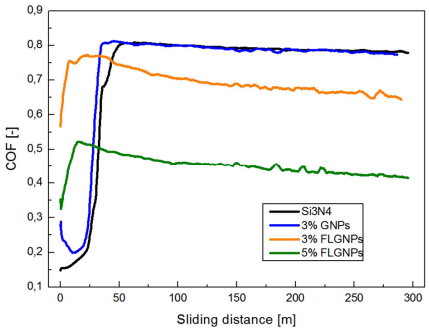

Figure 1 *Composites with 5wt% of FL-GNP addition display a highly-reduced friction coefficient.*

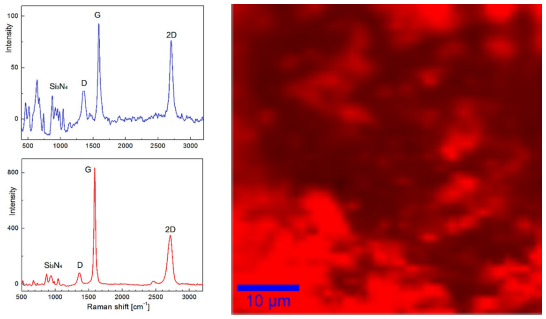

Figure 2 *Raman spectroscopy map of the graphene G peak* ***(a)*** *indicating a continuous few-layer graphene covarage of the wear track* ***(b)****.*

By confocal Raman spectroscopic mapping of the wear tracks we have shown that this outstanding improvement in the tribological properties can be attributed to the formation of a continuous protecting and lubricating tribo-film consisting of FL-GNPs of high structural quality (Fig. 2). There are key technological advantages in developing highly wear-resistant and low-friction ceramic composite materials. Components produced from such materials enable a substantial reduction of losses during operation, as well as a significant increase of their durability.

Developing an improved production technology for the ceramic block of the PorTL dosimeter system

(MTA EK project)

K. Balázsi, Zs. Fogarassy, S. Gurbán, V. Varga, Cs. Balázsi, I. Apáthy, A. Csőke, T. Pázmándi, P. Szántó, B. Zábori, and A. Hirn (MTA EK AEKI)

The portable thermoluminescent dosimeter (TLD) system PorTL consists of several dosimeter cells of compact and robust design and a light-weight battery-powered TLD reader. The TL block inside the PorTL cells consists of a ceramic plate with a miniature heater fixed on one side and a thermocouple and the Al_2O_3:C TL tablet on the other side. An improved production technology of the ceramic block has been developed based on attritor milling and hot isostatic pressing (HIP) using a novel Si3N4 ceramic nanocomposite material. The main objective was to decrease the manufacturing lead time of the PorTL cells and to extend the lifetime of the TL block (Fig 1).

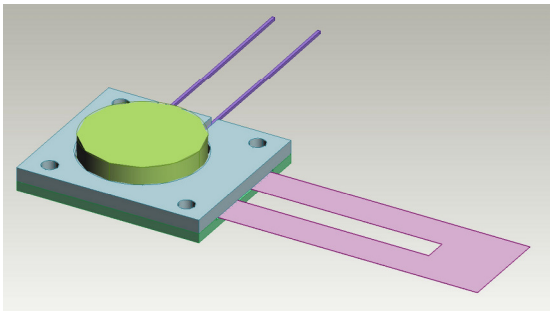

Figure 1 *The novel design of the PorTL block; the ceramic plates are prepared with HIP technology.*

Five of the ceramic materials tested had significant radioactive background radiation probably due to their potassium (^{40}K) content; only the Si_3N_4 ceramic nanocomposite material was found to be suitable for using as basic material of the TL block.
Since the sensitivity of Al_2O_3:C TL tablet dropped significantly after heating it at 1700 °C, the technology to produce the TL block was split into two: 1) production of ceramic components and 2) integration of the heater, the thermocouple, and the TL tablet into the block.

The advantages of this approach are:

- the use of Si_3N_4 material and the corresponding technology (HIP), with which the MTA EK MFA has already extensive experience;
- the manufacturing of the tools needed for the production of the ceramic block is relatively simple;
- much less work hours required than in the case of the original technology;
- shorter manufacturing lead times.

Graphitic films of group III nitrides and group II oxides: platform for fundamental studies and applications

(FLAG-ERA, MTA Postdoctoral Fellowship and bilateral scientific agreement between CNR and MTA)

I. Cora, L. Tóth, B. Pécz, R. Yakimova (IFM Sweden), A. Kakanakova (IFM Sweden), and F. Gianazzo (CNR-IMM, Italy)

In this cooperative project, range of structural and material properties of innovative van der Waals heterostructures of group III nitrides (AlN, GaN, and InN) with graphene and ultrathin graphitic films of group III nitrides was explored. MOCVD of AlN (Fig. 1) and GaN was performed in Linköping onto epitaxial graphene on 4H-SiC substrates within the temperature range of 1100-1410 °C, and with sequential introduction of precursors. Graphene templates were predominantly one monolayer, whereby a buffer layer exists at the interface with the SiC substrate.

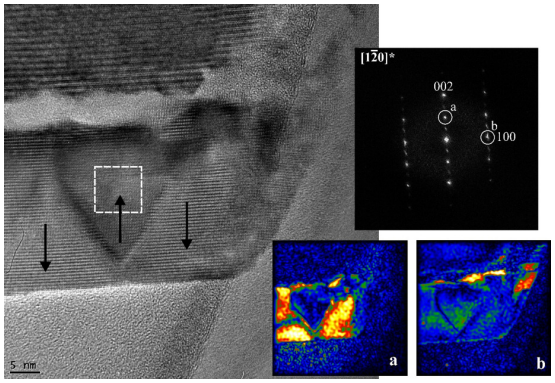

Figure 1 *HRTEM and FFT images show that AlN grows onto the substrate epitaxially and voids between them are common. Geometric phase maps calculated by the two reflections show that the layer is inhomogeneous and it grows in 3D.*

In our lab, structural characterization of the samples by TEM and AFM was performed. Raman characterization of the layers was done by the colleagues in Catania. With the TEM study of the work we could demonstrate how the growth parameters influence/affect the quality of the nitride layer and the stability of the graphene.

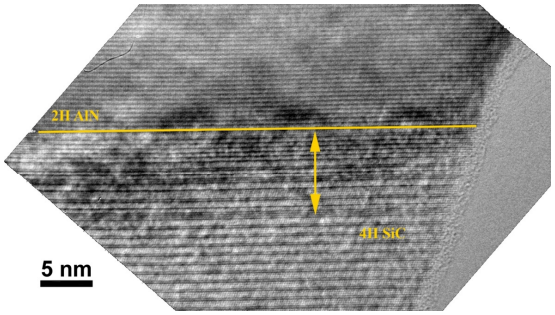

Figure 2 *HRTEM image of the AlN-SiC interface grown at 1410 °C. The 4H SiC show stacking disorder at the top and the AlN grows onto it epitaxially, while graphene diminishes from the interface.*

At 1410 °C the top surface of the SiC substrate shows stacking disorder, and the AlN grows epitaxially onto it, while the graphene layer diminishes (Fig. 2). Voids between the SiC and the AlN are common if the substrate is pre-treated by H_2/NH_3. At 1240 °C the AlN grows onto SiC with epitaxial orientation (Fig. 3). The AlN crystals grow in islands and at their coalescence threading dislocations are common. Graphene diminishes again. At 1100 °C graphene is still stable, but the layer is polycrystalline (Fig. 4).

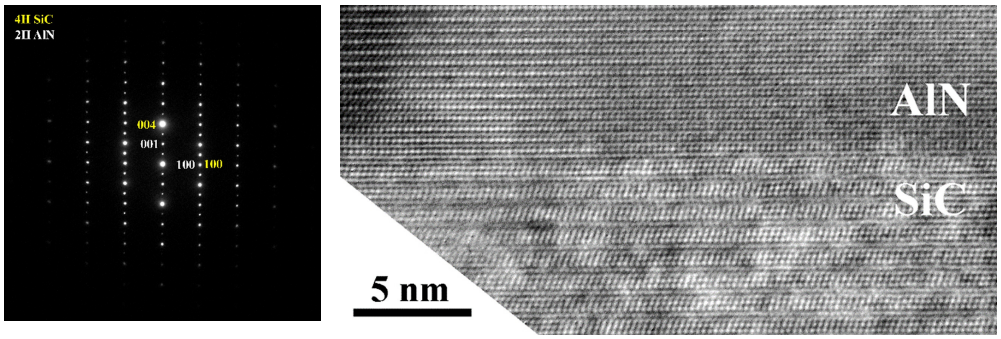

Figure 3 *HRTEM and SAED patterns show that AlN epitaxially grows onto the 4H SiC at 1240 °C, but graphene still lacks from the interface.*

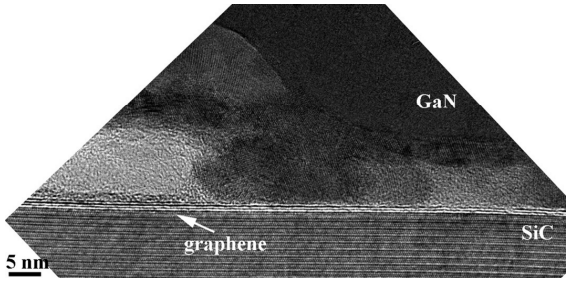

Figure 4 *HRTEM image of the sample grown at 1100 °C. Graphene remained at the interface, but the GaN layer is polycrystalline.*

TEM study of the as-deposited and annealed Ga_2O_3 films grown by vapor phase epitaxy

(MTA Postdoctoral Fellowship and bilateral scientific agreement between CNR and MTA)

I. Cora, B. Pécz, F. Mezzadri, F. Boschi, M. Bosi, R. Fornari (IMEM-CNR, Parma, Italy), M. Čaplovičová (STU, Bratislava, Slovakia), and I. Dódony (ELTE)

Ga_2O_3 is a wide bandgap semiconducting oxide (~4.7 eV), promising for UV optoelectronics and power electronics. Ga_2O_3 layers were grown onto (001) surface of α-Al_2O_3 by vapor phase epitaxy at 650 °C and were annealed at 1000 °C for 2 and 6

hours. The as-deposited layers and the two annealed samples were studied by high resolution transmission electron microscopy and X-ray diffraction.
Previous XRD studies on the as-deposited film showed that these films are single crystal epitaxial layers and exhibit hexagonal $P6_3mc$ space group symmetry, characterized by partial occupation of the Ga sites, which corresponds to the ε phase, -with disordered Ga atoms in the structure. In the present work detailed TEM studies allowed to investigate the real structure of this phase at the nanoscale (Fig. 1). The structure is ordered in 5-10 nm large (110)-twinned domains, and each domain has an orthorhombic structure with $Pna2_1$ space group symmetry, called κ-Ga_2O_3. This phase is a new polymorph among the Ga-oxides. Parallel XRD analysis carried out on thicker samples (9-10 μm) confirmed the same results, and permitted to provide the refined structural parameters.

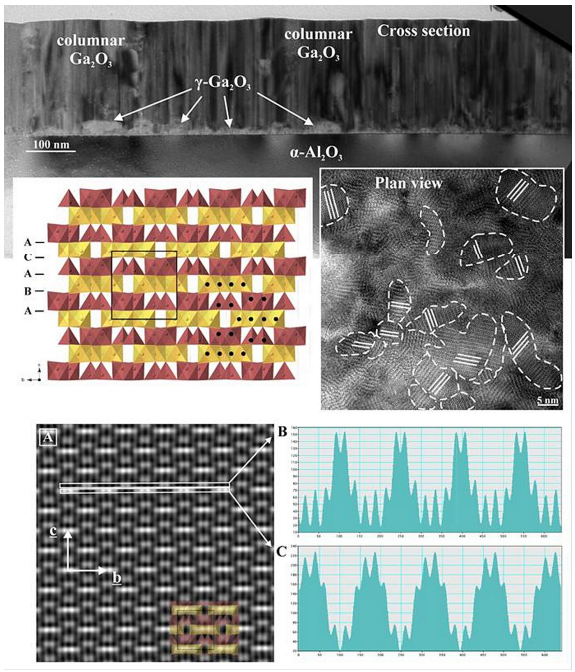

Figure 1 *TEM images of the cross section and the plan view TEM specimens of the as-deposited layers with the corresponding crystal structure of κ-Ga_2O_3. The structure is textured consisting of 5-10 nm large (110)-twinned orthorhombic domains. STEM image (at the bottom) with the corresponding line scans shows the Ga atoms in [102] projections. Spurious peaks are due to overlapping of the twin domains.*

The crystal structure of these Ga_2O_3 layers consists of an ABAC oxygen close-packed stacking, where Ga atoms in between occupy octahedral and tetrahedral sites forming two types of polyhedral layers parallel to (001). The edge-sharing octahedra and the corner-sharing tetrahedra form zig-zag ribbons along the [102] direction. Anti-phase boundaries are common inside the domains. The polar character of the structure is confirmed, in agreement with the characteristics of the $Pna2_1$ space group and explaining the ferroelectric nature measured earlier.
At 600-700 °C degree the sample starts to transform to β-Ga_2O_3. The duration of the thermal treatment at 1000 °C strongly influenced the crystallinity of the samples: while for a 2 hour annealing the sample was found to be polycrystalline and strongly textured, the sample annealed for 10 hours was almost single crystalline. The sample that was annealed for 2 hours, consists of pure β-Ga_2O_3. The layer is polycrystalline

and strongly textured: [-201] direction of each β-Ga_2O_3 crystal is perpendicular to the (001) of α-Al_2O3.
The 10 hours-long annealed sample is pure β-Ga_2O_3 and almost single crystalline: β-Ga_2O_3 grow onto the α-Al_2O_3 with epitaxy: (310)/[-13-1] β-Ga_2O_3 ‖ (001)/[1-10] α-Al_2O_3. The upper part of the layer grows with epitaxy but with a different orientation: (310)/[-130] β-Ga_2O_3 ‖ (001)/[1-10] α-Al_2O_3.

Highly Safe GaN Metal-Oxide-Semiconductor Transistor Switch (SAFEMOST)

(Hungarian National Scientific Foundation (OTKA) NN 118201

L. Tóth, I. Cora, B. Pécz, M. Tapajna (IEE SAS), J. Kuzmik (IEE SAS), B. Adamowicz (Silesian University of Technology), and T. Hashizume (Hokkaido University)

The present project started in 2016 is part of a multinational Slovakian-Japanese-Polish-Hungarian research project which was granted in the frame of the JST-V4 call of proposals. The research within the consortium is financed by the four national funding organizations as well as the International Visegrad Fund (IVF). The main goal of this project is to develop a GaN based metal-oxide-semiconductor (MOS) structure with a sufficiently low density of surface donor states at the gate-oxide/heterostructure interface thus allowing the realization of normally-off switching devices and decreasing conversion losses in electronics. Our Slovakian colleagues at IEE SAS manufactured several samples consisting of very thin gate dielectric layers prepared by various deposition techniques onto standard GaN/AlGaN/GaN heterostructures serving as substrates. All these layers were made of Al_2O_3 but the way of deposition varied from low temperature atomic layer deposition (ALD) using several precursors to a high temperature metalorganic chemical vapor deposition (MOCVD) process. The samples were studied by a complex way by the participants of the consortium. Electrical characterization and X-ray studies were performed in Bratislava, photo-capacitance investigation, Auger electron spectroscopy and photoluminescence in Gliwice, Poland, while XPS studies and modeling of the processes in Sapporo, Japan.
Our task in this cooperation was the structural characterization of the heterostructures, particularly of the dielectric film deposited on the top surface by means of transmission electron microscopy. In the first series of experiments Al_2O_3 layers deposited by ALD with different conditions were studied. These dielectric films were proved to possess somewhat higher density of surface donor states and so were regarded as less suitable for the required parameters than e.g. MOCVD deposited dielectrics. We have observed, however, that all these ALD layers show a crystalline microstructure – even those deposited as low as at 100 °C (Fig. 1). Also the study of MOCVD deposited dielectric layers has been started and will be continued next year.

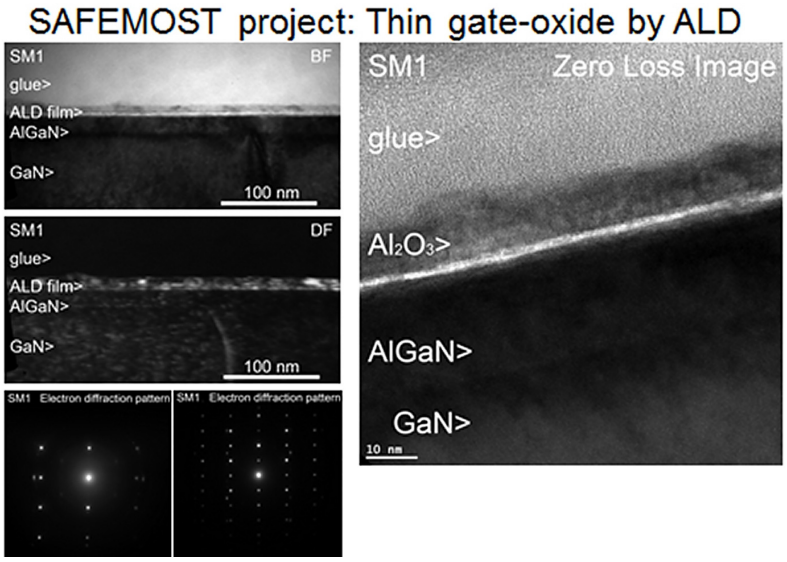

Figure 1 *Bright field and dark field micrographs (left) and high resolution image (right) of a 10 nm thick gate dielectric layer grown by atomic layer deposition (ALD) at 100 °C. The Al_2O_3 film was found crystalline as shown on the electron diffraction patterns below.*

Inclusions in Si whiskers obtained in metal (Ni) induced lateral crystallization of amorphous Si thin films

(TÉT-10-1-2011-0570, ESTEEM2-Graz)

Gy. Z. Radnóczi, E. Dodony, G.Battistig, B. Pécz, I. Stoimenos, N. Frangis, N. Vouroutzis (AU, Thessaloniki), D. Knez, and F. Hofer (TU Graz)

The crystalline silicon obtained in metal induced crystallization was further characterized based on the results from recent years. Si whiskers were investigated in detail to gather data on the tetrahedral $NiSi_2$ inclusions found in the whiskers earlier. Based on geometrical considerations and literature data a theoretical prediction was made on the atomic configuration of the $Si/NiSi_2$ interface that needed to be confirmed experimentally. High resolution STEM-HAADF images were taken on a spherical aberration corrected TEM to locate the Ni containing atomic columns inside the inclusions and determine their relative position to the Si lattice (Fig. 1(a)).
Based on the images taken on the lattice exactly aligned to the [110] zone and image simulation results (Fig. 1(b)) we identified the type Ia interface (Fig. 1(c)) in agreement with our prediction. The results also lead to the conclusion that the inclusions cannot form as precipitates during cool down as the amount of Ni inside the inclusions exceeds the solubility limit by several orders of magnitude. It is likely

that inclusions form during whisker growth at the leading edge of the whisker by trapping $NiSi_2$ from the $NiSi_2$ cluster leading the whisker growth.

The research leading to these results has received funding from the European Union Seventh Framework Programme under Grant Agreement 312483- ESTEEM2 (Integrated Infrastructure Initiative–I3).

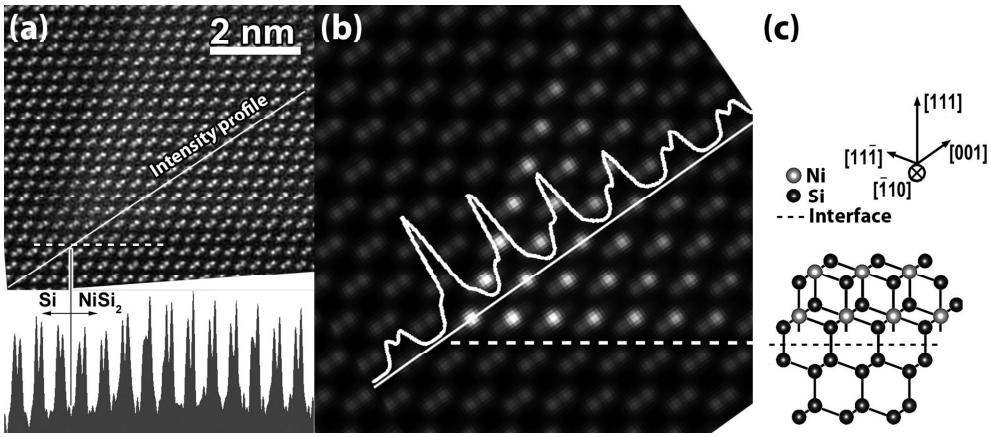

Figure 1 ***(a)****: noise filtered STEM –HAADF image of a $NiSi_2$ inclusion. The sample is viewed along the [110] direction.* ***(b)****: Simulated image of the same structure giving the same type of asymmetric dumbbells* ***(c)****: model of the identified atomic configuration at the interface.*

A comparative study of direct current magnetron sputtering (DCMS) and high power impulse magnetron sputtering (HiPIMS) processes for CN_x thin film growth with different inert gases

S. Schmidt (LiU), Zs. Czigány, J. Wissting (LiU), G. Greczynski (LiU), E. Janzén (LiU), J. Jensen (LiU), I. G. Ivanov (LiU), and L. Hultman (LiU)

Reactive DCMS and HiPIMS discharges of C in N_2/Ne, N_2/Ar, and N_2/Kr were investigated by positive ion mass spectrometry [107] in cooperation with Linköping University (LiU). The cation energies depend on the type of inert gas and the amount of N_2 in the sputter gas mixture. The sputter mode gains major significance with regards to the ionization of species originating from the target relative to the ionization of the sputter gases. HiPIMS processes yield approximately ten times higher flux ratio of ions originating from the target compared to those originating from the process gas (Fig. 1). For the case when graphite is sputtered in N_2/Ne mixtures containing up to ~20% N_2, the influence of the sputter mode on cation energies and degree of ionization was insignificant.

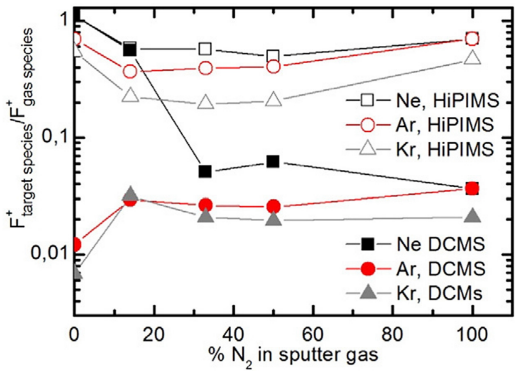

Figure 1 *Sum of the total ion flux of species originating from the target in relation to the sum of process gas ion species over the amount of N_2 in the inert gas for DCMS and HiPIMS discharges.*

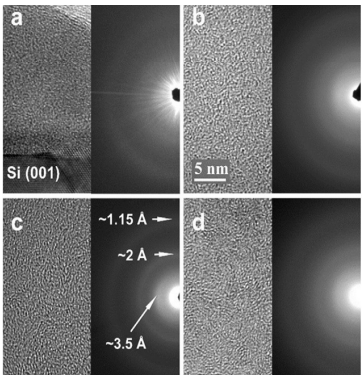

Figure 2 *Cross-sectional HRTEM images with corresponding SAED patterns of CN_x thin films deposited in Kr/14% N_2 by **a**): DCMS at T_s=110 °C, **b**): HiPIMS at T_s=110 °C, **c**): DCMS at T_s=430 °C, and **d**): HiPIMS, T_s=430 °C.*

The structure of the films deposited in 14% N_2/noble gas mixtures was investigated by transmission electron microscopy (TEM). It is shown that reactive DCMS and HiPIMS discharges using 14% N_2/noble gas mixtures at a substrate temperature of 430 °C produce graphitic or fullerene-like CN_x thin films, with one exception: the reactive HiPIMS discharge in N_2/Ne yields an amorphous structure. At a low substrate temperature of 110 °C the synthesized films are amorphous, only the CN_x film deposited by HiPIMS in reactive N_2/Kr atmosphere shows a weak graphitic short range ordered microstructure (Fig. 2).

A characteristic process in reactive sputtering of CN_x films is chemical sputtering which is described as the dynamic adsorption and desorption of plasma species at the substrate, where dangling C or CN bonds get passivated and structure-defining C_xN_y (x,y≤2) species adsorb, thus contributing to the film growth, additionally volatile C_xN_y (x,y≤2) clusters lift off. Therefore, high deposition rates and particle energies may counteract the formation of a fullerene-like structure. The structural evolution of CN_x thin films sputtered in HiPIMS mode was more pronounced, even though higher ion energies were measured for corresponding HiPIMS processes. The result suggests the occurrence of a pulse-assisted chemical sputter process not only at the substrate, but also at the target resulting increased number of sputtered C_xN_y (x,y≤2) species.

The film properties show a correlation to the substrate temperature, the applied inert gas and sputter mode. The mechanical performance of the films is mainly governed by their morphology and composition, but not by their microstructural short range order. Amorphous and fullerene-like $CN_{0.14}$ films (Fig. 2) exhibiting a hardness of ~15 GPa and an elastic recovery of ~90% were deposited at 110 °C in reactive Kr atmosphere by DCMS and HiPIMS.

FePt nanoparticles; colloid chemistry towards catalysts and magnetic recording media

A. Horváth, F. Somodi, A. Deák, and G. Sáfrán

In frame of an "Home-financed Project" of the Centre of Energy Research, a co-operative work of MFA and Institute for Energy Security and Environmental Safety, was carried out with the aim of preparation of FePt nanoparticles with fct ($L1_0$) structure and its testing (1) if they can be applied as catalyst for dry reforming of methane and (2) can we put FePt nanoparticles on a surface as separate and self-organized layer? The FePt particles after synthesis are, usually, paramagnetic and show fcc structure. Suitable annealing, however, may transfer the fcc phase to fct in which Fe and Pt are organized into discrete atomic rows (superlattice) and the alloy exhibits high magnetic anisotropy. The FePt nanoparticles have been synthesized in both aqueous (aq) and organic (org) media using reducing agents and precursors. On one hand, the FePt particles were deposited onto oxide substrates, on other hand they were encapsulated in silica shell and put on carbon coated TEM microgrid.

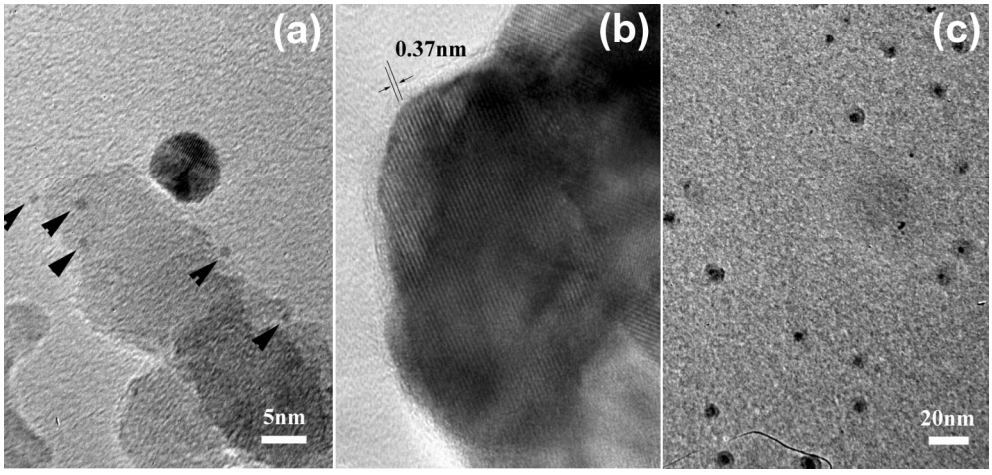

Figure 1 ***(a)****: TEM micrographs of FePt_org/Al_2O_3 TEM after 500 °C reduction;* ***(b)****: FePt aggregate with 0.37 nm period characteristic to the (100) lattice of L10,* ***(c)****: 2-5 nm size FePt particles in SiO_x shell (FePt_aq sample).*

The former samples were annealed in inert gas (5%H_2/Ar) atmosphere at 500 °C, while the latter were heat treated by means of UV excimer laser pulses. The function of the silica coating was the protection against oxidation and the separation of elemental magnets from each other. The ratio of the two constituting component was measured by EDS. The microstructure was characterized by TEM and HRTEM in the as deposited and in the heat treated state. The size of the FePt_org particles after 500 °C reduction treatment was non-uniform (Fig. 1(a)), while FePt_aq particles showed homogeneous size distribution. Based on their stability on Al_2O_3 and ZrO_2 substrates FePt_aq samples are promising candidates as catalysts in dry reforming of

methane. In nano-size particles it was not the case but in large FePt agglomerates the L10 ferromagnetic phase could be produced and observed (Fig. 1(b)) suggesting that the fcc phase was stabilized by small size and interaction with the substrate. It was possible to form the silica shell around FePt_aq nanoparticles prepared in aqueous media (Fig. 1(c)), however, the identification of developed phases due to laser treatment and the self-organization of silica-coated particles needs further studies.

A versatile nanopatterning technique using RF plasma etching through Langmuir-Blodgett films

J. Szívós (MTA EK MFA, Pannon University), M. Serényi, Sz. Pothorszky, G. Vértesy, and G. Sáfrán

The nanoscale modification of materials has attracted wide research interest recently. In a Ph.D. work a cheap and fast technique was proposed in 2014 [J. Szívós et al., Vacuum 109, 200 (2014)] to produce ordered nanopatterns directly for nanolithography and for nanoimprinting. This technique applies a monolayer of self-assembled silica nanospheres (Langmuir-Blodgett (LB) film) as a template and the sample surface is treated by a single UV laser (λ=248 nm) pulse through the LB film that results in nanocraters.

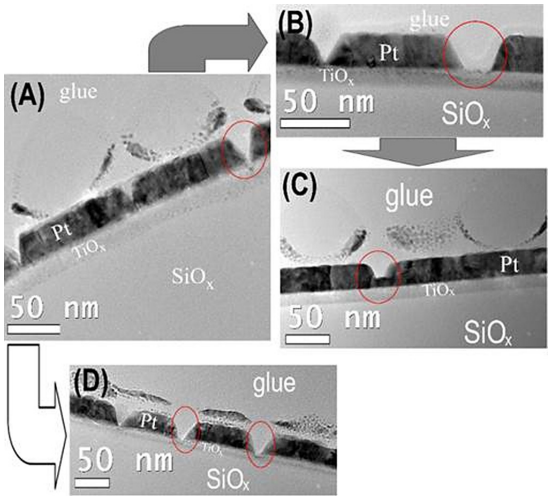

Figure 1 *Typical cross sectional (X-) TEM images of Pt samples RF plasma etched for 100 s,* ***(a)****:* U_{DC}*=1200 V and* P_{Ar}*=2.5*10^{-2} *mbar – 'basic settings';* ***(b)****:* U_{DC}*=1000 V and* P_{Ar}*=2.5*10^{-2} *mbar;* ***(c)****:* U_{DC}*=800 V and* P_{Ar}*=2.5*10^{-2} *mbar;* ***(d)****:* U_{DC}*=1200 V and* P_{Ar}*=2*10^{-2} *mbar.*

We could pattern Al-oxide but UV laser patterning was hardly effective for metal surfaces: the (quasi-)free electrons thermalize the lattice, thus the energy is absorbed nearly uniformly [M. S. Brown, C. B. Arnold: Springer Series in Materials Science Volume 135, 91-120 (2010)]. The next aim was to find a suitable solution for nanoscale patterning metallic, as well magnetic layers for increasing the capacity of FePt or CoPt magnetic layers by realizing Bit Patterned Media (BPM). In 2016 a technique to nanopattern diverse materials was introduced based on RF plasma

etching through the LB film [J. Szívós et al., Surf. Coat. Technol. 313, 115-120 (2017)]. The LB film-covered sample is placed at the „target" position of the RF sputtering source and is subjected to ~1 kV Ar plasma. The nanospheres of the LB film protect the surface and sputtering takes place between them. This way the hexagonal pattern can be replicated to almost any material's surface provided that the plasma parameters are set properly. The feature size is determined by the diameter of the nanospheres that, in principle, can be decreased to about 10 nm. Moreover, our technique can be easily scaled-up by using industrial RF sputterers. The operation of our technique was presented by nanopatterning Pt thin films. The etching time was fixed as 100 s in the experiments mentioned here. The effect of changing so-called DC wall potential (U_{DC}) and the pressure of the sputtering (Ar) gas (P_{Ar}) – is depicted in Fig. 1. Fig. 1(a) is the reference ('basic settings'), where U_{DC}=*1200 V* and P_{Ar}=*2,5*10*$^{-2}$ *mbar*. In Fig. 1(b) and Fig. 1(c) U_{DC} is set to *1000 V*, or *800 V*, respectively, at fixed P_{Ar} and etching time. The effect of setting P_{Ar} to *2*10*$^{-2}$ *mbar* (i.e. decreasing it by 20±1%) with the same U_{DC} and etching time is seen comparing Fig. 1(a) and Fig. 1(d). It can be concluded that lowering of U_{DC} yields in shallower pattern depth, but in turn, lowering P_{Ar} by 20% causes no remarkable effect. This result can be quantitatively verified by investigating the replicas of LB-film imperfections in the patterned Pt films (marked by the red circles in Fig. 1).

Moreover, versatility of our technique was demonstrated by fabricating ordered hexagonal nanopatterns in polycrystalline metal (Ti besides of Pt), single crystalline semiconductor (Si) and insulating oxides (AlO_x, SiO_x) and it worked well regardless of crystal structure and electrical properties. As an example, Fig. 2 shows X-TEM and plan view SEM image of the successfully nanopatterned AlO_x (Fig. 2(a) and Fig. 2(b)), and Si sample (Fig. 2(c) and Fig. 2(d)), respectively.

At the end of 2016, CoPt ($L1_0$) thin films were nanopatterned and the microstructural and magnetic properties will be investigated in a collaboration with the *Technical University of Tokyo*. We intend to show that an alternative implementation of Bit Patterned Magnetic Media is feasible by means of the technique described here.

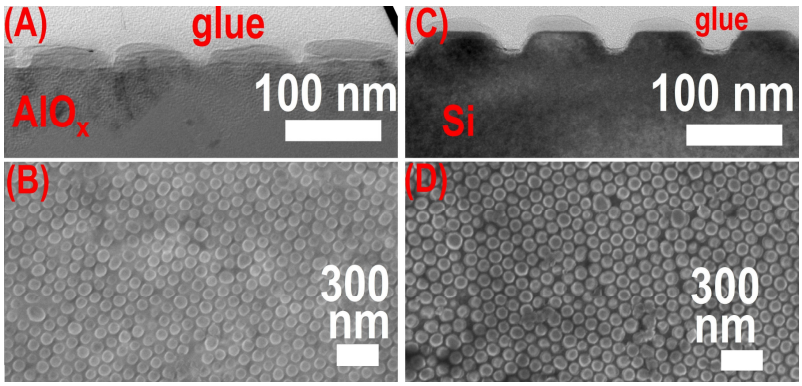

Figure 2 *Typical images of AlO_x (**(a)**: XTEM and **(b)**: SEM image) and Si (**(c)**: XTEM, **(d)**: SEM) samples nanopatterned by our RF plasma etching technique.*

Characterization of defect structure, mechanical properties and stability of electrodeposited nanocrystalline Ni films

T. Kolonits, Zs. Czigány, P. Jenei (ELTE), S. Zsurzsa (Wigner), J. Gubicza (ELTE), L. Péter (Wigner), and I. Bakonyi (Wigner)

The effect of various organic additives on the defect structure and mechanical properties of electrodeposited Ni films was investigated by X-ray diffraction (XRD) line profile analysis (eCMWP model) and transmission electron microscopy (TEM). The main task of the project is to investigate the effect of the additives on the grain structure and defect (dislocation and twin) density which influence the macroscopic properties and application of the layers.

The electrodeposited layers were deposited at room temperature at low current density onto various substrates (Al_2O_3, Cu, Si). The basic electrolyte mainly contained nickel sulfate ($NiSO_4 \cdot 7\ H_2O$) and boric acid (H_3BO_3).

XRD and TEM grain size and phase analysis was carried out to determine the microstructure (Fig. 1). Hardness, wear and friction tests were made to examine the mechanical properties. Heat treatment (near the melting point) was also applied to investigate the stability of the micro and macro properties.

According to our previous research [50] in the film deposited without additives, a columnar structure was observed, textured into direction <220>. Varying the additives in the bath and/or the substrate material, various microstructures were observed: textured (both in direction <220> or <200>), non-textured, twinned, ultra fine grained and nanocrystalline etc. Hardness and wear was related to the microstructure both before and after heat treatment. One of the additive-substrate combinations (trisodium-cytrate deposited on Cu substrate as cathode) showed outstanding hardness and thermal stability.

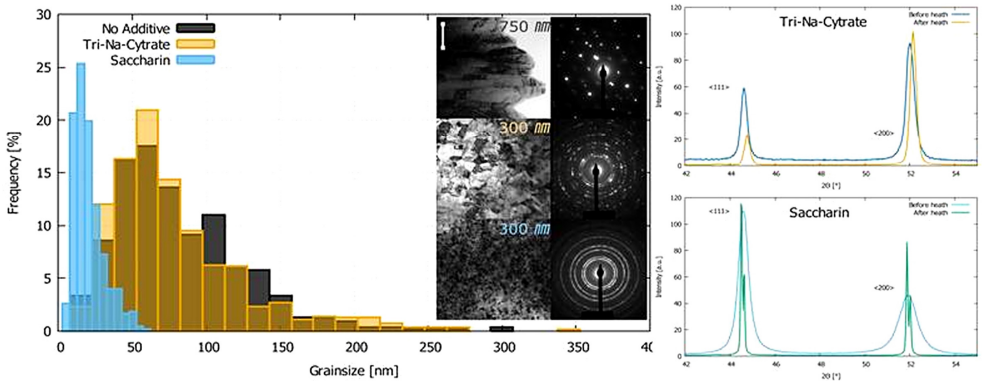

Figure 2 *Grain size distribution of nanocrystalline Ni film deposited with trisodium-cytrate and saccharine additives determined by TEM (left). Trisodium-cytrate causes larger, textured grains compared to saccharine; but has a greater thermal stability as the corresponding XRD patterns show it (right).*

Effect of high efficient attrition milling on 316L austenitic steel reinforced by ceramic nanoparticles

H. R. Ben Zine, K. Balázsi, and Cs. Balázsi

The elaboration of Oxide Dispersion Strengthened (ODS) Steels is having an interest as a good candidate for nuclear applications due to its good properties at high temperatures (>700 °C). Powder Metallurgy (PM) technology is the most used process to elaborate ODS steels, the preparation of this last is playing very important effect on the final properties of the alloy. The aim of our work is to study the effect of attrition milling on the 316L stainless steel reinforced by yttria ceramic nanoparticles. During this work a combined wet milling in ethanol and dry milling process of steel powders together with fine yttria nanoparticles was proposed by high agitator rotation speed; 600 rpm.

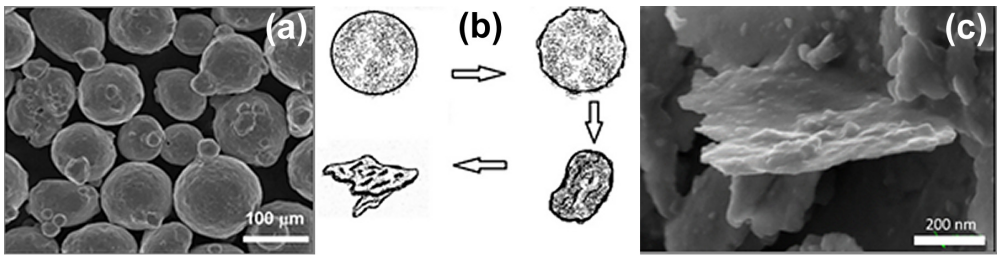

Figure 1 ***(a)****: 316L Starting powder.* ***(b)****: Schematic view of changes of powder grain morphology; the shape transformation process.* ***(c)****: Final powder grain shape after milling.*

A high efficiency attritor mill (Unio Process, type 01-HD/HDDM) equipped with a stainless steel setup working at 600 rpm was employed consecutively for wet (5h) and dry milling (5h). The morphological characterization of starting austenitic steel powder was performed by scanning electron microscopy (Fig. 1(a)), the sample consisted of globular particles with average particles size of 50–100 µm. The powder structure after 1 hour milling showed considerable differences to the starting powder with globular grains. Their average size is lower. The Fig. 1(b) shows schematic draw of powder grain changes and the evolution of grain morphology during milling process (Fig. 1(c)). The morphological investigations demonstrated the existence of small grains in few micrometer ranges among globular grains and drastically change in morphology. The sample consisted of bimodal grains, on the one hand very small austenitic grains with lamellar structure and on the other hand of few 80 µm size globular particles. The average size of lamellar particles in one dimension is nanometer range in thickness, whereas their length is few micrometers.

New type functional alloy films

(NN OTKA-112156)

F. Misják, B. R. Braeckman, Gy. Radnóczi, and D. Depla

Multi-component or high-entropy alloys contain at least five different metals in near-equimolar concentrations. It is expected that the large mixing entropy favors the formation of simple solid solutions instead of intermetallic phases. Mainly face-centered-cubic (FCC) or body-centered-cubic phases are formed (Fig. 1). The phase formation depends on the alloy composition and the synthesis method. High entropy alloys processed by non-equilibrium methods such as splat quenching, ball milling and magnetron sputtering exhibit in most cases a single-phase structure. High entropy alloy films and coatings can have favorable functional properties like relatively high hardness and plasticity, good electrical or magnetic as well as anticorrosion properties making them suitable for different applications

Five component CoCrFeNiCu (HEA) films were deposited at room temperature onto SiO_2 covered Si substrates with a deposition rate of 10 nm/min, corresponding to a metallic flux of approximately 1.4×10^{15} at/cm^{2}s. The average gaseous impurity flux provided by the base pressure in the vacuum chamber (5×10^{-4} Pa), corresponded to 1.42×10^{15} at/cm^{2}s. Hence, the (HEA) film was deposited with an average impurity-to-metal flux ratio of about 1. In addition to the residual gas in the vacuum chamber the powder target is a second source of impurities.

The (HEA) powder target is likely to contain a fraction of oxygen impurities as the powder grains are covered by metal-oxide surface layers. Hence, the use of powder targets further increases the impurity-to-metal flux ratio [14]. In the present work, the structure formation mechanism of the CoCrFeNiCu (HEA) model system was investigated. TEM measurements established that the structure and morphology of the crystalline film corresponds zone III structure in the structure zone model of the thin film growth and the grain size is 2-5 nm. No texture is observed. With increasing film thickness weakly developed columnar grains could be detected and a slight increase of the crystallite size is also observed (Fig 1). HREM measurements confirmed that the films are dens, homogeneous, free of pores (Fig. 2). The morphological and texture properties confirm that the CoCrCuFeNi film grew in the impurity-controlled conditions which involve hindered growth of crystallites due to the formation of covering layers and repeated nucleation of the crystalline HEA phase in the thickness of the film. The nano-size grain structure (zone III type microstructure) and the lack of crystallographic texture are the consequence of this growth mechanism [Materials Surface Processing by Directed Energy Techniques. Amsterdam, Oxford, Elsevier, 2006. pp.443-474.], [Metallic Films for Electronic, Optical and Magnetic Applications: Structure, Processing and Properties. Cambridge, Elsevier, 2014. pp. 67-120.].

The formation of elongated in the growth direction grains and their increase in cross section close to the film surface indicates a remaining possibility of competing growth, characteristic of zone T. As a result, the main processes being active in the

HEA film formation are: Nucleation and growth of the FCC HEA phase, the formation of a covering layer– presumably oxide-, repeated nucleation of the HEA phase on the surface of covering layer. Parallel to these the growing HEA crystallites can compete in growth among each other, preferably due to different surface capability or mechanism to incorporate oxygen. This process is leading to the V shape columnar like morphology of grains near the surface (Fig. 2).

Figure 1 *Cross section TEM images of the CoCrFeNiCu (HEA) film: bright field image (top), dark field image (bottom). The diffraction pattern corresponds to a random FCC structure, no texture is detected.*

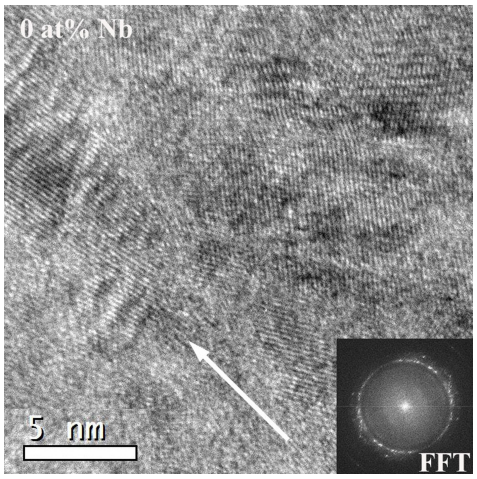

Figure 2 *High resolution image of the HEA film. The arrow shows the growth direction. No second phase (crystalline or amorphous) is detected in the grain boundaries.*

Processing of faint, diffuse diffraction rings from amorphous materials

(Nanomegas project)

J. L. Lábár

Electron diffraction pattern (SAED) from amorphous materials is extremely faint. The intensity, plotted as a function of the length of the scattering vector is frequently a monotonically decreasing function (see Fig. 1). Furthermore, the width of the diffraction peaks (in the 1D representation, which is averaging by the azimuthal angle) also varies in a wide range in contrast to the narrower range observed for the narrower peaks of crystalline materials. That is why the methods (e.g. [Microsc. Microanal. 15, 20–29, 2009]) established for crystalline materials are not performing perfectly for amorphous patterns when center and elliptical distortion are to be determined.

We developed a new approach to process such patterns by applying the Levenberg-Marquardt (non-linear fitting) method to two distinct problems. In the first step two intervals are selected at the two sides of a "peak" in the 1D intensity distribution calculated for the entire angular range. The position of the peak is determined by fitting a background + peak composite function. In the second step the pattern is divided into sectors and the above fitting is performed in each sector. A peak-position vs. azimuthal angle function results and a combination of two trigonometrical functions is fitted to it. Shifting of the center cause a cos(α), while elliptical distortion a cos(2α) type dependence. Amplitudes and phases of these functions provide magnitude and direction of shift and distortion.

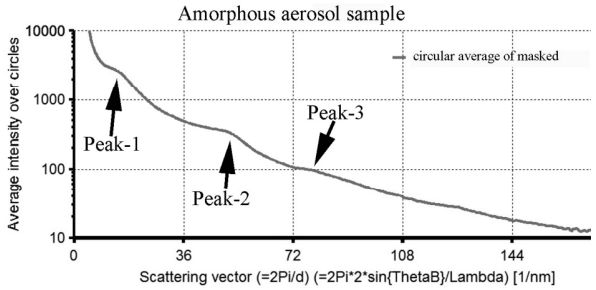

Figure 1 *The intensity plotted as a function of the length of the scattering vector.*

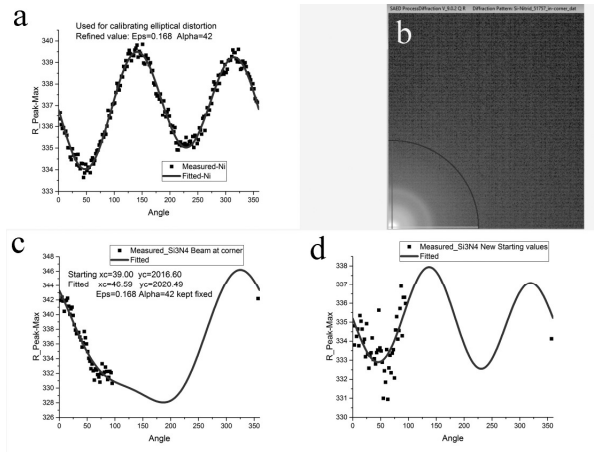

Figure 2 *Calibration process of the distortion.*

If the direct beam is shifted to the corner of the pattern to protect the camera than only a fraction of the angular range is available from the measurement. In such cases we cannot obtain all parameters from a single pattern. The problem is circumvented by prior calibration of the distortion in a standard sample and fitting the shift of the pattern center only, while keeping distortion fixed (Fig. 2). The procedure still remains robust and result in the same center irrespective of the starting position (within a reasonable range), although the shape of the fitted functions is different (see Figs. 2(c,d)).

Nanobiosensorics Group

Head: Róbert HORVÁTH, Ph.D., Senior Scientist

Research Staff

- Róbert HORVÁTH, Ph.D.
- Sándor KURUNCZI, Ph.D.
- Inna SZÉKÁCS, Ph.D.
- Dániel PATKÓ, Ph.D.

Ph.D. students

- Boglárka KOVÁCS, Ph.D. student
- András SAFTICS, Ph.D. student
- Enikő FARKAS, PhD. student
- Rita UNGAI-SALÁNKI, PhD. student
- Judit NÁDOR, PhD. student
- Beatrix PÉTER, PhD. student

Diploma workers

- Bálint KOVÁCS, B.Sc. student
- Aurél PRÓSZ, B.Sc. student
- Barbara TÜRK, M.Sc. student
- Dávid CSIKAI, B.Sc. student
- Milán SZTILKOVICS, B.Sc. student
- Olga NÉMETH, B.Sc. student
- Dóra PALOTÁS, B.Sc. student
- Bennó MÜLLER, B.Sc. student
- Martin NOVÁK, B.Sc. student
- Attila BÍRÓ, B.Sc. student
- Szilvia HEGYESI, B.Sc. student
- Petra PRAJCZER, B.Sc. student

The Nanobiosensorics Group was established in 2012 in the framework of the "Lendület" program of the Hungarian Academy of Sciences. The "Lendület program" funds young researchers in Hungary aiming at the establishment of their own independent research groups. The research profile of the Nanobiosensorics Group is the development and application of label-free optical biosensors, the mathematical modeling of the relevant biological and biophysical processes. Building on their broad national and international collaborative network the group conducts research in the fields of instrument development, monitoring of cell secreted extracellular vesicles, development of protein-based functional coatings, adhesion studies on human cancer and immune cells, and theoretical modeling. In 2014, the application for an ERC Consolidator Grant by the head of the research group received qualification category "A (fully meets the ERC excellence criteria and should be funded if sufficient funds are available)" after the interview in Brussels, but the funding line did not reach this proposal due to budgetary constraints. However, using this achievement the Group could successfully apply for funding from NKFIH in the framework of the ERC_HU call. In the framework of this project they aim single cell manipulation and label-free sensing.

Hydrogel film fabrication for biosensing

(Lendület Program , Bolyai Research Scholarship)

A. Saftics, B. Türk, S. Kurunczi, and R. Horváth

Fabrication of a stable and reproducible surface with the required chemical functions is one of the major challenge in the development of label-free biosensors. Polysaccharide dextran interface layers are able to improve the sensitivity of biosensors, owing to the anti-fouling property and the high receptor immobilization capacity of the dextran chains.

Carboxymethyl-dextran (CMD) was synthesized in our laboratory from the native dextran. Grafting methods based on covalent coupling to aminosilane- and epoxysilane-functionalized surfaces were applied to obtain thin CMD layers. The carboxyl moiety of the CMD was coupled to the aminated surface by EDC-NHS reagents, while CMD coupling through epoxysilane molecules was performed without any additional reagents. The surface analysis following the grafting procedures consisted of x-ray photoelectron spectroscopy (XPS), attenuated total reflection infrared spectroscopy (ATR-IR), as well as atomic force microscopy (AFM), which proved the presence of the 1-2 nm thick CMD layer, and verified its covalent grafting to the surface. The *in situ* optical waveguide lightmode spectroscopy (OWLS) measurements were suitable to devise the structure of the interfacial dextran layers by the evaluation of the optogeometrical parameters. We found that the extent of the layer anisotropy was dependent both of the grafting procedure (using epoxysilane or aminosylane coatings) and the pH of the CMD solution applied for the grafting (Fig. 1). The apparent refractive index of the CMD layer was unrealistically higher than the reference values in the literature, which suggested parallel chain conformation to the surface. The developed methodologies allowed to design and fabricate nanometer scale ultrathin CMD layers with well-controlled surface structure, which are otherwise very difficult to characterize in aqueous environments using available instrumentation [104].

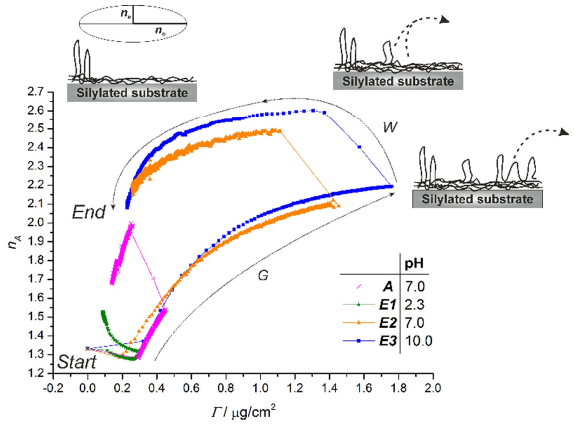

Figure 1 *In situ OWLS measurements on the covalent grafting experiments of the CMD (**n_A**: apparent refractive index of the CMD layer, **Γ**: areal mass density of the deposited CMD; **A, E**: surface with aminosilane or epoxysilane coating, respectively; **G, W**: grafting or washing sections of the experiment).*

ZnO nanostructure templates as a cost-efficient mass-producible route for the development of cellular networks

("Lendület" grant LP2012-26/2012 of HAS)

E. Makarona (NCSR "Demokritos", Greece), B. Péter, I. Székács, C.Tsamis (NCSR "Demokritos", Greece), and R. Horváth

The development of artificial surfaces which can regulate or trigger specific functions of living cells, and which are capable of inducing in vivo-like cell behaviors under in vitro conditions has been a long-sought goal over the past twenty years. In our work, an alternative, facile and cost-efficient method for mass-producible cellular templates is presented. The proposed methodology consists of a cost-efficient, two-step, all-wet technique capable of producing ZnO-based nanostructures on predefined patterns on a variety of substrates. ZnO—apart from the fact that it is a biocompatible material—was chosen because of its multifunctional nature which has rendered it a versatile material employed in a wide range of applications. Si, Si_3N_4, emulated microelectrode arrays and conventional glass cover slips were patterned at the micrometer scale and the patterns were filled with ZnO nanostructures. Using HeLa cells, we demonstrated that the fabricated nanotopographical features could promote guided cellular adhesion on the pre-defined micron-scale patterns only through nanomechanical cues without the need for further surface activation or modification (see Fig. 1) [64]. The suggested methodology is extremely promising for the creation of engineered cellular networks through purely nanomechanical cues.

One of the most important results of this study was a better understanding of the dynamics of selective cellular adhesion and the implication of time as a controlling factor that must be combined with nanomechanosensation. Further studies are foreseen for the evolvement of the method into a technology that can be readily transferred to mass-production and the development of real-life viable products [64].

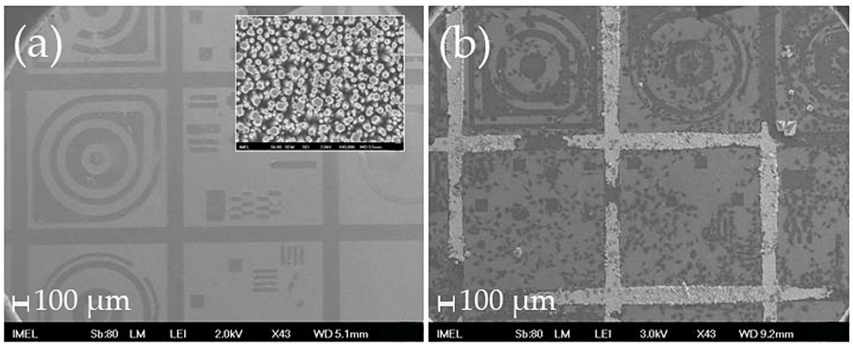

Figure 1 *SEM images of* ***(a)****: the Si wafer with larger patterns and flat areas (the darker areas contain the ZnO nanorods shown in the zoom-in inset image; scale bar: 100 nm);* ***(b)****: the same samples with HeLa cells after 4 days in culture, where the cells mostly adhere onto the flat areas (the white areas are the nanorods that have been covered by salts from the nutrient medium that was not fully removed after washing).*

Self-assembled, nanostructured coatings for water oxidation by alternating deposition of Cu-branched peptide electrocatalysts and polyelectrolytes

("Lendület" grant LP2012-26/2012 of HAS, ERC_HU Program of NKFIH, POMOST/2012-5/9 and PIEF-GA-2012-329969)

E. Farkas, D. Srankó (MTA EK), Zs. Kerner (MTA EK), B. Setner (University of Wrocław, Poland), Z. Szewczuk (University of Wrocław, Poland), W. Malinka (Wrocław Medical University), R. Horváth, L. Szyrwiel (Wrocław Medical University, Poland, CNRS/UPPA, LCABIE, UMR5254, France), and J. S. Pap (MTA EK)

In the past few decades the importance of the LbL (Layer-by-Layer) technique has grown, especially to build up functional multilayers or surface-based nanodevices and surface modifications. The LbL method is based on the alternating exposure of a surface to oppositely charged polyelectrolytes. Those polymers are called polyelectrolytes (PEs), whose repeating units are ionic groups and have high molecular weight. The PLL (poly-L-lysine) and PAH (poly-(allylamine hydrochloride)) are positively charged PEs, these were used in our experiments. The advantages of the PEs have been taken to build heterogeneous catalytic layers with Cu-peptides on indium-tin-oxide (ITO) conducting OWLS chip surface, with the use of the principle of the LbL technique. The Cu-peptides were known to accelerate the half-reaction of water oxidation that has significance in envisioned water splitting systems to generate H2 as renewable fuel. The peptide ligands bind to the metal in the equatorial positions at high pH and capable of stabilizing higher oxidation states occurring in catalysis. The applied complexes contain L-2,3-diaminopropionic acid (dap) linkers that provide branched structure with a glycine (Cu-3G) or a histidine (Cu-2GH) residue at the C-terminus.

Initially suitable polyelectrolyte pairs were sought to the Cu-peptides and Optical Waveguide Lightmode Spectroscopy (OWLS) was applied to monitor the build-up process of the nanocomposite multilayers in situ. The Cu-2GH paired with PAH and Cu-3G coupled with PLL were suitable for further studies. The layer-buildup-mechanism is supposed to involve secondary binding forces beside the electrostatic interactions. Phosphate is also incorporated into the layers.

Optimization was also supported by electrochemical methods. Conditions of pH 9-10 and Cu-complex concentration of 0.1-0.5 mM were optimal for stable LbL formation. These layers show electrocatalytic activity at high positive (>1.1 V) potential and the measurement on EC-OWLS (OWLS with electrochemical function) shows, that the surface mass density is somewhat decreased after the alternating potential cycles, but the layers don't lose their activity (Fig. 1).

Other surface analyses included XPS (X-ray photoelectron spectroscopy) to detect the Cu(II) in an organic N-donor environment, and AFM that shows an inhomogeneous surface with nanoporous structure. The profilometric section demonstrates that the Cu-2GH multilayers are smoother and thinner, than that of Cu-3G.

In conclusion, with the use of OWLS/EC-OWLS it was possible to examine functional thin layers and define their properties. The Cu-peptide/PE film is electrochemically active stable, heterogeneous catalyst layers. This catalyst heterogenization method could lead to a cheaper, more economic and environmentally friendly technology.

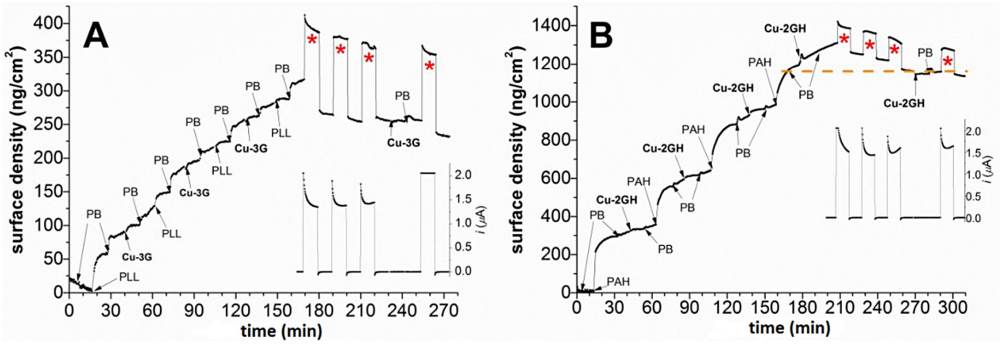

Figure 1 ***(A)****: three deposition cycles of PLL and Cu-3G (0.5 mM) in phosphate buffer (PB) (0.1 M) at pH = 10.12 and concomitant 3×10 min runs of CPE at 1.1 V vs. Ag/AgCl with intermittent breaks of 10 minutes and concomitant attempt to supply the electrolyzed surface with Cu-3G at an ITO-coated chip placed in an EC-OWLS cell;* ***(B)****: the same sequence applied to PAH and Cu-2GH layers.*

Self-assembly and structure of flagellin–polyelectrolyte composite layers: polyelectrolyte induced flagellar filament formation during the alternating deposition process

("Lendület" grant LP2012-26/2012 of HAS, OTKA NN117849 and K104726 grants, ERC_HU project of NKFIH)

E. Farkas, D. Patkó, N. Q. Khánh, E. Tóth (Pannon University), F. Vonderviszt, and R. Horváth

The simple and cost-effective bottom-up fabrication of complex functionalized nanostructures is extensively researched today. Here, the alternating deposition of the negatively charged protein flagellin and a positively charged polyelectrolyte are studied. The multilayer buildup was followed in situ using Optical Waveguide Lightmode Spectroscopy (OWLS) revealing the deposited surface mass density in real time during the alternating deposition process. The nanostructure of the assembled films was investigated by Atomic Force Microscopy (AFM) measurements. When flagellin was applied in its natural filamentous form no distinct multilayer buildup was observed, the filaments assembled mainly into bundles. In contrast, when thermally treated filament solution or pure flagellin monomer solution was used a systematic linearly growing buildup was seen, and thick, relatively smooth

films were fabricated. The structural investigation (Fig. 1) revealed that the fabricated films are relatively smooth, what is in close connection with the assembling mechanism, having a tendency of filling up possible holes. We also concluded that the flagellin monomers assembled into nanofilaments inside the multilayer and even a single layer of polycation could induce the self-assembly of filaments, possibly by helping the adsorption of flagellin monomers close to each other. Both the filament formation and the multilayer buildup were completely absent when a truncated flagellin variant – missing the disordered terminal regions – was applied. Since these regions are necessary for filament formation, we conclude that the linearly growing nature of the layer is a clear consequence of filament formation.

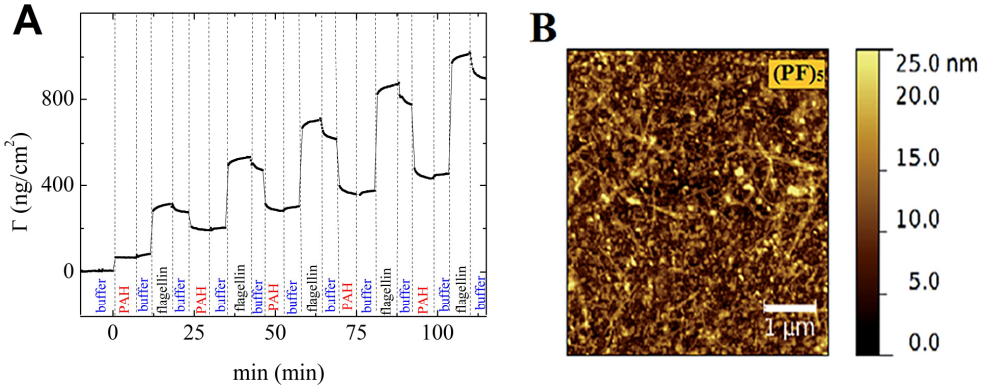

Figure 1 ***A****: Formation of 5 bilayer of flagellin and PAH polyelectrolyte monitored by OWLS.* ***B****: AFM picture of 5 bilayer of flagellin and PAH polyelectrolyte.*

Therefore, this study first reveals a new type of linearly growing polyelectrolyte multilayer buildup mechanism, when one of the components induces the self-assembly of the oppositely charged component, creating a complex, stable and smooth filamentous nanostructured coating. These composite films can find diverse applications in nanotechnology and in biomedical sciences since the variable D3 domain of flagellin subunits can be easily modified to express enzymatic, fluorescent or molecular binding properties on the surfaces of the filaments. The present work therefore opens up novel routes in the bottom-up fabrication of complex nanostructured coatings.

Cell adhesion measurements with a label-free optical biosensor

("Lendület" Program of the HAS the ERC_HU grant from NKFIH, K104838 OTKA grant, Bolyai Scholarship, MedInProt)

N. Orgován, R. Ungai-Salánki, Sz. Lukácsi (ELTE), N. Sándor (ELTE), Zs. Bajtay (ELTE), A. Erdei (ELTE), B. Szabó (ELTE), and R. Horváth

Monocytes, dendritic cells (DCs), and macrophages (MFs) are closely related immune cells that differ in their main functions [105]. To study the inherently and essentially dynamic aspects of these cells, dynamic cell adhesion assays were performed with a high-throughput label-free optical biosensor [Epic BenchTop (BT)] on surfaces coated with either fibrinogen (Fgn) or the biomimetic copolymer PLL-g-PEG-RGD [84]. We found that, all three cell types induced a larger biosensor signal on Fgn than on PLL-g-PEG-RGD.

The results obtained with evanescent-field-based label-free optical biosensor were compared with three different techniques in this study: the classical fluorescence reader-based adherence assay, the flow chamber technique, and the automated micropipette [42]. The results obtained with the different techniques demonstrate that there are significant differences between the adhesion of the three cell types on Fgn. Monocytes were found to be the less adhesive than MFs and DCs. Furthermore, DCs adhered stronger than MFs; this is in accordance with the fact that DCs have larger expression levels of β2 integrins than MFs (Fig. 1). Hence, it seems that the expression levels of β2 integrins fundamentally influence the adhesion capacity of these immune cells.

These techniques confirmed the results obtained with the high-temporal-resolution Epic BT, but could only provide end-point data. In contrast, complex, non-monotonic cell adhesion kinetics measured by the high-throughput optical biosensor is expected to open a window on the hidden background of the immune cell–extracellular matrix interactions.

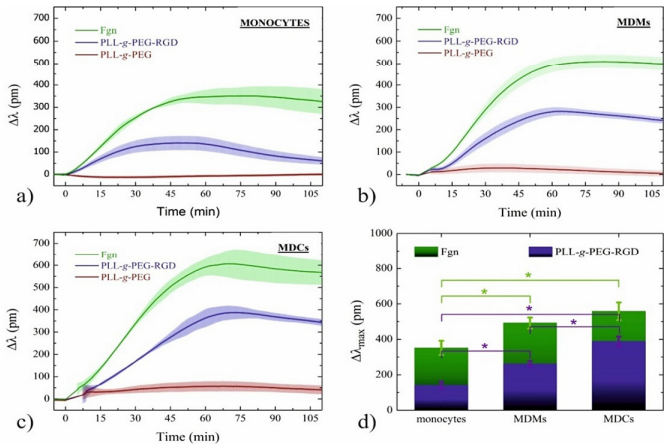

Figure 1 *Time-dependent adherence of monocytes, monocyte-derived macrophages (MFs), and monocyte-derived dendritic cells (DCs) on PLL-g-PEG- and Fgn-coated surfaces, as was measured with the Epic BT in dynamic cell adhesion (DCA) assays. Representative kinetic profiles provoked by adhering and spreading monocytes, MFs, and DCs are shown in panels* ***a)****,* ***b)****, and* ***c)****, respectively. PLL-g-PEG-coated surfaces were used as negative control. The background-corrected maximum biosensor signals induced by different cells on PLL-g-PEG-RGD- and Fgn-coated surfaces are shown in panel* ***d)****. In all panels data are shown as means, error bars represent standard deviations. * indicates statistical significance with p<0.05 (t-test).*

Label-free optical biosensor for on-line monitoring the integrated response of human B cells upon the engagement of stimulatory and inhibitory immune receptors

("Lendület" grant LP2012-26/2012 of HAS)

I. Kurucz (ELTE), B. Péter, A. Prosz, I. Székács, R. Horváth, and A. Erdei (ELTE)

The majority of current cell-based assays relies on the measurement of a single event at a predetermined time point in a specifically chosen signaling path-way, let it be second messenger release, reporter-gene production or target translocation. These measurements require the use of labeled compounds, sometimes the modification of cells to express the target in larger amount or to produce a reporter molecule to be able to monitor receptor engagement. The mentioned manipulations can be toxic for the cells and can interfere with normal cellular physiology of the target receptors or their environment and the applied fluorescence and colored compounds may induce elevated background [Sensors and Actuators B, 240, 528–535 (2017)]. Consequently, functional cellular assays which can report from different signaling events in real time without the application of molecular engineering (in providing the suitable cellular partner) and without the use of labeling would be of high value for both theoretical and practical studies even if they are more complex and less specific than cell-based biochemical assays.

To be able to obtain holistic pictures about B cell responses to complex interlocking stimulations Epic BT optical biosensor was applied and set to establishing the method using human B cell lines, derived from Burkitt's lymphomas. We successfully immobilized non-adherent B cells on the surface of the biosensors, without the ligation of any specific receptors or adhesion molecules. This way we were able to demonstrate that engagement of the antigen specific B cell receptors (BCR) induced reproducible dynamic mass redistribution (DMR) inside the cells as a measure of receptor activation (see Fig. 1). The initiated DMR response proved to be specific, since only antibodies recognizing the BCR could generate the response; neither the assay-buffer, nor high concentration of indifferent proteins or non-specific antibodies had any effect. The measure of cell activation was sensitive, concentration dependent, and specifically and dose-dependently inhibited by the Syk inhibitor BAY 61-3606. The BCR-triggered DMR response was evoked from three human Epstein-Barr virus (EBV) negative B cell lines, but could not be elicited in two EBV-positive BL cell lines, where the presence of the EBV-derived LMP2A protein desensitizes the cells' response to the BCR-induced signaling.

Therefore, our work opens new avenues to study complex signaling events and to decipher interactions within the signaling network during B cell activation [Sensors and Actuators B, 240, 528–535 (2017)].

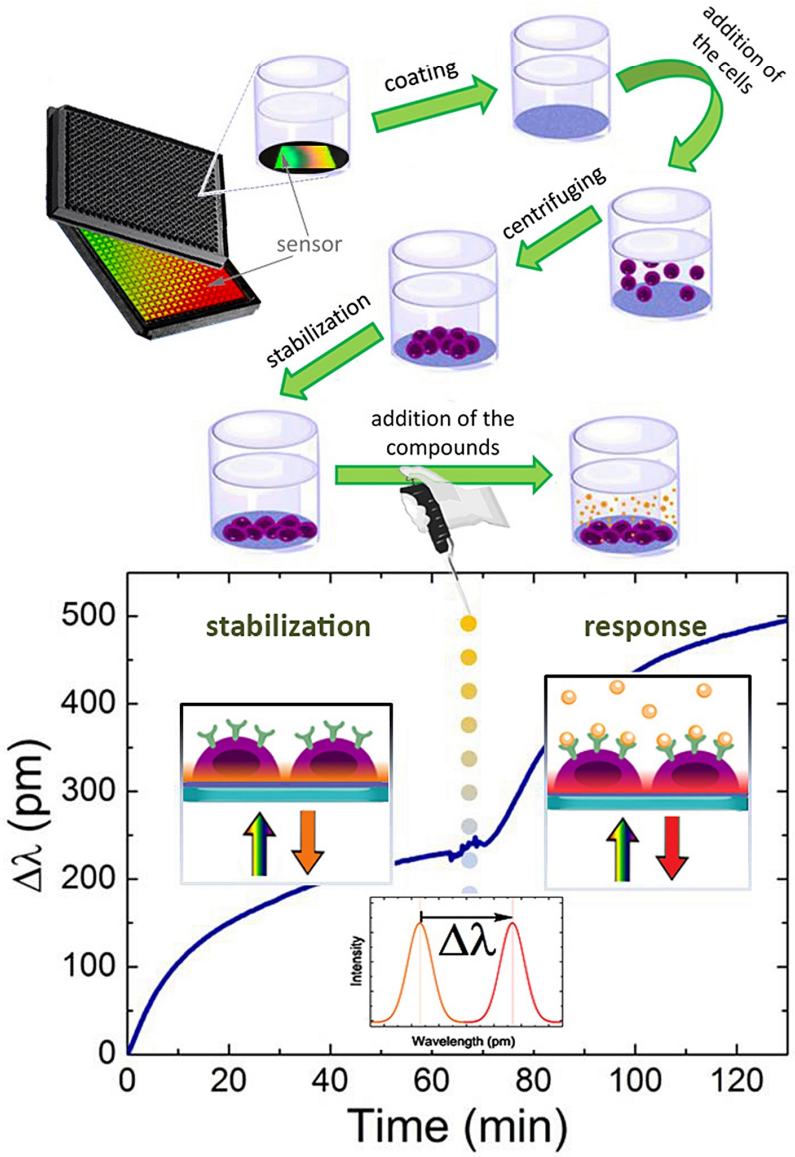

Figure 1 *Experimental setup to perform real-time measurement of dynamic mass redistribution (DMR) using B-cell lines* ***(A)****; and schematic illustration of the principle of DMR detection* ***(B)****.*

Complex Systems Department

Head: György SZABÓ, D.Sc., scientific advisor

Research Staff

- István BORSOS
- Zoltán JUHÁSZ, Ph.D.
- Géza ÓDOR, D.Sc., scientific advisor
- Attila SZOLNOKI, D.Sc., scientific advisor

Ph.D. students / Diploma workers

- Balázs KIRÁLY, Ph.D. student
- Kinga S. BODÓ, M.Sc. student
- Kristóf HÓDSÁGI, M.Sc. student
- Gergely BUNTH, M.Sc. student
- Vince VARGA, B.Sc. student

The main research area of the group is the theoretical investigations of non-equilibrium systems by means of statistical physics and solid state theory. The research topics include a wide scale of evolutionary games, different dynamical processes on random networks, and analyses of the relatedness hidden in the databases of folk songs and genetic data.

A review paper is published on the evolutionary potential games on lattices. During the preparation of this survey *Szabó* and *Borsos* have developed methods for the identification of potential games as well as for the evaluation of potential if it exists. One of these methods is based on the concept of matrix decomposition when the payoff matrices are built up as linear combinations of four types of elementary games representing games with self- and cross-dependent payoffs, coordination type interactions and cyclic dominances.

In different social dilemmas the systematic consideration of methods and mechanisms supporting the maintenance of cooperative behavior among selfish players is surveyed in one of the Highlights papers.

The analysis of the dynamical processes on networks is extended for those realistic networks that are observed experimentally when quantifying real connections in human brain. The topological investigations of large Open Connectome networks of human brain and the study of dynamical processes on it has clearly indicated the relevance of those topological features that are currently missing in the traditional model systems.

The analysis of folk music is focused on the identification of a suitable set of characteristic melodies that can be used for quantifying the relatedness between different nations and cultures. In our new algorithm the number of the possible characteristic melodies was also the subject of an evolutionary process. The mentioned method is also adapted to the numerical analyses of genetic data.

Anisotropic invasion and its consequences

(OTKA K-120785)

Gy. Szabó, L. Varga, and M. Szabó

In the simplest spatial evolutionary games players are located at the sites of a square lattice, they play game with their four nearest neighbors and sometime they are allowed to adopt the strategy of a neighbor having higher income. For two-strategy evolutionary games the noisy imitations can result in anisotropic invasion velocities along the interface separating the territory of the two homogeneous strategy distributions denoted by black and white domains in Figs. 1 and 2.

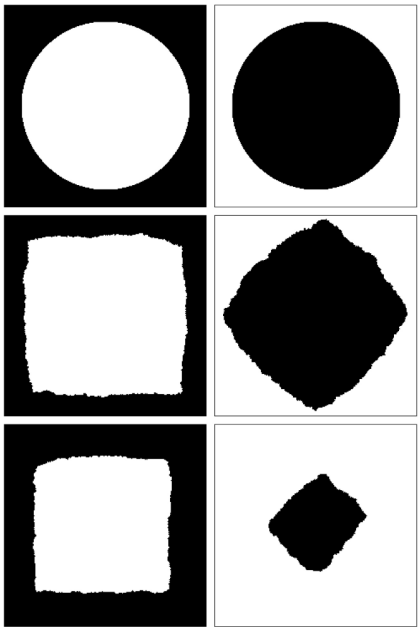

Figure 1 *Evolution of white and black circular domains (from top to bottom the times are t=0, 500, and 4000 MCS) for imitation at low noises on a square lattice.*

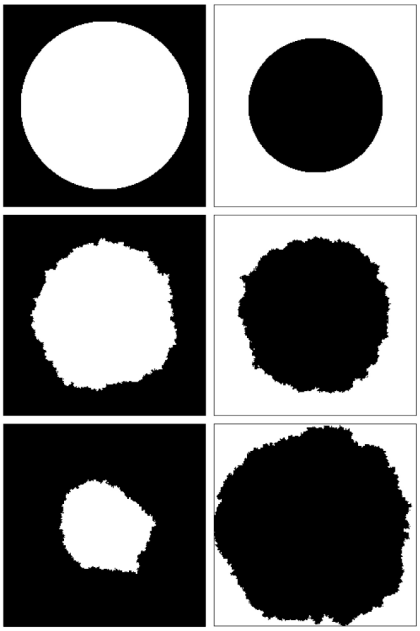

Figure 2 *Evolution of circular white and black domains at a high noise level for the same payoff parameters used in Fig. 1.*

In this system the pair interaction is composed of a coordination interaction of unit strength, and self- and cross-dependent payoff components with tunable strengths. For certain strengths of the tunable components the black domain can invade the territory of the white one along the horizontal and vertical interfaces. At the same time the opposite process (black domains invade the white's territories) can be observed for tilted (45°) interfaces. As a result, both the circular white and black islands shrink and vanish after forming square and diamond faceted territories for the same model parameters at low noises as illustrated in Fig. 1. This unusual feature is related to the advantage of cooperation when imitation controls the evolution.

At high noises the smooth interfaces become irregular that suppress the anisotropy of the invasion velocities and then the black territories always invade the white domains. The latter behavior occurs typically in thermodynamic systems.
The above phenomenon has interesting consequences at low noise levels when the random initial state evolves into one of the homogeneous absorbing states. The selection of the final state is related to a percolation process. According to the continuous percolation theory if one of the phases percolates horizontally then it also will percolate vertically in the large size limit and the percolating phase can be considered as a sea in which the islands shrink and disappear at the end of evolution. In these regions of parameters both homogeneous absorbing phases can be realized in the final frozen state by choosing suitable portions of strategies in the initial state as it is illustrated in Fig. 3. [118].

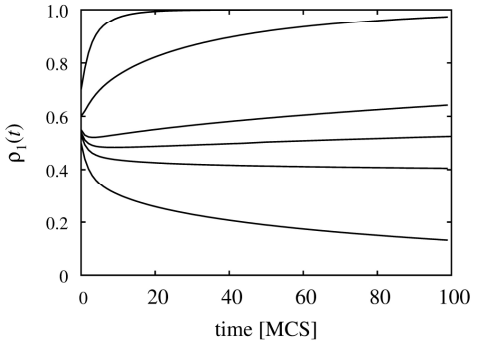

Figure 3 *Frequency of white strategies versus time if the system is started from a random initial state with different portion of white strategies at t=0 for large sizes (L=1000).*

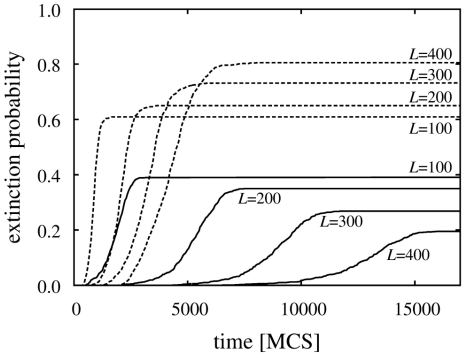

Figure 4 *Extinction probability of the black (solid lines) and white (dashed lines) strategies as a function of time for different small system sizes indicated by the labels.*

Summarizing the essence, in contrary to the thermodynamic systems the present evolutionary games can develop into one of the two absorbing states with probabilities dependent on the size and initial composition. These features result in complex phase diagrams and technical difficulties in the numerical evaluation of the phase boundaries when tuning the model parameters.

mtDNA analysis of 174 Eurasian populations using a new iterative rank-correlation method

Z. Juhász, H. Pamjav, T. Fehér, E. Németh, and G. Bárány

In this study, we analyzed 27-dimensional mtDNA haplogroup distributions of 174 Eurasian, North-African and American populations, including numerous ancient data as well. The main contribution of this work was the description of the haplogroup

distribution of recent and ancient populations as compounds of certain hypothetic ancient core populations immediately or indirectly determining the migration processes in Eurasia for a long time. To identify these core populations, we developed a new iterative algorithm determining clusters of the 27 mtDNA haplogroups having strong rank-correlation among each other within a definite subset of the populations.
Based on this study, the current Eurasian populations can be considered as compounds of 3 early core populations regarding to maternal lineages. We wanted to show that a simultaneous analysis of ancient and recent data using a new iterative rank-correlation algorithm and the weighted SOC learning technique may reveal the most important and deterministic migration processes in the past. This technique allowed us to determine geographically, historically and linguistically well interpretable clusters of our dataset having a very specific, hardly classifiable structure. The method was validated using a 2-dimensional stepping-stone model [44].

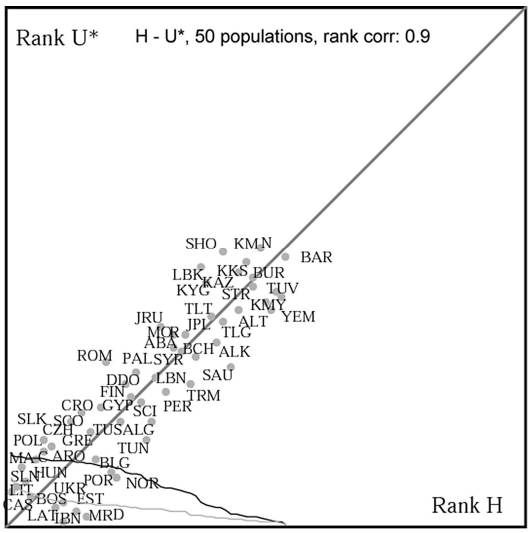

Figure 1 *An example for iterative rank-correlation algorithm output.The 50-element subset of the 174 populations where the rank-correlation of haplogroups H and U* is 0.9. Point coordinates correspond to the rank values of the populations within the rank hierarchies of Hg-s H and U**

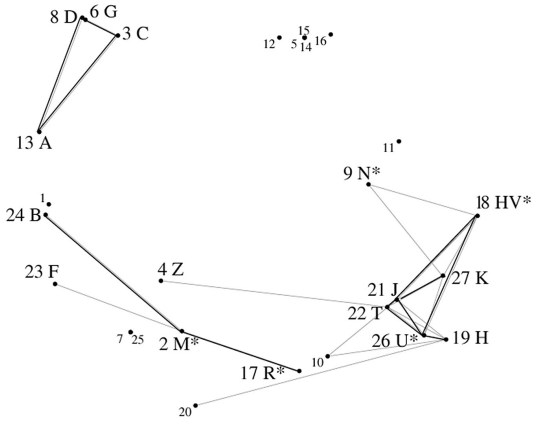

Figure 2 *MDS map of (1-rank correlations) of 27 Hg-s. We found 3 disjunctive Correlating Hg-clusters (CHgC):*

1. *18-HV*, 19-H, 21-J, 22-T, 26-U*, 27-K, (weaker links: 4-Z, etc.) – „Western"*

2. *2-M, 17-R, 24-B (weaker link: 23-F) - „Eastern"*

3. *3-C, 6-G, 8-D, 13-A – „Siberian"*

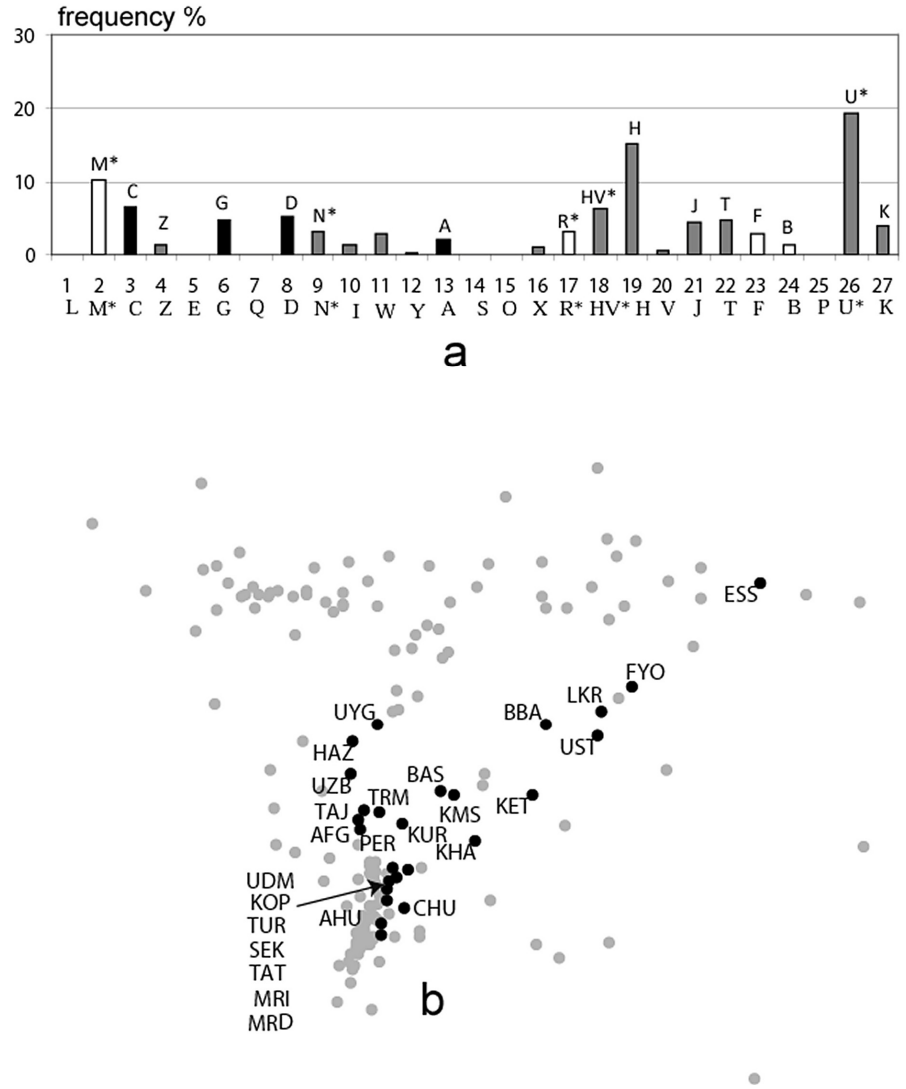

Figure 3

a*: The average of the haplogroup distributions constructing one of the most important clusters of our 174 populations, called S/5. Western, Siberian and Eastern haplogroups are denoted by grey, black and white columns.*

b*: MDS map of the 174 Hg-distributions, highligting the members of Cluster S/5. 27 populations: UDMurt, KOmi, TURkish, SzEKler (Hungarian), TATar, MaRI, MoRDvin, CHUvash, KHAnty, Konda-ManSi, BAShkir, PERsian, AFGhan, UZBek, HAZara, UYGhur, KET, ESkimo. UST, BBA, LKR, FYO are ancient populations belonging to the Andronovo culture (2000 – 800 BC), AHU is an ancient Hungarian population (9th century).*

MFA Seminar Talks

2016.01.27	**Géza ÓDOR** (MTA EK MFA, Budapest, Hungary): *"Lassú, villanásos dinamikák, Griffiths effektusok agyhálózatokban"*
2016.02.01-03	**MFA** (MTA EK MFA, Budapest, Hungary): *"Intézeti beszámolók"*
2016.02.10	**Erzsébet DÓDONY** (MTA EK MFA, Budapest, Hungary): *"Patterson térképezés"*
2016.03.09	**István GROMA** (ELTE, Budapest, Hungary): *"Plasztikus deformáció nano-rudakban"*
2016.03.16	**MFA** (Gifu University, Japan): *"Fiatal Kutatók (FIKU) meghallgató napja"*
2016.03.18	**Mutsuhiro Shima** (MTA EK MFA, Budapest, Hungary): *"Tailored Synthesis of Magnetic Nanostructures"*
2016.04.06	**Péter PETRIK** (MTA EK MFA, Budapest, Hungary): *"Nanofotonika"*
2016.04.20	**Rita SALÁNKI** (MTA EK MFA, Budapest, Hungary): *"Ph.D. házivédés"*
2016.04.27	**András PATKÓS** (ELTE, Budapest, Hungary): *"A sötét anyag és sötét energia kihívása"*
2016.05.11	**Sándor KURUNCZI** (MTA EK MFA, Budapest, Hungary): *"Dextrán rétegek fejlesztése bioszenzorikai alkalmazásokhoz"*
2016.05.18	**Áron SZABÓ** (Integrated Systems Laboratory, ETH Zürich, Switzerland): *"Ab initio transzport szimulációk kétdimenziós félvezető eszközökben"*

2016.05.25	**Dániel ZÁMBÓ** (MTA EK MFA, Budapest, Hungary): *"Ph.D. házivédés"*
2016.06.15	**Beatrix PÉTER** (MTA EK MFA, Budapest, Hungary): *"Ph.D. házivédés"*
2016.06.24	**MFA** (MTA EK MFA, Budapest, Hungary): *"MFA Nyári Iskola – beszámoló nap"*
2016.06.28	**Judit NÁDOR** (MTA EK MFA, Budapest, Hungary): *"Ph.D. házivédés"*
2016.10.19	**Zoltán SZABÓ** (MTA EK MFA, Budapest, Hungary): *"Kódfejtő szeminárium – kriptográfia röviden"*
2016.11.16	**András DEÁK** (MTA EK MFA, Budapest, Hungary): *"Optika és kolloidkémia"*

Research and Development Partners, Foreign Visitors

AMARAL, Marco A. *(Univ. Federal de Minas Gerais, Brazil)*
ANLANMERT, Beril *(Industrial Product Design Isik Univ., Istanbul, Turkey)*
ANTIPINA, Lubov *(Technological Institute for Superhard and Novel Carbon Materials, Russia)*
BIETTI, Sergio *(Univ. of Milano, Italy)*
BOIKO, Vitalii *(Institute of Physics of the National Academy of Sci., Kiev, Ukraine)*
BOSCHI, Francesco *(Istituto CNR-IMEM, Italy)*
CAYREL, Frederic *(Univ. of Tours, France)*
CHERNOZATONSKIJ, Leonid *(RAS, Russia)*
DEFFORGE, Thomas *(Univ. of Tours, France)*
DEMIN, Victor *(Emanuel Institute of Biochemical Physics, Moscow, Russia)*
DOVBESHKO, Galina *(NASU, Ukraine)*
DUSZA, Jan *(Institute of Materials Research, Slovak Academy of Sci., Slovakia)*
FERREIRA, Silvio C. *(Univ. Federal de Vicosa, Brazil)*
FIORENZA, Patrick *(Italian National Research Council, Rome)*
FISICHELLA, Gabriele *(Italian National Research Council, Rome)*
FRIGERI, Cesare *(Istituto CNR-IMEM, Italy)*
GAUTIER, Gael *(Univ. of Tours, France)*
HRISTOVA-VASILEVA, Temenuga *(Bulgarian Academy of Sci., Bulgaria)*

HWANG, Chanyong *(KRISS, South Korea)*
JAKAB-FARKAS, László *(Sapientia Univ., Marosvásárhely, Romania)*
KARA, Alpagut *(Anadolu Univ., Eskisehir, Turkey)*
KELLING, Jeffrey *(Helmholtz-Zentrum, Dresden, Germany)*
KNIESZ, Oliver L. *(3DZ Budapest Kft.)*
KURODA, Takashi *(National Institute for Materials Sci., Tsukuba, Ibaraki, Japan)*
KUZHIR, Polina *(Belarusian State Univ., Minsk)*
KVASHIN, Dmitry *(Energoprom Group, Rostov, Russia)*
LAMBIN, Philippe *(Univ. of Namur, Belgium)*
LANYI, Stefan *(Slovak Academy of Sci., Bratislava, Slovakia)*
LATHUS, Guillaume *(France)*
LOBOTKA, Peter *(Institute of Electrical Engineering, SAS, Slovakia)*
MAI, Viola *(Mathys Ltd., Bertlach, Switzerland)*
MANO, Takaaki *(National Institute for Materials Science, Tsukuba, Ibaraki, Japan)*
MARQUEZ NAVARRO, Emilio *(Univ. of Cadiz, Spain)*
MOREAU, Stephan *(Setaram, Caluire, France)*
NADZEYA, I. Valynets *(Institute for Nuclear Problems, Belarusian State Univ., Minsk)*
NENADOVIC, Milos *(Institute of Nuclear Sci. "Vinca", Serbia)*
NGUYEN NGUYEN, Viet *(SEMILAB, Japan)*
NOWAK, Jakub *(The Univ. of Edinburgh, Scotland)*
PERC, Matjaz *(Univ. of Maribor, Slovenia)*
PEREDERI, Alexander *(Technology Solutions Professional - Surface bei Microsoft, Cologne Area, Germany)*
RAMSDEN, Jeremy *(UK)*
SANGUINETTI, Stefano *(Univ. of Milano Bicocca, Italy)*
SEVERIN, Ivan *(National Technical Univ. of Ukraine, Kiev)*
SHIMA, Mutsuhiro *(GIFU Univ., Japan)*
SIEMEN, Wilhelm *(Staatliches Museum für Porzellan, Hohenberg a. d. EgerSelb, Germany)*
SOPACK, Tibor *(Institute of Materials Research, Slovak Academy of Sci., Slovakia)*
SOROKIN, Pavel B. *(RAS, Russia)*
STOIMENOS, Ioannis *(Aristotle Univ. of Thessaloniki, Greece)*
STRECKOVA, Maggdalena *(Institute of Materials Research, Slovak Academy of Sci., Slovakia)*
SUCHÁNEK, Martin *(ChartMogul, Berlin, Germany)*
SUGIMOTO, Yu *(Hokkaido Univ., Sapporo, Japan)*
SUK-JOONG, Kang *(President of Korea Institute of Ceramic Engineering and Technology, KICET)*
SZABÓ, Pavol *(UEF SAV, Slovakia)*
TAKAGI, Toshiyuki *(Tohoku Univ., Sendai, Japan)*
TOMAS, Ivan *(Institute of Physics, Prague, Czech Republic)*
TURAN, Sevet Turan *(Anadolu Univ., Eskisehir, Turkey)*
WALTER, R. Thomas *(Helmholtz-Zentrum, Potsdam, Germany)*

Publications in 2016

1. **Anaya J**, Rossi S, Alomari M, Kohn E, Tóth La, Pécz B, Hobart KD, Anderson TJ, Feygelson TI, Pate BB, Kuball M: "Control of the in-plane thermal conductivity of ultra-thin nanocrystalline diamond films through the grain and grain boundary properties", *Acta Materialia 103: pp.141-152. (2016)*
2. **Balázsi K**: "Influence of deposition parameters on structure of TiC/a:C nanocomposite coatings", In: *M Michalka, A Vincze (Eds.), 19th School of Vacuum Technology, Vacuum and New Materials, Strbske Pleso, Slovakia, 2016.11.09-2016.11.12., Strbske Pleso: Slovak Vacuum Society, 2016. pp.75-79. (ISBN:978-80-971179-7-9)*
3. **Bányász I**, Berneschi S, Fried M, Havranek V, Khánh NQ, Nagy GUL, Németh A, Nunzi-Conti G, Pelli S, Rajta I, Righini C, Szilágyi E, Veres M, Zolnai Zs: "The use of ion beam techniques for the fabrication of integrated optical elements", In: *Ferrari M, Dorosz D, Marciniak M (Eds.), 18th International Conference on Transparent Optical Networks (ICTON), Trento, Italy, 2016.07.10-2016.07.14. pp.1-4.*
4. **Bányász I**, Pelli S, Nunzi-Conti G, Righini GC, Berneschi S, Szilágyi E, Németh A, Fried M, Lohner T, Petrik P, Zolnai Zs, Khánh NQ, Rajta I, Nagy GUL, Havranek V, Vosecek V, Lavrentiev V, Veres M, Himics L: "Design and fabrication of integrated optical elements in glasses and crystals by various ion beam techniques", In: *Cole P (Eds.), 12th International Topical Meeting on Nuclear Applications of Accelerators (AccApp '15), Washington, USA, 2015.11.10-2015.11.13., Kensington: American Nuclear Society, 2016. pp.389-415.*
5. **Bársony I**, Zolnai Zs, Battistig G (Eds.): "Procedia Engineering: Proceedings of the 30th anniversary Eurosensors Conference – Eurosensors 2016", *Budapest, Hungary, 2016.09.04 -2016.09.07., Budapest: Elsevier; Akadémiai Kiadó, (2016). 1766 p. (168)*
6. **Battistig G**, Gurbán S, Sáfrán G, Sulyok A, Németh A, Panjan P, Zolnai Zs, Menyhárd M: "Wafer-scale SiC rich nano-coating layer by Ar^+ and Xe^+ ion mixing", *Surface and Coatings Technology 302: pp.320-326. (2016)*
7. **Battistig G**, Zolnai Zs, Németh A, Panjan P, Menyhárd M: "Nanoscale SiC production by ballistic ion beam mixing of C/Si multilayer structures", *J Physics D-Applied Physics 49:(18) Paper 185303. (2016)*
8. **Bérces Zs**, K Tóth, Márton G, I Pál, B Kováts-Megyesi, Fekete Z, Ulbert I, Pongrácz A: "Neurobiochemical changes in the vicinity of a nanostructured neural implant", *Scientific Reports 6: Paper 35944. (2016)*
9. **Berecz T**, Jenei P, Csóré A, Lábár JL, Gubicza J, Szabó PJ: "Determination of dislocation density by electron backscatter diffraction and X-ray line profile analysis in ferrous lath martensite", *Materials Characterization 113: pp.117-124. (2016)*
10. **Bíró F**, Radnóczi GyZ, Takács M, Baji Zs, Dücső Cs, Bársony I: "Pt Deposition Techniques for Catalytic Activation of Nano-structured Materials", *Procedia Engineering 168: pp.1148-1151. (2016), Proc 30th Anniversary Eurosensors Conference – Eurosensors 2016, Budapest, Hungary: 2016.09.04-2016.09.07.*
11. **Biró LP**, Lambin P: "Chapter 7. Grain Boundaries in Chemical Vapor Deposition-Grown Graphene", In: *Aliofkhazraei M, Ali N, Milne WI, Ozkan CS, Mitura S, Gervasoni JL*

(Eds.), Graphene Science Handbook: Mechanical and Chemical Properties, Boca Raton FL: CRC Press, 2016. pp.107-126. (ISBN:978-1-4665-9123-3)

12. **Bosi M**, Attolini G, Negri M, Ferrari C, Buffagni E, Frigeri C, Calicchio M, Pecz B, Riesz F, Cora I, Osváth Z, Jiang L, Borionetti G: "Defect structure and strain reduction of 3C-SiC/Si layers obtained with the use of a buffer layer and methyltrichlorosilane addition", *CrystEngComm 18:(15) pp.2770-2779. (2016)*
13. **Bouvet-Marchand A**, Loubat M, Graillot A, Volk J, Dauksevicius R, Saoutieff E, Viana A, Christian B, Lebedev V, Sturm C, Loubat C: "UV-crosslinked Polymeric Materials for Encapsulation of ZnO Nanowires in Piezoelectric Fingerprint Sensors", *Procedia Engineering 168: pp.1135-1139. (2016), 30th Eurosensors Conference, Eurosensors 2016, Budapest, Hungary: 2016.09.04-2016.09.07.*
14. **Braeckman BR**, Misják F, Radnóczi Gy, Depla D: "The influence of Ge and In addition on the phase formation of CoCrCuFeNi high-entropy alloy thin films", *Thin Solid Films 616: pp.703-710. (2016)*
15. **Chen X**, Szolnoki A: "Individual wealth-based selection supports cooperation in spatial public goods games", *Scientific Reports 6: Paper 32802. 8 p. (2016)*
16. **Christian B**, Volk J, Lukács IE, Sautieff E, Sturm C, Graillot A, Dauksevicius R, O'Reilly E, Ambacher O, Lebedev V: "Piezo-force and Vibration Analysis of ZnO Nanowire Arrays for Sensor Application", *Procedia Engineering 168: pp.1192-1195. (2016), 30th Eurosensors Conference, Eurosensors 2016, Budapest, Hungary: 2016.09.04-2016.09.07.*
17. **Cora I**, Pekker P, Dódony I, Janovszky D: "Single crystal structure determination and refinement of $AgZrCu_4$ and Ag-containing $Cu_{10}Zr_7$ by precession electron diffraction and tomography techniques", *J Alloys and Compounds 658: pp.678-683. (2016)*
18. **Cota W**, Ferreira SC, Ódor Gé: "Griffiths effects of the susceptible-infected-susceptible epidemic model on random power-law networks", *Phys Rev E-Stat Nonlin 93:(3) Paper 032322. 9 p.(2016)*
19. **Dabóczi M**, Albert E, Agócs E, Kabai-Faix M, Hórvölgyi Z: "Bilayered (silica-chitosan) coatings for studying dye release in aqueous media: The role of chitosan properties", *Carbohydrate Polymers 136: pp.137-145. (2016)*
20. **Daróczi CsS** (Eds.): "MTA EK MFA Yearbook 2015", *Budapest: MTA Műszaki Fizikai és Anyagtudományi Kutatóintézet (MFA), 2016. 136 p.* http://www.mfa.kfki.hu/system/files/MFA_Yearbook_2016.pdf
21. **Dódony I**, Németh T, Kovács-Kis V: "Report on the natural occurrence of a silica-clay nanocomposite", *Resolution and Discovery 2016: pp.1-6. (2016)*
22. **Dózsa L**, Galkin NG, Pécz B, Osváth Z, Zolnai Zs, Galkin KN, Chernev IM, Shevlyagin AV, Dotsenko SA: "Structural, microscopic, and optical properties of Mg_2Si-Mg_2Sn alloy heterostructures on silicon", In: *Galkin NG (Eds.), Proc Third Asian School-Conference on Physics and Technology of Nanostructured Materials: ASCO-NANOMAT 2015, 262 p., Vladivostok, Russia, 2015.08.19-2015.08.26. Vladivostok: Trans Tech Publications, 2016. pp.63-67, (ISBN:978-3-03835-682-0;978-5-8044-1556-4)*
23. **Duta L**, Stan GE, Stroescu H, Gartner M, Anastasescu M, Fogarassy Zs, Mihailescu N, Szekeres A, Bakalova S, Mihailescu IN: "Multi-stage pulsed laser deposition of aluminum nitride at different temperatures", *Appl Surf Sci 374: pp.143-150. (2016)*

24. **El-Tahawy M**, Gubicza J, Huang Y, Choi H, Choe H, Lábár JL, Langdon TG: "Evolution of Microstructure, Phase Composition and Hardness in 316L Stainless Steel Processed by High-Pressure Torsion", *Materials Science Forum 879: pp.502-507. (2016), THERMEC'2016 - International Conference on Processing & Manufacturing of advanced Materials, Graz, Ausztria: 2016.05.29-2016.06.03.*

25. **Farkas E**, Patkó D, Khánh NQ, Tóth EL, Vonderviszt F, Horváth R: "Self-assembly and structure of flagellin-polyelectrolyte composite layers: Polyelectrolyte induced flagellar filament formation during the alternating deposition process", *RSC Advances 6:(95) pp.92159-92167. (2016)*

26. **Farkas E**, Sranko D, Kerner Zs, Setner B, Szewczuk Z, Malinka W, Horváth R, Szyrwiel L, Pap JS: "Self-assembled, nanostructured coatings for water oxidation by alternating deposition of Cu-branched peptide electrocatalysts and polyelectrolytes", *Chemical Science 7: pp.5249-5259. (2016)*

27. **Fekete B**, Trampus P, Jandova D, Kasl J, Jóni B, Misják F, Radnóczi Gy: "Low cycle thermomechanical fatigue of VVER-440 reactor pressure vessel steels: Investigation the fatigue kinetics and development of a life assessment model", *Procedia Structural Integrity 2: pp.2164-2172. (2016), 21st European Conference on Fracture, ECF21 Catania, Italy: 2016.06.20-2016.06.24.*

28. **Fekete Z**, Pálfi E, Márton G, Handbauer M, Bérces Zs, Ulbert I, Pongrácz A, Négyessy L: "Combined in vivo recording of neural signals and iontophoretic injection of pathway tracers using a hollow silicon microelectrode", *Sensors and Actuators B-Chemical 236: pp.815-824. (2016)*

29. **Fodor B**, Agócs Emil, Bardet B, Defforge T, Cayrel F, Alquier D, Fried M, Gautier G, Petrik P: "Porosity and thickness characterization of porous Si and oxidized porous Si layers – an ultraviolet-visible-mid infrared ellipsometry study", *Microporous and Mesoporous Materials 127: pp.112-120. (2016)*

30. **Fodor B**, Kozma P, Burger S, Fried M, Petrik P: "Effective medium approximation of ellipsometric response from random surface roughness simulated by finite-element method", *Thin Solid Films 617: pp.20-24. (2016)*

31. **Fogarassy Zs**: "Fizikai és kémiai módszerekkel gőzfázisból leválasztott szerkezetek kialakítása és jellemzése", *Ph.D. Thesis, 117 p., 2015., Supervisor(s): Lábár JL, (2016)*

32. **Gastner MT**, Ódor Gé: "The topology of large Open Connectome networks for the human brain", *Scientific Reports 6: Paper 27249. 11 p. (2016)*

33. **Ghegin E**, Nemouchi F, Perrin C, Hoummada K, Lábár J, Zhiou S, Rodriguez P, Sagnes I, Jany C: "Metallurgical studies of integrable Ni-based contacts for their use in III–V/Si heterogeneous photonics devices", In: *IEEE (Eds.), 2016 IEEE Silicon Nanoelectronics Workshop (SNW), Honolulu, USA, 2016.06.12-2016.06.13., Honolulu: IEEE, 2016. pp.214-215. (ISBN:978-1-5090-0726-4)*

34. **Godzsak M**, Pekker P, Cora I, Veres Zs: "Investigation of the intermediate layers formed by austenitic nitrocarburizing", *Int J Microstructure and Materials Properties 11:(1-2) pp.34-47. (2016)*

35. **Gubicza J**, El-Tahawy M, Huang Y, Choi H, Choe H, Lábár JL, Langdon TG: "Microstructure, phase composition and hardness evolution in 316L stainless steel

processed by high-pressure torsion", *Mater Sci Eng A-Structural Materials Properties Microstructure and Processing 657: Pp.215-223. (2016)*

36. **Henry A**, Chubarov M, Czigány Zs, Garbrecht M, Högberg H: "Early stages of growth and crystal structure evolution of boron nitride thin films", *Jap J Appl Phys 55:(5S) Paper 05FD06. 5 p. (2016)*
37. **Horváth Á**, Balázsi K, Balázsi Cs: "Nanoszerkezetű ODS acélfejlesztés Hungaryon", *Nukleon 9: Paper 199. 5 p. (2016)*
38. **Horváth Á**, Nagy N, Schiller R: "Particle irradiation and electron work function: Fe single crystal bombarded with Ar^+ ions", *Radiation Physics and Chemistry 124: pp.38-40. (2016)*
39. **Horváth R**: "Bioszenzorika és bio-nanotechnológia", *Magyar Tudomány 1: pp.70-77. (2016)*
40. **Horváth ZsJ**: "Possible physical origins of non-ideal temperature dependence of current-voltage characteristics of Schottky junctions", In: *J Vajda, I Jamnicky (Eds.), Applied Physics of Condensed Matter, 4 p., Strbske Pleso, Slovakia, 2016.06.22-2016.06.24., Bratislava: Slovak University of Technology in Bratislava, 2016. pp.227-230., Applied Physics of Condensed Matter (ISBN:978-80-227-4572-7)*
41. **Hovsepian PE**, Mandal P, Ehiasarian AP, Sáfrán G, Tietema R, Doerwald D: "Friction and wear behaviour of Mo-W doped carbon-based coating during boundary lubricated sliding", *Appl Surf Sci 366: pp.260-274. (2016)*
42. **Jani PK**, Schwaner E, Kajdácsi E, Debreczeni ML, Ungai-Salánki R, Dobó J, Doleschall Z, Rigó JJr, Geiszt M, Szabó B, Gál P, Cervenak L: "Complement MASP-1 enhances adhesion between endothelial cellsand neutrophils by up-regulating E-selectin expression", *Molecular Immunology 75: pp.38-47. (2016)*
43. **Juhász Z**: "A népzene kultúrkörei", *Magyar Kultúra Kiadó, 2016, Győr (ISBN:978-615-80195-8-3)*
44. **Juhász Z**, Fehér T, Németh E, Pamjav H: "mtDNA analysis of 174 Eurasian populations using a new iterative rank correlation method", *Mol Genet Genomics 291:493–509 (2006)*
45. **Kelling J**, Ódor Gé, Gemming S: "Bit-Vectorized GPU Implementation of a Stochastic Cellular Automaton Model for Surface Growth", *p. online. p. (2016), 2016 IEEE International Conference on Intelligent Engineering Systems, 2016. INES '16 (IEEE, 2016)*
46. **Kelling J**, Ódor Gé, Gemming S: "Universality of (2+1)-dimensional restricted solid-on-solid models", *Phys Rev E-Stat Nonlin 94:(2) Paper 022107. 7 p. (2016)*
47. **Kis-Kovacs V**, Shumilova T, Masaitis V: "HRTEM study of Popigai impact diamond: heterogeneous diamond nanostructures in native amorphous carbon matrix", *Physics and Chemistry of Minerals 43:(9) pp.661-670. (2016)*
48. **Kiss ÁK**, Lábár JL: "Determining Projections of Grain Boundaries from Diffraction Data in Transmission Electron Microscope", *Microscopy and Microanalysis 22:(3) pp.551-564. (2016)*
49. **Kiss ÁK**, Rauch EF, Lábár JL: "Highlighting material structure with transmission electron diffraction correlation coefficient maps", *Ultramicroscopy 163: pp.31-37. (2016)*

50. **Kolonits T**, Jenei P, Tóth BG, Czigány Zs, Gubicza J, Péter L, Bakonyi I: "Characterization of Defect Structure in Electrodeposited Nanocrystalline Ni Films", *J Electrochemical Society 163:(3) pp.D107-D114. (2016)*
51. **Koós AA**, Vancsó P, Magda GZ, Osváth Z, Kertész K, Dobrik G, Hwang C, Tapasztó L, Biró LP: "STM study of the MoS_2 flakes grown on graphite: A model system for atomically clean 2D heterostructure interfaces", *Carbon 105: pp.408-415. (2016)*
52. **Kovács B**, Orgován N, Patkó D, Székács I, Kurunczi S, Tóth B, Vonderviszt F, Horváth R: "The modulation of human cell adhesion by oriented flagellin monolayers revealed by label-free optical biosensors", *Biosensors 2016, Göteborg, 2016. May 25-27, poster (2016)*
53. **Kovács B**, Patkó D, Szekács I, Orgován N, Kurunczi S, Sulyok A, Khánh NQ, Tóth B, Vonderviszt F, Horváth R: "Flagellin based biomimetic coatings: From cell-repellent surfaces to highly adhesive coatings", *Acta Biomaterialia 42: pp.66-76. (2016)*
54. **Kovács B**, Patkó D, Székács I, Orgován N, Kurunczi S, Tóth B, Vonderviszt F, Horváth R: "The modulation of human cell adhesion by genetically modified flagellin monolayers revealed by label-free optical biosensors", *Műszaki Kémiai Napok 2016, Veszprém, 2016. April 26-28, oral presentation (2016)*
55. **Kovács-Kis V**, Németh T, Dódony I: "Nanostructural changes in montmorillonite upon cyclic wetting-and-drying. An electron diffraction study", In: *Valúchová J (Eds.), 8th Mid-European Clay Conference (MECC 2016): Book of Abstracts, 207 p. Kosice, Slovakia, 2016.07.06-2016.07.08., Kosice: ELFA s.r.o., 2016. p.172. 1 p. (ISBN:978-80-972288-0-4)*
56. **Lázár K**, Kovács-Kis V, Len A, Kasztovszky Zs, Markó A, T Biró K: "Novel investigations on the mineralogy of Carpathian mahogany obsidian", *p. 47. International Obsidian Conference, Lipari, Italy, 2016. June 1-3, Poster (2016)*
57. **Leiterer C**, Bronstrup G, Jahr N, Talkenberg F, Radnóczi GyZ, Pecz B, Christiansen S, Sivakov V: "Index matching at the nanoscale: light scattering by core-shell Si/SiOx nanowires", *Nanotechnology 27:(43) Paper 435202. 6 p. (2016)*
58. **Li K**, Szolnoki A, Cong R, Wang L: "The coevolution of overconfidence and bluffing in the resource competition game", *Scientific Reports 6:(2) Paper 21104. 9 p. (2016)*
59. **Li L**, Ungár T, Tóth LS, Skrotzki W, Wang YD, Ren Y, Choo H, Fogarassy Zs, Zhou XT, Liaw PK: "Shear-Coupled Grain Growth and Texture Development in a Nanocrystalline Ni-Fe Alloy during Cold Rolling", *Metal Mater Trans-A-Physical Metallurgy and Materials Science 47:(12) pp.6632-6644. (2016)*
60. **Lohner T**, Serényi M, Petrik P: "Spectroellipsometric Characterization of Sputtered Silicon Nitride Films Using Two Different Dispersion Relations", *Int J New Horizons in Physics 3:(1) pp.7-10. (2016)*
61. **Lu Bin**, Defforge T, Fodor B, Morillon B, Alquier D, Gautier G: "Optimized plasma-polymerized fluoropolymer mask for local porous silicon formation", *J Appl Phys 119:(21) Paper 213301. 7 p. (2016)*
62. **M Kiss**, P Földesy, Fekete Z: "Optimization of a Michigan-type silicon microprobe for infrared neural stimulation", *Sensors and Actuators B-Chemical 224: pp.676-682. (2016)*

63. **Makai JP**: "Simultaneous spatial and angular positioning of plane specular samples by a novel double beam triangulation probe with full auto-compensation", *Optics and Lasers in Engineering 77: pp.137-142. (2016)*

64. **Makarona E**, Péter B, Székács I, Tsamis C, Horváth R: "ZnO Nanostructure Templates as a Cost-Efficient Mass-Producible Route for the Development of Cellular Networks", *Materials 9:(4) Paper 256. 23 p. (2016)*

65. **Márk GI**, Vancsó P, Biró LP, Kvashnin DG, Chernozatonskii L, Chaves A, Rakhimov KY, Lambin P: "Wave Packet Dynamical Calculations For Carbon Nanostructures", In: *Maffucci A, Maksimenko SA (Eds.), Fundamental and Applied Nano-Electromagnetics, 290 p., Doedrecht: Springer Netherlands, 2016. pp.89-102. (NATO Science for Peace and Security Series B: Physics and Biophysics, VIII) (ISBN:978-94-017-7476-5)*

66. **Maros MB**, Németh AK, Zoltán K, Bódis E, Maros Zs, Tapasztó O, Balázsi K: "Tribological characterisation of silicon nitride/multilayer graphene nanocomposites produced by HIP and SPS technology", *Tribology International 93:(Part A) pp.269-281. (2016)*

67. **Márton G**, P Baracskay, B Cseri, B Plósz, G Juhász, Fekete Z, Pongrácz A: "A silicon-based microelectrode array with a microdrive for monitoring brainstem regions of freely moving rats", *J Neural Engineering 13:(2) Paper 026025. 12 p. (2016)*

68. **Matsumoto T**, Uchimoto T, Takagi T, Vértesy G: "Evaluation of chill structure in ductile cast iron by incremental permeability method", *Int J Appl Electromagnetics and Mechanics 52:(2016) pp.1599-1605. (2016)*

69. **Mayer M**, Malinsky P, Schiettekatte F, Zolnai Zs: "Intercomparison of ion beam analysis software for the simulation of backscattering spectra from two-dimensional structures", *Nucl Instrum Meth B-Beam Interactions with Materials and Atoms 385: pp.65-73. (2016)*

70. **Molnár Gy**, Dózsa L, Erdélyi R: "Local electrical characteristics of iron silicide nanostructures on Si substrates", In: *Galkin NG (Eds.), Proc Third Asian School-Conference on Physics and Technology of Nanostructured Materials: ASCO-NANOMAT 2015, 262 p., Vladivostok, Russia, 2015.08.19-2015.08.26. Vladivostok: Trans Tech Publications, 2016. pp.95-98. (ISBN:978-3-03835-682-0;978-5-8044-1556-4)*

71. **Nádas J**, Rakovics V: "Bandwidth widening of semiconductors with luminescent layer", In: *Dariusz Sawicki, Piotr Pracki (Eds.), Proc VI. IEEE Lighting Conference of the Visegrad Countries LUMEN V4. 294 p., Karpacz, Poland, 2016.09.13-2016.09.16., Karpacz: IEEE, 2016. Paper 7745519. 4 p. (ISBN:978-1-5090-3304-1)*

72. **Nádas J**, Rakovics V: "Félvezető fényforrások a közeli infravörös spektroszkópiában", In: *Vonderviszt F, Bokrossy-Csiba M, Törcsváryné Kovács Zs (Eds.), Műszaki Kémiai Napok 2016: 172 p., Veszprém, Hungary, 2016.04.26-2016.04.28. Veszprém: Pannon Egyetem Műszaki Informatikai Kar, Műszaki Kémiai Kutatóintézet, 2016. pp.70-75. (ISBN:978-963-396-087-5)*

73. **Nádor J**, Kalas B, Saftics A, Agócs E, Kozma P, Körösi L, Székács I, Fried M, Horváth R, Petrik P: "Plasmon-enhanced two-channel in situ Kretschmann ellipsometry of protein adsorption, cellular adhesion and polyelectrolyte deposition on titania nanostructures", *Optics Express 24:(5) pp.4812-4823. (2016)*

74. **Nagy N**, Zámbó D, Pothorszky Sz, Gergely-Fülöp E, Deák A: "Identification of dewetting stages and preparation of single chain gold nanoparticle rings by colloidal lithography", *Langmuir 32:(4) pp.963-971. (2016)*

75. **Nazirizadeh Y**, Behrends V, Prósz A, Orgován N, Horváth R, Ferrie AM, Fang Y, Selhuber-Unkel C, Gerken M: "Intensity interrogation near cutoff resonance for label-free cellular profiling", *Scientific Reports 6: Paper 24685. 6 p. (2016)*

76. **Nemcsics Á**, Pődör B, Tóth La, Balázs J, Dobos L, Makai J, Csutorás M, Ürmös A: "Investigation of MBE grown inverted GaAs quantum dots", *Microelectron Reliability 59: pp.60-63. (2016)*

77. **Németh M**, Zarándy Á, Földesy P: "Dual-pixel CMOS APS Architecture for Intra-frame Speed Measurement", In: *IEEE (Eds.), IEEE 19th International Symposium on Design and Diagnostics of Electronic Circuits & Systems (DDECS). 4 p., Kosice, Slovakia, 2016.04.20-2016.04.22., Bratislava: Slovak University of Technology in Bratislava, 2016. pp.12-15. (ISBN:978-80-8086-256-5)*

78. **Németh M**, Zarándy Á, Földesy P: "Pixel-level APS Sensor Integration and Sensitivity Scaling for Vision Based Speed Measurement", *Procedia Engineering 168: pp.1321-1324. (2016), Proc 30th Anniversary Eurosensors Conference – Eurosensors 2016, Budapest, Hungary: 2016.09.04-2016.09.07.*

79. **Németh T**, Máthé Z, Pekker P, Dódony I, Kovács-Kis V, Sipos P, Cora I, Kovács I: "Clay mineralogy of the Boda Claystone Formation (Mecsek Mts., SW Hungary)", *Open Geosciences 8:(1) pp.259-274. (2016)*

80. **Ódor Gé**: "Critical dynamics on a large human Open Connectome network", *Phys Rev E-Stat Nonlin 94:(6) Paper 062411. 7 p. (2016)*

81. **Oláh N**, Fogarassy Zs, Sulyok A, Szívós J, Csanádi T, Balázsi K: "Ceramic TiC/a:C protective nanocomposite coatings: Structure and composition versus mechanical properties and tribology", *Ceramics International 42:(10) pp.12215-12220. (2016)*

82. **Oláh N**, Fogarassy Zs, Sulyok A, Veres M, Kaptay G, Balázsi K: "TiC crystallite formation and the role of interfacial energies on the composition during the deposition process of TiC/a:C thin films", *Surface and Coatings Technology 302: pp.410-419. (2016)*

83. **Orgován N**, Szabó B, Horváth R: "Optical waveguide-based biosensor for label-free monitoring of living cells", In: *Pranjal Chandra (Eds.), Nanobiosensors for Personalized and Onsite Biomedical Diagnosis, 624 p., Stevenage: Institution of Engineering and Technology (IET), 2016. pp.165-180. (ISBN:9781849199506)*

84. **Orgován N**, Ungai-Salánki R, Lukácsi Sz, Sándor N, Bajtay Zs, Erdei A, Szabó B, Horváth R: "Adhesion kinetics of human primary monocytes, dendritic cells, and macrophages: Dynamic cell adhesion measurements with a label-free optical biosensor and their comparison with end-point assays", *Biointerphases 11:(3) Paper 031001. 11 p. (2016)*

85. **Osváth Z**, Gergely-Fülöp E, Deák A, Hwang C, Biró LP: "Mapping the nanomechanical properties of graphene suspended on silica nanoparticles", *J Experimental Nanoscience 11:(13) pp.1011-1018. (2016)*

86. **Osváth Z**, Molnár Gy, Kertész K, Deák A, Nagy N, Hwang C, Biró LP: "The structure and properties of graphene suspended on nanoparticles", In: *Kónya Z, Kukovecz Á (Eds.), 7th Szeged International Workshop on Advances in Nanoscience: SIWAN 7, Szeged,*

Hungary, 2016.10.12-2016.10.15., Szeged: Akadémiai Kiadó, 2016. pp.29-30. (ISBN:978-963-05-9801-9)

87. **Paddubskaya A**, Valynets N, Kuzhir P, Batrakov K, Maksimenko S, Kotsilkova R, Velichkova H, Petrova I, Biró I, Kertész K, Márk GI, Horváth ZE, Biró LP: "Electromagnetic and thermal properties of three-dimensional printed multilayered nano-carbon/poly(lactic) acid structures", *J Appl Phys 119:(13) Paper 135102. 9 p. (2016)*
88. **Pálinkás A**, Molnár Gy, Hwang C, Biró LP, Osváth Z: "Determination of the STM tip-graphene repulsive forces by comparative STM and AFM measurements on suspended graphene", *RSC Advances 6:(89) pp.86253-86258. (2016)*
89. **Pálinkás A**, Molnár Gy, Osváth Z: "Grafén/arany hibrid nanoszerkezetek vizsgálata pásztázó alagútmikroszkópiával", In: *Keresztes Gábor (Eds.), Spring Wind 2016. Tanulmánykötet. I. kötet: Agrártudomány, állam- és jogtudomány, föld- és fizikatudomány, had- és rendészettudomány, 574 p., Budapest, Hungary, 2016.04.15-2016.04.17. Budapest: Doktoranduszok Országos Szövetsége, 2016. pp.274-288. (ISBN:978-615-5586-09-5)*
90. **Pálinkás A**, Süle P, Molnár Gy, Hwang C, Biró LP, Osváth Z: "Investigation of graphene-gold hybrid nanostructures by scanning tunnelling microscopy and spectroscopy", In: *Kónya Z, Kukovecz Á (Eds.), 7th Szeged International Workshop on Advances in Nanoscience: SIWAN 7, Szeged, Hungary, 2016.10.12-2016.10.15., Szeged: Akadémiai Kiadó, 2016. pp.30-31. (ISBN:978-963-05-9801-9)*
91. **Pálinkás A**, Süle P, Szendrő M, Molnár Gy, Hwang C, Biró LP, Osváth Z: "Moiré superlattices in strained graphene-gold hybrid nanostructures", *Carbon 107: pp.792-799. (2016)*
92. **Palla-Papavlu A**, Filipescu M, Schneider CW, Antohe S, Ossi PM, Radnóczi Gy, Dinescu M, Wokaun A, Lippert T: "Direct laser deposition of nanostructured tungsten oxide for sensing applications", *J Physics D-Applied Physics 49:(20) Paper 205101. 8 p. (2016)*
93. **Pekker Á**, Németh G, Botos Á, Tóháti HM, Borondics F, Osváth Z, Biró LP, Walker K, Khlobystov AN, Kamarás K: "Cloaking by p-electrons in the infrared", *Phys Status Solidi B-Basic Research 253:(12) pp.2457-2460. (2016)*
94. **Petkov N**, Volk J, Erdélyi R, Lukács IE, Nagata T, Sturm C, Grundmann M: "Contacting ZnO Individual Crystal Facets by Direct Write Lithography", *ACS Appl Materials Interfaces 8:(36) pp.23891-23898. (2016)*
95. **Piszter G**, Kertész K, Bálint Z, Biró LP: "Pretreated Butterfly Wings for Tuning the Selective Vapor Sensing", *Sensors 16:(9) Paper 1446. 9 p. (2016)*
96. **Piszter G**, Kertész K, Bálint Z, Biró LP: "Variability of the structural coloration in two butterfly species with different prezygotic mating strategies", *Plos One 11:(11) Paper e0165857. 19 p. (2016)*
97. **Pothorszky Sz**, Zámbó D, Deák A: "Structural and Optical Properties of Gold/Silica “Mushroom” Particles Prepared by Interfacial Templating", *Particle & Particle Systems Characterization n.a: Paper 1600291. (2016)*
98. **Pothorszky Sz**, Zámbó D, Deák T, Deák A: "Assembling patchy nanorods with spheres: Limitations imposed by colloidal interactions", *Nanoscale 8:(6) pp.3523-3529. (2016)*
99. **Radnóczi GyZ**, Dódony E, Battistig G, Vouroutzis N, Kavouras P, Stoemenos J, Frangis N, Kovács A, Pécz B: "Structural characterization of nanostructures grown by Ni metal

induced lateral crystallization of amorphous-Si", *J Appl Phys 119:(6) Paper 065303. 16 p. (2016)*

100. **Radnóczi GyZ**, Stelzner Th, Sivakov VA, Stoimenos J, Christiansen SH, Pécz B: "Microstructure of silicon nanorods for novel solar cells", *Resolution and Discovery 1:(1) pp.21-26. (2016)*
101. **Rajta I**, Huszánk R, Szabó ATT, Nagy GUL, Szilasi S, Fürjes P, Holczer E, Fekete Z, Járvás G, Szigeti M, Hajba L, Bodnár J, Guttman A: "Tilted pillar array fabrication by the combination of proton beam writing and soft lithography for microfluidic cell capture: Part 1 Design and feasibility", *Electrophoresis 37:(3) pp.498-503. (2016)*
102. **Rakovics V**, Dücső Cs, Réti I, Battistig G: "Vízben oldott motorhajtóanyagok meghatározása UV abszorpció és lumineszcencia alapján", In: *Vondervisztt F, Bokrossy-Csiba M, Törcsváryné Kovács Zs (Eds.), Műszaki Kémiai Napok 2016: Proc. 172 p., Veszprém, Hungary, 2016.04.26-2016.04.28., Veszprém: Pannon Egyetem Műszaki Informatikai Kar, Műszaki Kémiai Kutatóintézet, 2016. pp.89-95. (ISBN:978-963-396-087-5)*
103. **Sáfrán G**, Tóth AL, Illés L: "Mikrostély tartó transzmissziós elektromikroszkópos minták fókuszált ionsugaras megmunkálására", *NSZO: H01J37/20 G21K5/08, 230423, (2010), P1000683 (2016) Hungary*
104. **Saftics A**, Kurunczi S, Szekrényes Zs, Kamarás K, Khánh NQ, Sulyok A, Bősze Sz, Horváth R: "Fabrication and characterization of ultrathin dextran layers: time dependent nanostructure in aqueous environments revealed by OWLS", *Colloids Surf B-Biointerfaces 146: pp.861-870. (2016)*
105. **Sándor N**, Lukacsi S, Ungai-Ungai-Salánki R, Orgován N, Szabó B, Horváth R, Erdei A, Bajtay Z: "CD11c/CD18 Dominates Adhesion of Human Monocytes, Macrophages and Dendritic Cells over CD11b/CD18", *Plos One 11:(9) Paper e0163120. 17 p. (2016)*
106. **Sautner É**, Papp K, Holczer E, Ungai-Salánki R, Szabó B, Fürjes P, Prechl J: "Label-free Microfluidic Sensing by Detection of Interaction-triggered Change in Blood Flow Characteristics", *Procedia Engineering 168: pp.1406-1409. (2016)*
107. **Schmidt S**, Czigány Zs, Wissting J, Greczynski G, Janzén E, Jensen J, Ivanov IG, Hultman L: "A comparative study of direct current magnetron sputtering and high power impulse magnetron sputtering processes for CN_x thin film growth with different inert gases", *Diamond and Related Materials 64: pp.13-26. (2016)*
108. **Seifikar M**, O'Reilly EP, Christian BP, Lebedev V, Volk J, Erdelyi R, Lukács IE, Dauksevicius R, Gaidys R: "Enhanced pressure response in ZnO nanorods due to spontaneous polarization charge", In: *IEEE (Eds.), 15th International Conference on Nanotechnology: IEEE-NANO 2015, Rome, Itally, 2015.07.27-2015.07.30. [s.l.] - IEEE, 2016. pp.1465-1468. (ISBN:9781467381550)*
109. **Sepsi Ö**, Pothorszky Sz, Nguyen TM, Zámbó D, Újhelyi F, Lenk S, Koppa P, Deák A: "Preparation and characterization of two-dimensional metallic nanoparticle and void films derived from a colloidal template layer", *Optics Express 4:(2) pp.A424-A429. (2016)*
110. **Serényi M**, Lohner T, Sáfrán G, Szívós J: "Comparison in formation, optical properties and applicability of DC magnetron and RF sputtered aluminum oxide films", *Vacuum 128: pp.213-218. (2016)*

111. **Serényi M**, Sulyok A, Menyhárd M, Baradács E, Parditka B, Cserháti Cs, Langer GA, Erdélyi Z: "Electron irradiation induced SiO_2 growth at Al_2O_3/Si interface", In: *Janez Kovac, Gregor Jaksa (Eds.), JVC-16, Joint Vacuum Conference, Programme and book of abstracts, Portoroz, Slovenia, 2016.06.05-2016.06.09., Ljubljana: Slovenian Society for Vacuum Technique, 2016. p. 81. (ISBN:978-961-92989-8-5)*

112. **Sipos P**, Kovács-Kis V, Németh T, Balázs R: "Effect of iron oxyhydroxide removal on the metals' partition at particle level following their sorption in soil", In: *Valúchová J (Eds.), 8th Mid-European Clay Conference (MECC 2016): Abstracts, 207 p., Kosice, Slovakia, 2016.07.06-2016.07.08., Kosice: ELFA s.r.o., 2016. p. 174. 1 p. (ISBN:978-80-972288-0-4)*

113. **Sipos P**, Kovács-Kis V, Németh T, Balázs R: "TEM-EDS study of metals' partition at particle level after their sorption in soil", *Geophysical Research Abstracts 18: Paper 12686. 1 p. (2016), EGU General Assembly 2016, Wien, Austria: 2016.04.17-2016.04.22.*

114. **Stolarczyk JK**, Deák A, Dermot F Brougham: "Nanoparticle clusters: assembly and control over internal order, current capabilities and future potential", *Advanced Materials 28:(27) pp.5400-5424. (2016)*

115. **Szabó Gy**, Borsos I: "Evolutionary potential games on lattices", *Physics Reports-Review Section of Physics Letters 624: pp.1-60. (2016)*

116. **Szabó Gy**, Hodsagi K: "The role of mixed strategies in spatial evolutionary games", *Physica A - Statistical Mechanics and its Applications 462: pp.198-206. (2016)*

117. **Szabó Gy**, Király B: "Extension of a spatial evolutionary coordination game with neutral options", *Phys Rev E-Stat Nonlin 93:(5) Paper 052108. 7 p. (2016)*

118. **Szabó Gy**, Varga L, Szabó M: "Anisotropic invasion and its consequences in two-strategy evolutionary games on a square lattice", *Phys Rev E-Stat Nonlin 94:(5) Paper 052314. (2016)*

119. **Szabó Z**, Baji Z, Basa P, Czigány Zs, Bársony I, Wang H-Y, Volk J: "Homogeneous transparent conductive ZnO:Ga by ALD for large LED wafers", *Appl Surf Sci 379: pp.304-308. (2016)*

120. **Székács I**, Horváth R, Székács A: "Label-Free Optical Biosensors for Monitoring Cellular Processes and Cytotoxic Agents at Interfaces Using Guided Modes and Advanced Phase-Contrast Imaging Techniques", In: *Dimitrios NP, Georgia-Paraskevi N (Eds.), Biosensors for Security and Bioterrorism Applications, Cham, Switzerland: Springer International Publishing, 2016. pp.443-468. (ISBN:978-3-319-28926-7)*

121. **Székács I**, Klátyik Sz, Darvas B, Horváth R, Székács A: "A glyphosate formázott készítményének és formázó anyagának citotoxicitási vizsgálatai holografikus mikroszkópia segítségével", In: *Darvas B, Bakonyi G, Győri J, Major J, Székács A (Eds.), VI. Ökotoxikológiai Konferencia előadás és poszter kötete, 44 p., Budapest, Hungary, 2016.11.18 Budapest: Magyar Ökotoxikológiai Társaság, 2016. pp.36-37. (ISBN:978-963-89452-6-6)*

122. **Székács I**, Klátyik Sz, Darvas B, Horváth R, Székács A: "Cytotoxicological Assessment Of Glyphosate, Its Herbicide Product And The Surfactant Used For Its Formulation By Holographic Microscopy", In: *Universidad de Santiago de Compostela (Eds.), 9th European Conference on Pesticides and Related Organic Micropollutants in the Environment: 15th Symposium on Chemistry and Fate of Modern Pesticides, Santiago de*

Compostela, Spain, 2016.10.04-2016.10.07., Santiago de Compostela: Universidad de Santiago de Compostela, 2016. pp.393-394. (ISBN:978-84-945958-1-3)

123. **Szenes G**, Pécz B: "Anomalous effect of ion velocity on track formation in GeS", *Nucl Instrum Meth B-Beam Interactions with Materials and Atoms 389–390: pp.17-22. (2016)*
124. **Szolnoki A**, Chen X: "Cooperation driven by success-driven group formation", *Phys Rev E-Stat Nonlin 94:(4) Paper 042311. 8 p. (2016)*
125. **Szolnoki A**, Perc M: "Biodiversity in models of cyclic dominance is preserved by heterogeneity in site-specific invasion rates", *Scientific Reports 6: Paper 38608. 9 p. (2016)*
126. **Szolnoki A**, Perc M: "Collective influence in evolutionary social dilemmas", *Europhysics Letters 113:(5) Paper 58004. 6 p. (2016)*
127. **Szolnoki A**, Perc M: "Competition of tolerant strategies in the spatial public goods game", *New J Physics 18:(8) Paper 083021. 11 p. (2016)*
128. **Szolnoki A**, Perc M: "Leaders should not be conformists in evolutionary social dilemmas", *Scientific Reports 6: Paper 23633. 8 p. (2016)*
129. **Szolnoki A**, Perc M: "Zealots tame oscillations in the spatial rock-paper-scissors game", *Phys Rev E-Stat Nonlin 93:(6) Paper 062307. 6 p. (2016)*
130. **Takács M**, Zámbó D, Deák A, Pap AE, Dücső Cs: "WO_3 nano-rods sensitized with noble metal nano-particles for H2S sensing in the ppb range", *Materials Research Bulletin 84: pp.480-485. (2016)*
131. **Tapasztó O**, Tapasztó L, Lemmelb H, Puchy V, DuszaJ, Balázsi Cs, Balázsi K: "High orientation degree of graphene nanoplatelets in silicon nitride composites prepared by spark plasma sintering", *Ceramics International 42:(1) pp.1002-1006. (2016)*
132. **Toke O**, Vonderviszt F: "Amphipathic helical ordering of the flagellar secretion signal of Salmonella flagellin", *Biochemical and Biophysical Research Communications 476:(4) pp.641-647. (2016)*
133. **Tomas I**, Vértesy G: "Adaptive Testing For Nondestructive Evaluation Of Degraded Materials", *J Electrical Eng-Elektrotechnicky Casopis 67:(4) pp.273-278. (2016)*
134. **Toporkov M**, Demchenko DO, Zolnai Zs, Volk J, Avrutin V, Morkoc H, Özgür Ü: "Lattice parameters and electronic structure of BeMgZnO quaternary solid solutions: Experiment and theory", *J Appl Phys 119:(9) Paper 095311. 9 p. (2016)*
135. **Ungai-Salánki R**, T Gerecsei, Fürjes P, Orgován N, Sándor N, Holczer E, Horváth R, Szabó B: "Automated single cell isolation from suspension with computer vision", *Scientific Reports 6: Paper 20375. 9 p. (2016)*
136. **Vágó A**, Szakacs G, Sáfrán G, Horváth R, Pécz B, Lagzi I: "One-step green synthesis of gold nanoparticles by mesophilic filamentous fungi", *Chemical Physics Letters 645: pp.1-4. (2016)*
137. **Vancsó P**, Magda GZ, Pető J, Noh JY, Kim YS, Hwang C, Biró LP, Tapasztó L: "The intrinsic defect structure of exfoliated MoS2 single layers revealed by Scanning Tunneling Microscopy", *Scientific Reports 6: Paper 29726. (2016)*
138. **Vértesy G**, Gasparics A, Pávó J, Gyimóthy Sz: "Detection of low density magnetic nanoparticles by Fluxset type magnetic probe", *Int J Appl Electromagnetics and Mechanics 52:(1-2) pp.453-460. (2016)*

139. **Vértesy G**, Uchimoto T, Takagi T, Tomás I: "Correlation between conductivity and magnetic hysteresis measurements in flake graphite cast iron", In: *Noritaka Yusa, Uchimoto T, Hiroaki Kikuchi (Eds.), Electromagnetic Nondestructive Evaluation (XIX), Amsterdam: IOS Press, 2016. pp.110-117., Studies in Applied Electromagnetics and Mechanics 41. (ISBN:978-1-61499-638-5)*

140. **Wang Z**, Szolnoki A, Perc M: "How Much Interconnected Should Networks be for Cooperation to Thrive?", In: *Antonios Garas (Eds.), Interconnected Networks. 125 p., Zürich: Springer International Publishing, 2016. pp.125-139. (Understanding Complex Systems) (ISBN:978-3-319-23945-3)*

141. **Watanabe K**, Nagata T, Seungjun Oh, Wakayama Y, Sekiguchi T, Volk J, Nakamura Y: "Arbitrary cross-section SEM-cathodoluminescence imaging of growth sectors and local carrier concentrations within micro-sampled semiconductor nanorods", *Nature Communications 7: Paper 10609. 9 p. (2016)*

142. **Zámbó D**, Deák A: "Optical Simulations of Self-assembly Relevant Gold Aggregates: A Comparative Study", *Periodca Polytechnica-Chemical Engineering 60:(4) pp.244-251. (2016)*

143. **Zámbó D**, Pothorszky Sz, Brougham DF, Deák A: "Aggregation kinetics and cluster structure of amino-PEG covered gold nanoparticles", *RSC Advances 6:(32) pp.27151-27157. (2016)*

144. **Zámbó D**, Suzuno K, Pothorszky Sz, Bárdfalvy D, Holló G, Nakanishi H, Wang D, Ueyama D, Deák A, Lagzi I: "Self-assembly of like-charged nanoparticles into Voronoi diagrams", *Physical Chemistry Chemical Physics 18:(36) pp.25735-25740. (2016)*